Intended for
Energinet Eltransmission A/S

Document type
Report

Date
July 2021

HESSELØ EXPORT CABLE ROUTE

CABLE ROUTE SURVEY REPORT

RAMBØLL

Revision	**2**
Date	**02/09/2021**
Made by	**JROU, JOPR, TBGR**
Checked by	**RUBJ**
Approved by	**UTN**
Description	**Cable Route Survey Report**

Ref Hesselø_ECR_Cable_Route_Survey_Rev1

CONTENTS

APPENDICES

Abbreviations	
AGC	Automatic Gain Control
CPT	Cone Penetration Test
DGNSS	Differential Global Navigation Satellite System
DTM	Digital Terrain Model
DTU18	Danish Technical University 2018
DVR90	Danish Vertical Reference 1990
EGN	Empirical Gain Normalization
ETRS89	European Terrestrial Reference System 1989
GL	Gilleleje
GNSS	Global Navigation Satellite System
GPS	Global Positioning System
GSD	Geometric Standard Deviation
IHO	International Hydrographic Organization
IMU	Inertial Motion Unit
KP	Kilometer Point
MAG	Magnetometer
MBES	Multibeam Echosounder
nT	Nanotesla
OWF	Offshore Windfarm
POS MV	Position and Orientation System for Marine Vessels
QC	Quality Control
RPL	Route Position List
RTK	Real-time Kinematic
SBET	Smoothed Best Estimates Trajectory
SBP	Sub-bottom Profiler
SSS	Side Scan Sonar
SVP	Sound Velocity Profiler
THU	Total Horizontal Uncertainty
TPE	Total Propagated Error
TVG	Transverse Gradiometer
TVU	Total Vertical Uncertainty
USBL	Ultra-Short Baseline
UTM	Universal Transverse Mercator
VC	Vibrocore
WP	Work Package

1. EXECUTIVE SUMMARY

For the Hesselø cable route survey Ramboll has gathered data using geophysical methods: side scan sonar (SSS), multibeam echo sounder (MBES), magnetometry (MAG) and sub-bottom profiling (SBP). Furthermore, a geotechnical campaign was completed which includes 60 vibrocores and CPT's with a penetration of 3m and 6m. The aim of the geotechnical investigation including the laboratory tests was to provide data for the burial assessment. Also, 55 grab samples were collected to support seabed interpretation and for laboratory testing. For the onshore part an airborne lidar survey was performed in order to build a terrain model and identify any onshore obstacles. The data gathered was in generally of good quality.

The MBES data was of good quality and the resolution allow to detect targets down to 30cm and even smaller. The MBES results shows a relatively flat seabed ranging from 0.8m at landfall to 34.0m at the deepest offshore parts. The MBES indicates a seabed with dense boulder fields located on the southern part of the cable route where the boulders are building up small reefs whereas the remaining cable route are heavily affected by trawl marks besides a minor boulder field further offshore located on the western arm.

The SSS data was used for seabed geology and substrate interpretation supported by the backscatter data. In addition, the SSS data was used to detect all man-made objects as well as natural objects with the size of 0.5 m or larger in at least one dimension- except within the boulder field areas, where all objects with the minimum size of 2 m in at least one dimension have been identified. The predominant seabed surface geology along the corridor is Sand and Muddy sand, although the area is characterized by the outcrop of glacial Till and Quaternary Clay at the seabed. The outcrops are primarily located in the southern part of the corridor. The Muddy sand (or gyttja) is primarily a constitute of clay, silt, fine sand and with shell fragments.

The magnetometer data were used for detection of any ferrous objects. In total 1299 anomalies down to 5 nT was detected most of these are inside boulder fields and most likely related to geology and mineral composition. Also, outside the boulder fields the main part of the anomalies can't be correlated with the MBES or SSS data meaning that the anomalies are just below the mudline or too small for MBES and SSS resolution. However, these anomalies should be taken into consideration.

The SBP data were used to interpret the subsurface conditions in the upper 10m. Different horizons were interpreted along the cable route and to verify the reflections the SBP data were correlated with the geotechnical results. Glacial tills are outcropping the seabed or are present at shallow depths below the seabed in the southernmost part of the cable corridor (KP=0.0-9.2) as well as in the central part of the corridor, north-east from Lysegrund (KP=27.0-35.0, western arm). The central segment, between KP=(18.0-27.0, western arm) and KP=(21.75-27.0, eastern arm) located east from Lysegrund can be characterized by presence of a relatively thick succession of Late Glacial to Post Glacial sands found below approx. 0.5-2.0m thick cover of Holocene fine-grained sediments. Along the remaining part of the route, the Post Glacial deposits are underlain by Late Glacial clays. The acquired SBP data did not penetrate to the lower boundary of the unit as it can reach significant thicknesses of up to 75m. The Holocene succession is 0-13m thick (typically between 0.5-6.0m) and present throughout entire cable corridor, except along its southern part where the Holocene deposits are local and found at selected location only.

The onshore lidar measurements result in a detailed terrain model together with an orthophoto to identify potential obstacles. Only two monuments were found and beside these a steep cliff with dense vegetation on top indicates the transition from the beach to the coastline found as a grass field.

2. INTRODUCTION

Energinet has commissioned Ramboll Denmark A/S to perform a cable route survey between Gilleleje and the upcoming offshore windfarm, Hesselø OWF. These investigations include geophysical survey, onshore airborne lidar survey and geotechnical investigations.

The cable route survey is split into four different work packages:

- WP A Offshore survey (MBES, SSS, SBP, MAG and Grab Sampling)
- WP B Nearshore and onshore survey (MBES, SSS, SBP, MAG, Grab Sampling and Airborne Lidar)
- WP C Geotechnical investigations (CPT, VC)
- WP D Hydrographic survey (later, planned to be in September 2021)

The aim of the investigations is to provide greater knowledge of the nature of the seabed, sedimentary materials and environmental conditions prior to installation of new export cable. The survey must map the static and dynamic elements of the seabed and upper soil stratification to ca. 10m below seabed. The results of the survey should be able to be used as basis for:

- Initial marine archaeological site assessment
- Planning of environmental investigations
- Assessment of subsea cable burial design
- Assessment of installation conditions for subsea cables

Ramboll in cooperation with MEWO S.A. from Poland have gathered data using the following four geophysical methods: side scan sonar (SSS), multibeam echosounder (MBES), magnetometry (MAG), sub bottom profiling (SBP). Also, an onshore Lidar mapping were performed by ALM. Furthermore, a geotechnical campaign was carried out to acquire vibrocores and CPT.

The delivered data includes: Bathymetry of the seabed, lidar ground models and orthophoto, high/low frequency side scan imaging of the seabed with accompanying seabed classifications, mapping of the magnetic anomalies in the survey area, interpretations of layers in the sub bottom and soil parameters from the vibrocore and CPT.

Figure 2-1 shows an overview of the survey corridor (SN2020_032_SURVEYS_POL) and the main line defined by provided RPL (REV_03_2020-10-30_NHW). The corridor width has a nominal width of 1000m with local extensions up to 1400m. The length of the route is approx. 70 km.

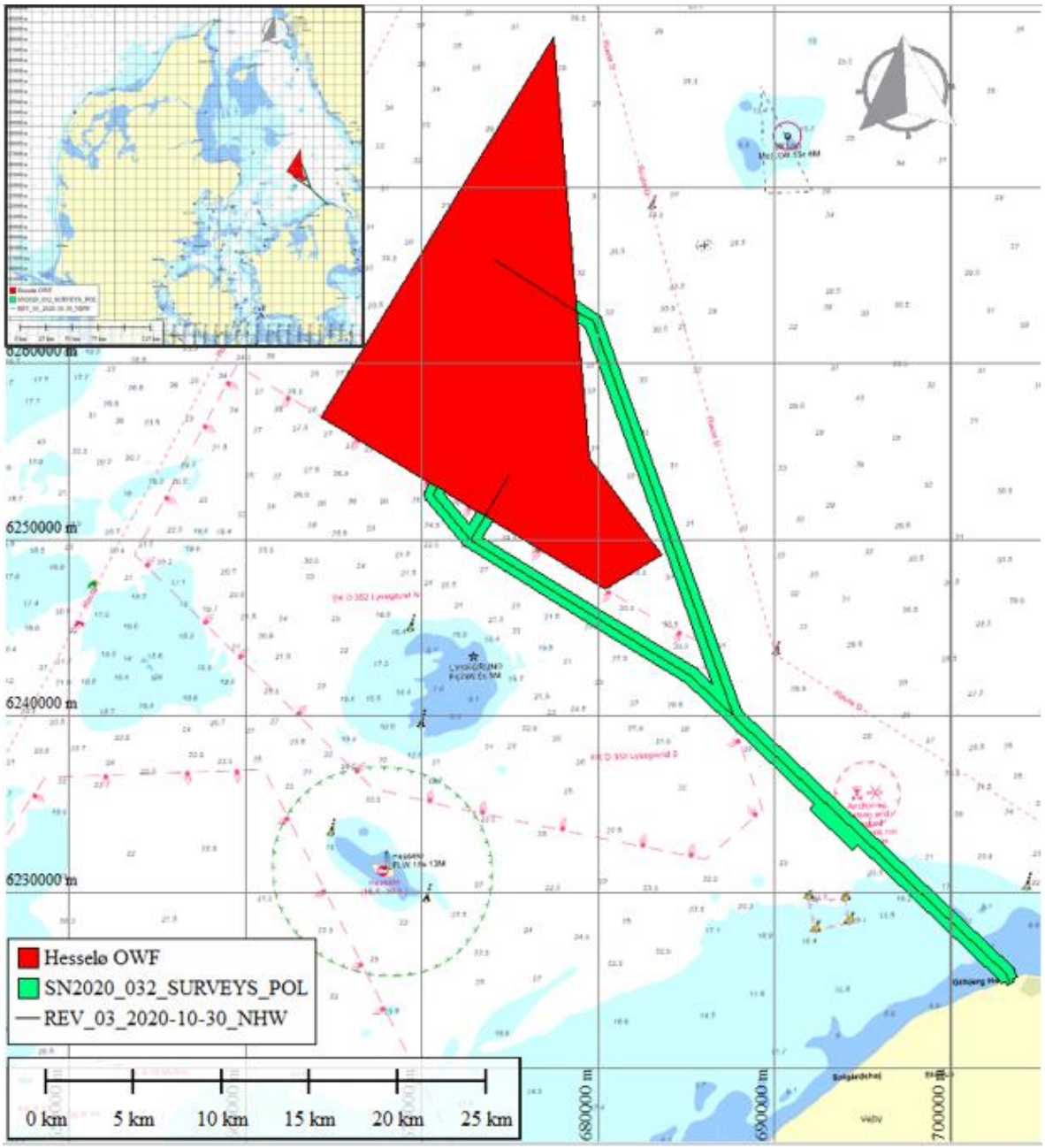

Figure 2-1 Overview of the survey area

3. EQUIPMENT

3.1 Geophysical equipment

The geophysical offshore and nearshore survey (WP A and WP B) were performed using four survey vessels, "Mintaka I" equipped with full spread (MBES, SSS, MAG and SBP), "Hydrocat" equipped with MBES and MAG, "Hydrocat 2" were equipped with SBP and SSS and last "Rambunctious" were equipped with MBES and SBP. The onshore lidar survey was acquired by "Twin-Engine Cessna 337 Skymaster" which were equipped with camera and laser scanner. The geotechnical campaign was acquired by "Glomar Vantage" equipped with CPT and Vibrocore. Mintaka I, Hydrocat. Hydrocat 2 and Glomar Vantages was operated by MEWO with assistance from Rambøll, Rambunctious was operated by Rambøll, whereas the Cessna Skymaster was operated by ALM. The vessels used for WP A and WP B can be seen in Figure 3-1 to Figure 3-6. Equipment and vessel specifications can be found in Appendix 5.

Figure 3-1: Survey vessel "Mintaka I" at quayside in Gilleleje

Figure 3-2: Survey vessel "Hydrocat" on quayside at Kolobrzeg

Figure 3-3: Survey vessel "Hydrocat 2" on quayside in Kolobrzeg

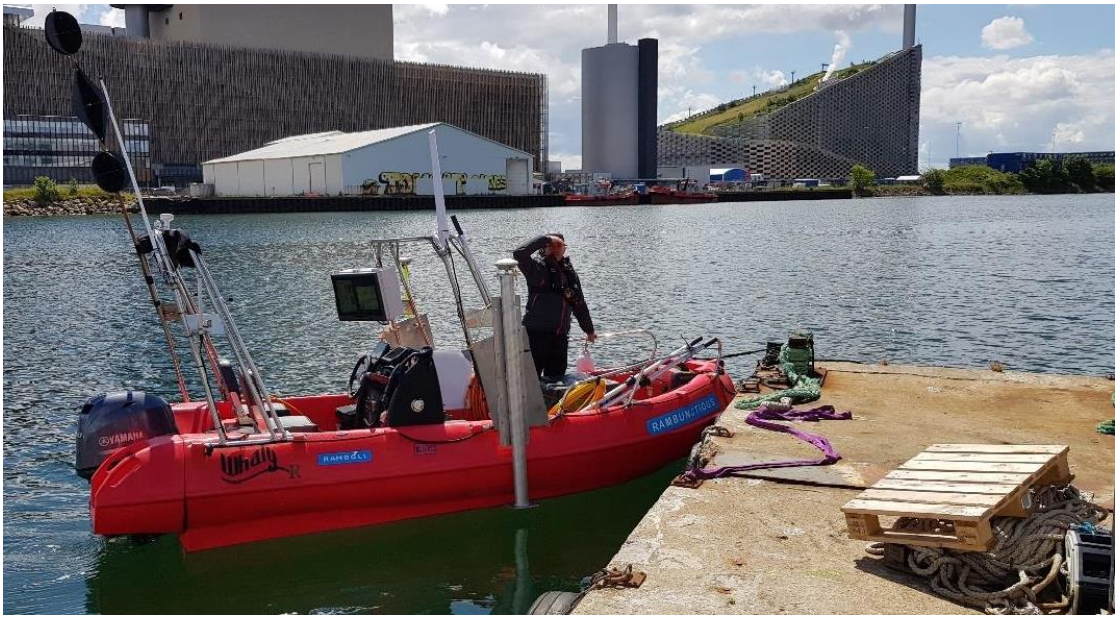

Figure 3-4: Survey vessel "Rambunctious" on quayside at Lynette Harbour

Figure 3-5: Airplane "Twin-Engine Cessna 337 Skymaster" used for Lidar mapping

Table 3-1 lists the instruments used during the geophysical survey, WP A and WP B

Table 3-1 Instrumentation used for data acquisition of WP A and WP B

Equipment	Type	Vessel	WP
Navigation and Acquisition software	QINSy, Edgetech Discovery, SESWIN, MAGlog	Mintaka I	A
Primary GPS and IMU	POSMV WaveMaster II	Mintaka I	A
Secondary GPS	Trimble BX982	Mintaka I	A
Side Scan Sonar	EdgeTech 4205 Series Dual Frequency	Mintaka I	A
Multibeam Echosounder	Reson SeaBat T50	Mintaka I	A
Sub-Bottom Profiler	Innomar SES-2000 Standard	Mintaka I	A
Magnetometer	2x Geometrics G-882 Caesium Vapor	Mintaka I	A
USBL	Sonardyne Scout PRO	Mintaka I	A
SVP	SWIFT SVP	Mintaka I	A
Grab Sampler	Van Veen Grab	Mintaka I	A
Navigation and Acquisition software	QINSy, MAGlog	Hydrocat	B
Primary GPS and IMU	SBG Apogee Navsight	Hydrocat	B
Secondary GPS	Trimble BX982	Hydrocat	B
Multibeam Echosounder	Reson SeaBat T50	Hydrocat	B
Magnetometer	2x Geometrics G-882 Caesium Vapor	Hydrocat	B
USBL	Sonardyne Scout PRO	Hydrocat	B
SVP	SWIFT SVP	Hydrocat	B
Navigation and Acquisition software	QINSy, Edgetech Discovery, SESWIN	Hydrocat 2	B
Primary GPS and IMU	C-NAV 3050	Hydrocat 2	B
Secondary GPS	C-NAV 3050	Hydrocat 2	B

Equipment	Type	Vessel	WP
Side Scan Sonar	EdgeTech 4200 Series Dual Frequency	Hydrocat 2	B
Sub-Bottom Profiler	Innomar SES-2000 Standard	Hydrocat 2	B
USBL	Sonardyne Scout PRO	Hydrocat 2	B
Grab Sampler	Van Veen Grab	Hydrocat 2	B
Navigation and Acquisition software	NaviPac, NaviScan, SESWIN	Rambunctious	B
Primary GPS and IMU	Trimble SP852	Rambunctious	B
Secondary GPS	Norbit iWBMSh with integrated Applanix OceanMaster	Rambunctious	B
Multibeam Echosounder	Norbit iWBMSh	Rambunctious	B
Sub-Bottom Profiler	Innomar SES-200 Standard	Rambunctious	B
SVP	AML Minos X	Rambunctious	B
Navigation and Acquisition software	Applanix MMS, RiProcess	Cessna Skymaster	B
GPS	Applanix POSAV 150	Cessna Skymaster	B
IMU	OxTS Inertial+	Cessna Skymaster	B
Laser Scanner	Riegl VQ480i	Cessna Skymaster	B
Camera	Hasselblad A6D, HC50 II	Cessna Skymaster	B

3.2 Geotechnical equipment

The geotechnical investigations (WP C) were performed by Glomar Vantage seen in Figure 3-6. Equipment and vessel specifications can be found in Appendix 5.

Figure 3-6 Geotechnical vessel, "Glomar Vantage"

The equipment used for the geotechnical investigation is listed below in Table 3-2.

Table 3-2: Geotechnical Equipment Spread

Equipment	Type
Navigation software	QINSy
Primary GNSS	Trimble BX992
CPT unit	RONSON 100
Vibrocore unit	VKG 3-6-9
USBL	Sonardyne Ranger PRO

3.3 Instrument calibration

3.3.1 Geophysical Survey Campaign

The instrument calibration was performed for all vessels before commencement. The Acceptance Test Reports are enclosed in Appendix 6 for WP A and WP B.

List of Acceptance Test Reports

1) WP A – Mintaka I
2) WP B - Hydrocat
3) WP B - Hydrocat 2
4) WP B - Rambunctious and Cessna Skymaster
5) WP C – Glomar Vantage

3.4 Accuracy and estimates of spatial uncertainty

The accuracy of the different equipment is tested in the Acceptance Test Reports. The uncertainties can be seen in Table 3-3. More detailed information can be seen in Appendix 6 which contains Acceptance Test Reports for WP A, B and C.

Table 3-3: Uncertainties for the different sensors for WP A and B found during the acceptance test.

Equipment	Easting [m]	Northing [m]	Depth [m]
SSS (Mintaka I)	0.48	1.11	n/a
SBP (Mintaka I)	0.05	0.05	n/a
MBES (Mintaka I)	0.05	0.05	0.08
MAG (Mintaka I)	0.63	0.52	n/a
SSS (Hydrocat 2)	1.97	0.38	n/a
SBP (Hydrocat 2)	1.06	0.27	n/a
MBES (Hydrocat)	0.006	0.005	0.02
MAG (Hydrocat)	0.76	0.94	n/a
MBES (Rambunctious)	0.02	0.02	0.018
SBP (Rambunctious)	0.91	0.70	n/a
Lidar Mapping	0.003	0.001	0.005

The accuracy of the MBES is tested by multiple runs with differences less than 10 cm.

Afterwards the towed equipment position was validated by different runs in the same and in different directions above a suitable object which showed differences in position of less than 2 m.

The accuracy depends on the combined uncertainties of all elements in the process. E.g. the accuracy of the bathymetry is affected by the combined uncertainties of the following processes: i) height of reference position of vessel by GNSS RTK ii) roll and pitch of vessel by motion sensor iii) vector from reference point to multibeam transponder iv) mounting angles of multibeam transponder v) timing accuracy in the combination of position, angles and data stream from transponder.

Uncertainties can be estimated a-priori by calculating Total Propagated Error, TPE. The contributions from the separate processes are combined based on an assumption of uncorrelated and normal distributed errors. A-posterior estimates are derived for the DGNSS positioning and the bathymetry.

Besides the instrumental uncertainty results are affected by the natural variability of the seabed; few surfaces in nature are smooth. The representation of this natural variability must be added to the instrumental uncertainty.

In the following all references to error, uncertainty or accuracy are by the value of two times the standard deviation. Error contributions from various sensors and processes are shown in Table 3-4.

Table 3-4: Bathy error contributions from separate sensors and processes

System	Vertical error	Horizontal error	Source
GPS Positioning	0.02 m	0.02 m	Estimate
Gyro heading		$0.02° \rightarrow r^{1)} \times tan(0.02°)$	Specifications
Motion sensor	$0.01° \rightarrow r \times tan(0.01°)$	$0.01° \rightarrow r \times tan(0.01°)$	Specifications
Echosounder transducer	0.01 m		Estimate
Pole movement	0.05 m	0.05 m	Estimate

1) *r denotes radial distance to bespoken sensor*

By combination of the above separate error contributions the total propagated error, TPE, can be estimated for the resulting data products: The bathymetry, the sonar gram etc. Calculated Total Propagated Error is presented in Table 3-5. The calculation assumes each error source independent and normally distributed. Thus, the variance of the sum of the error distributions equals the sum of the variances: $\sigma_{\sum i^2} = \sum \sigma_i^2$.

Table 3-5: Calculated TPE for the bathymetry

Data type	Vertical TPE	Horizontal TPE
Bathymetry (Mintaka I)	0.088	0.052
Bathymetry (Hydrocat)	0.076	0.034
Bathymetry (Rambunctious)	0.084	0.029

In addition to the theoretical calculation of the obtainable accuracy it is important to observe the fact the any acoustic ranging to the seabed has a certain acoustic 'foot print' on the seabed and the result of the measurement depends in a complicated way of the average within this foot print. For this reason, there is a lower limit to the accuracy of acoustic ranging. This is estimated to be comparable to the short-scale roughness of the seabed.

4. SURVEY DETAILS

4.1 Survey blocks

During the survey the corridor which represents the Hessel Export Cable Route is divided into twelve block during the data acquisition of WP A and WP B in order to optimise data acquisition and post-processing. The cable route is divided into the following blocks ranging from GL01 to GL12 where GL01 is the block closest to the landfall at Gilleleje. GL01 consist of data acquired by Hydrocat, Hydrocat 2, Rambunctious and onshore lidar mapping. The remaining blocks (GL02 to GL12) are acquired by Mintaka I.

In Figure 4-1 the twelve survey blocks can be seen.

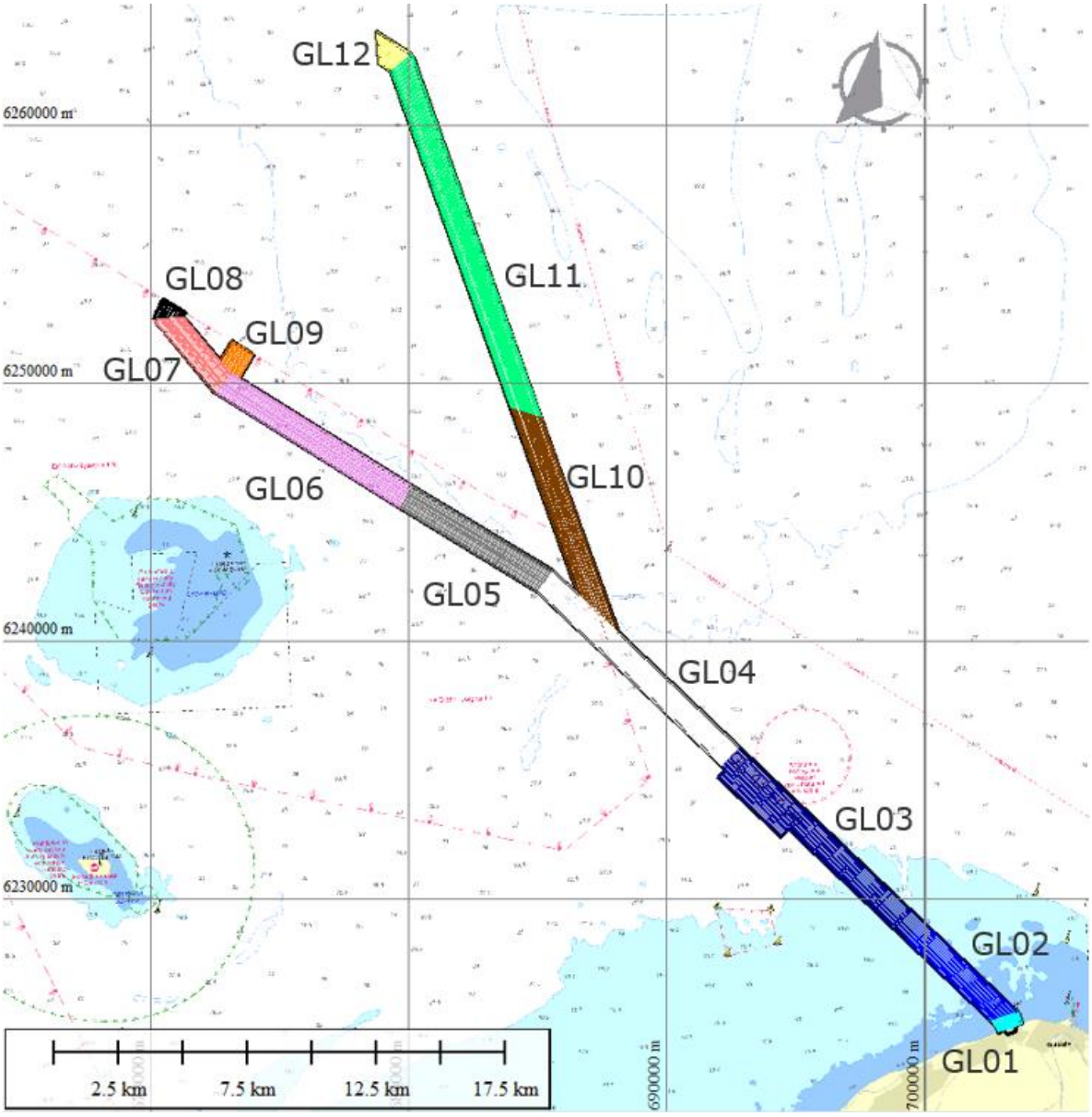

Figure 4-1: Overview of the survey corridor divided into survey blocks with the main line

The below Table 4-1 shows the twelve-survey blocks together with start and end KP for each block.

Table 4-1 Lists the survey blocks and their start and end KP values

Survey blocks	Start KP	End KP
GL01	0.06	0.67
GL02	0.67	5.54
GL03	5.54	15.36
GL04	15.36	25.02
GL05	25.02	31.52
GL06	31.52	39.73
GL07	39.73	43.04
GL08	43.04	43.54
GL09	39.73	41.39
GL10	22.74	31.32
GL11	31.32	45.48
GL12	45.48	46.66

4.2 Survey lines

Lines are planned to ensure 100% MBES coverage and 200% SSS coverage inside the provided survey polygon "SN2020_032_SURVEYS_POL". Also, survey lines are planned to be parallel to the provided RPL "REV_03_2020-10-30_NHW". The RPL includes KP values going form KP 0 at the landfall part to KP 52 along the eastern going arm and to KP 43.96 along the western going arm. The RPL can be found in Appendix 7.

Table 4-2 shows the planned line spacing for WP A and WP B which also were achieved during acquisition.

Table 4-2: Shows the linespacing used during data acquisition for WP A and WP B

	MBES	MAG	SSS	SBP
GL01 (Rambunctious)	11m	n/a	n/a	20m
GL01 (Hydrocat & Hydrocat 2)	15m to 25m	20m	15m to 45m	45m
GL02 to GL12 (Mintaka)	45m	45m	45m	45m

All data was QC'd online and checked on daily basis to ensure quality and coverage. If sufficient quality or coverage wasn't achieved infill lines was planned. Infill lines was in most cases caused by:

1) SSS data below 200% coverage due to thermoclines
2) MBES data below 100% coverage – only for nearshore surveys due to shallow water
3) RTK drops-outs mostly offshore near the windfarm site

Table 4-3 shows the accumulated acquired survey line kilometres for each sensor during WP A and WP B including infill lines. Also, the quantity of Grab samples, CPT and vibrocores are listed.

Table 4-3 Accumulated line kilometres per sensor incl. infill

Geophysical survey	Total line kilometres
MBES	1929 km
MAG [1)]	3531 km
SSS	1864 km
SBP	1822 km
Geotechnical Investigation	**Quantity**
Grab Samples [2)]	55 (5)
CPT	60
Vibrocores	60

[1)]The MAG survey consists of two magnetometers and the total line kilometres are for all
[2)]The number in parenthesis is the number of empty grabs samples which is excluded from total numbers, 55

4.3 Acquired data quality

4.3.1 MBES

In general, the acquired MBES data from all three vessels are of good quality. With a density of at least 18-21 pings/m^2 and a standard deviation that does not exceed 0.30. The TVU and THU are in most blocks within IHO special order specifications which means the THU is below 2.0m and TVU is below 0.34m for 30m water depths and below 0.26 for 10m water depths. However, in some cases both the THU and TVU exceeds 2.0m. The reason for this is due to dropouts in the RTK signal this includes only smaller areas and how these minor dropouts are fixed during MBES processing is described further in section 6.1.

Figure 4-2 and 4-3 shows the TVU and THU grid along the corridor.

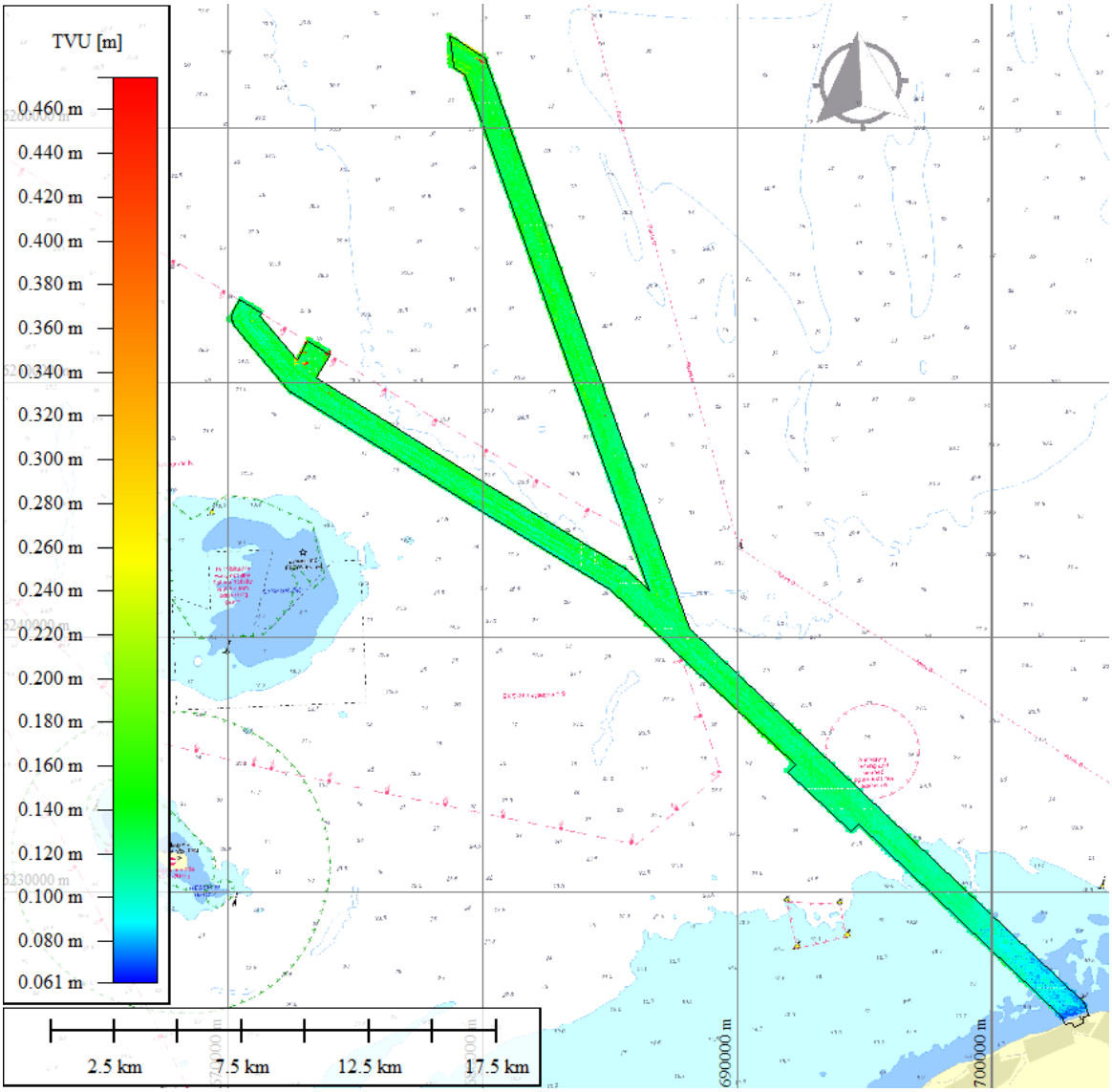

Figure 4-2 TVU along the cable route

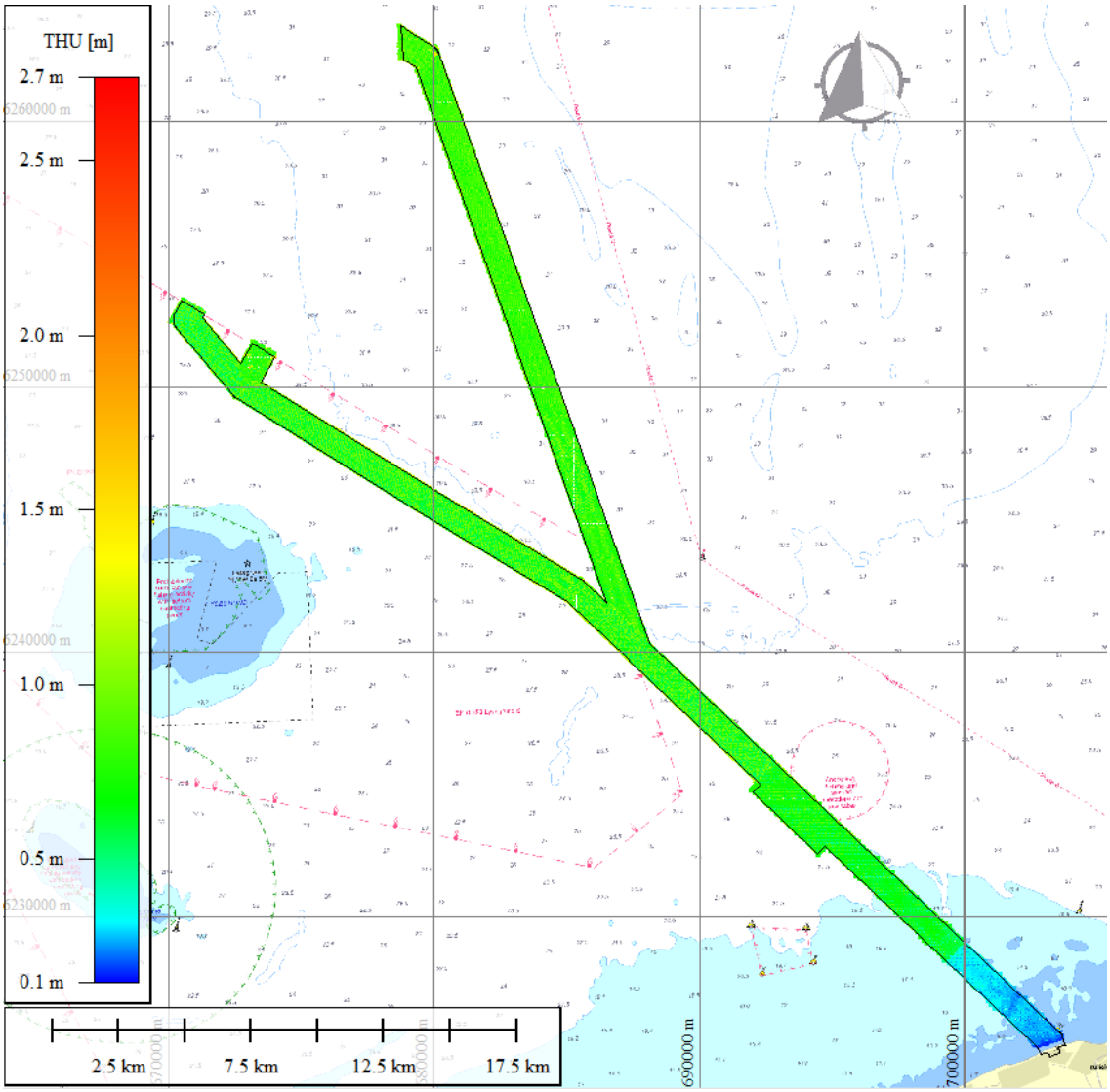

Figure 4-3 THU along the cable route

In block GL02 to GL03 small empty pixels of 25cm in size are sporadically distributed without data, seen in Figure 4-4. The reason is that in the dense boulder fields and larger boulders will cast a shadow behind the boulder compared to the MBES transducer head on the outer beams even if the density of 16 pings/m^2 are met. These small pixels are only visible in the 25cm average grid.

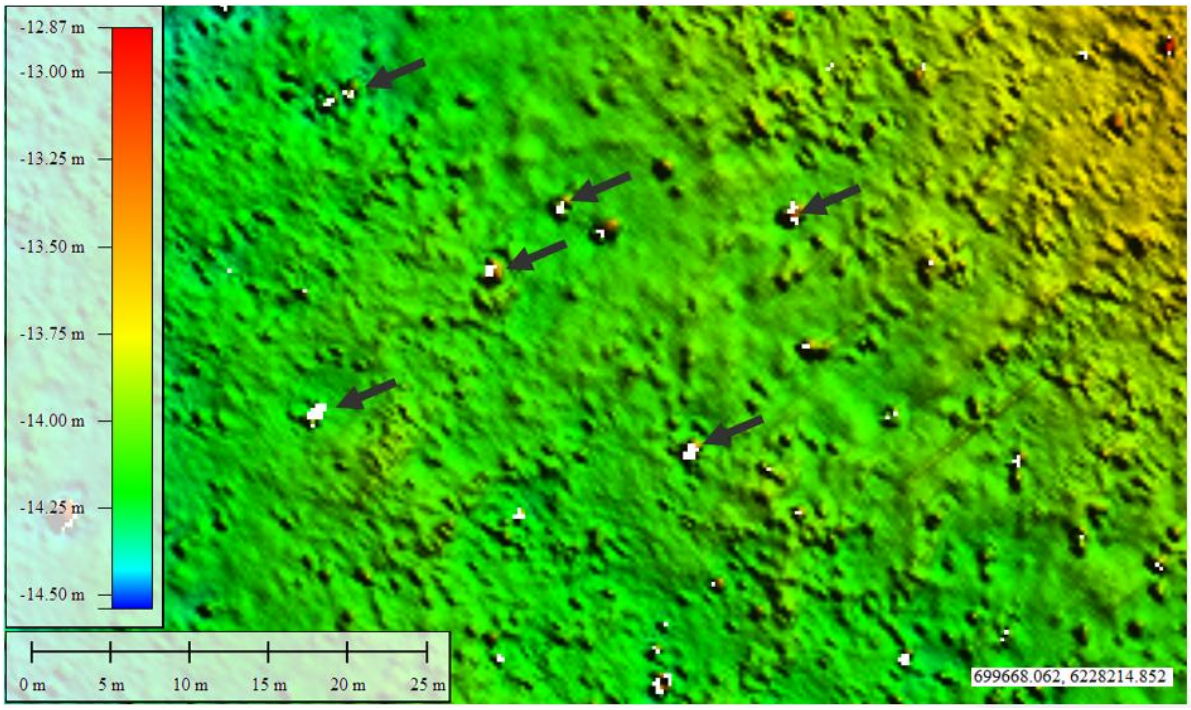

Figure 4-4: Minor pixels in the average 25 cm grid without data due to shadow effects caused by the dense boulder fields. Arrows indicates places with these minor pixels of 25cm in size.

Backscatter data was in general of good quality which supported the SSS data very well during the data interpretation. The Backscatter data was acquired using a time series mode and SSS mode where the intensities are well normalized between the three survey vessels. Only due to the data density the nadir in some areas is still visible and is not fully normalized but this doesn't interrupt any seabed interpretation, can be seen in Figure 4-5. Also, when comparing with the SSS data the different seabed changes can be followed clearly on both sensors as seen in Figure 4-6.

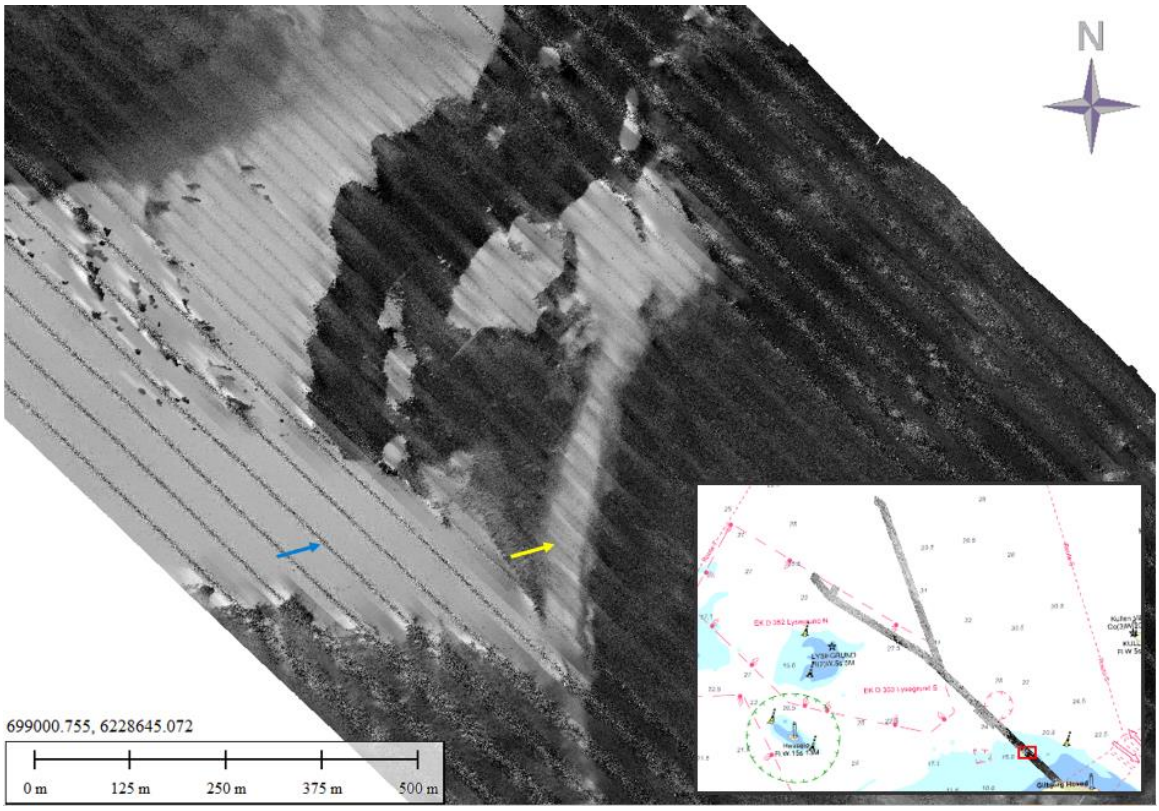

Figure 4-5 Example of the backscatter quality. Yellow arrow indicates area with high density data where the nadirs almost are normalized and the blue arrow indicates area with a little less data density where the nadirs are not fully normalized.

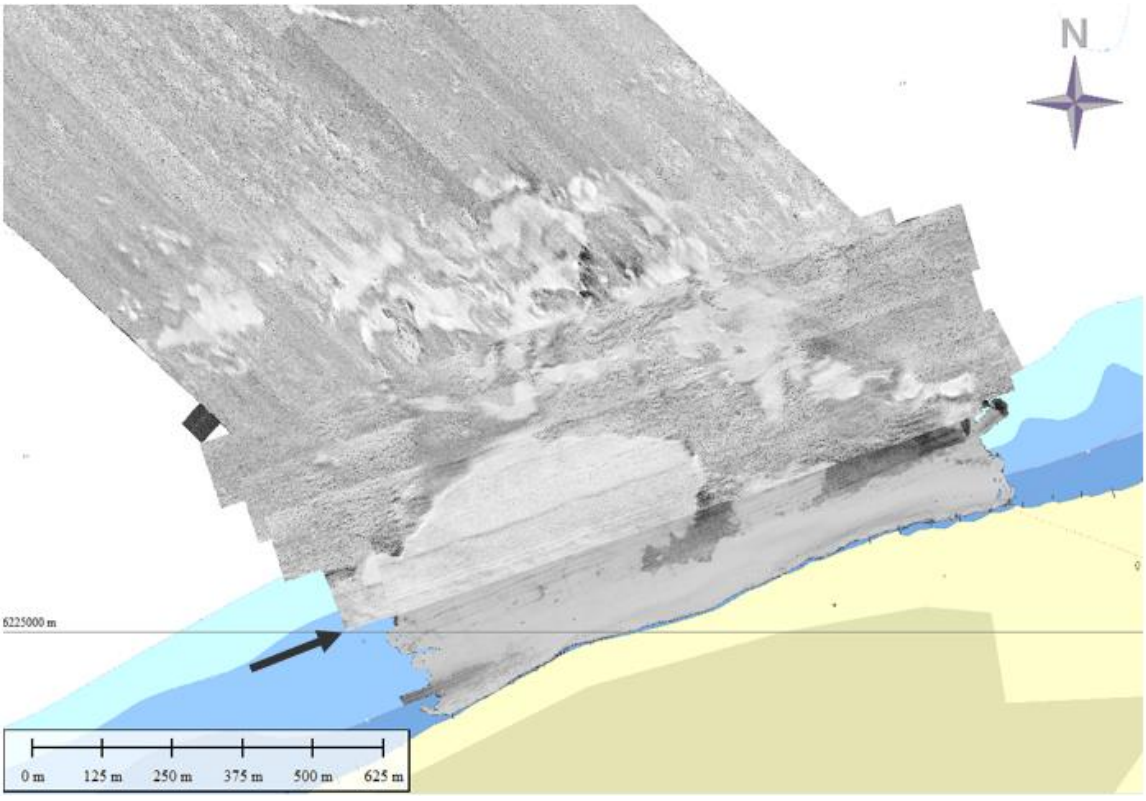

Figure 4-6 An example of the nearshore backscatter data beneath the SSS LF mosaic. The arrow indicates the transition from SSS data to backscatter data.

4.3.2 SSS

The data quality of the SSS data was good and it was possible to resolute objects down to 0.5m in size along the smallest axis, even smaller objects can be identified from the SSS data. Also,

the acquired SSS data correspond across the different survey lines, shown in Figure 4-7 where trawl marks correlates well across the different lines.

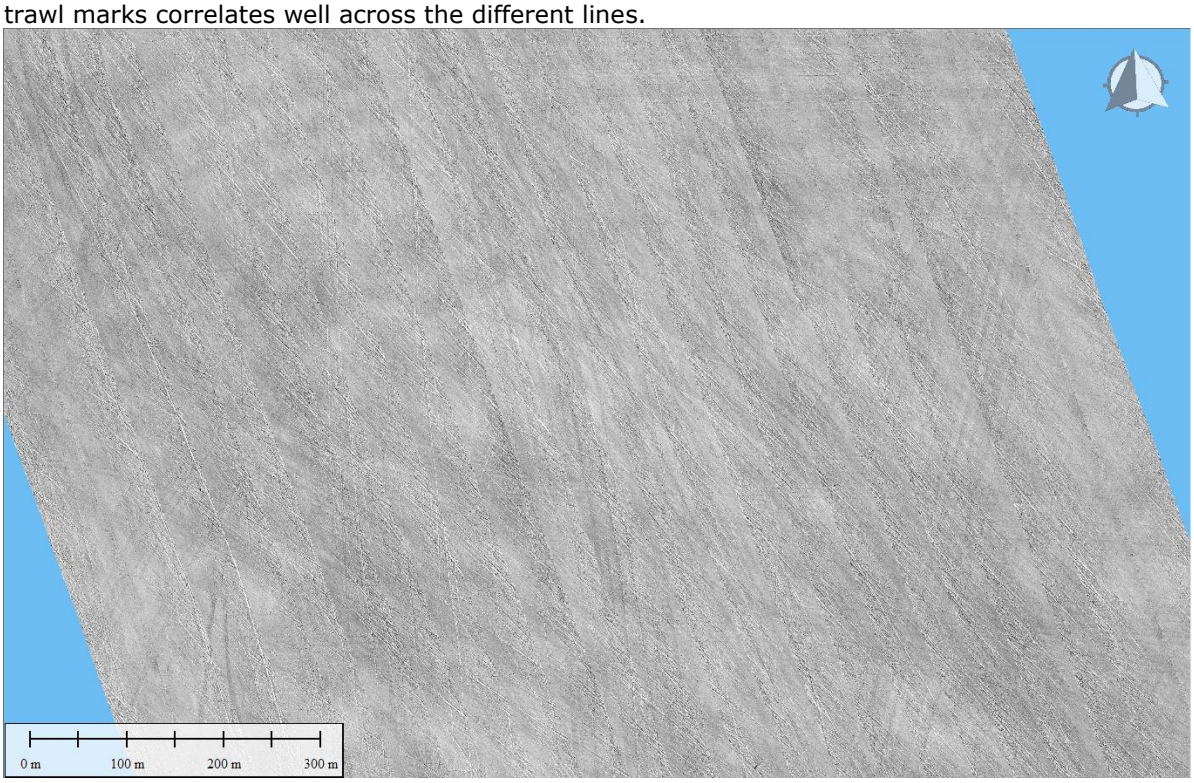

Figure 4-7: Image of SSS HF 0.2m mosaics where trawls correspond well across the acquired survey lines – in block GL10.

When comparing the mosaics with the MBES data the two datatypes also correlate well, seen in Figure 4-8. In some cases, there is an offset of approx. 2m which is expected as the MBES is acquired and processed using RTK signal whereas the SSS data positioning is derived from the USBL system.

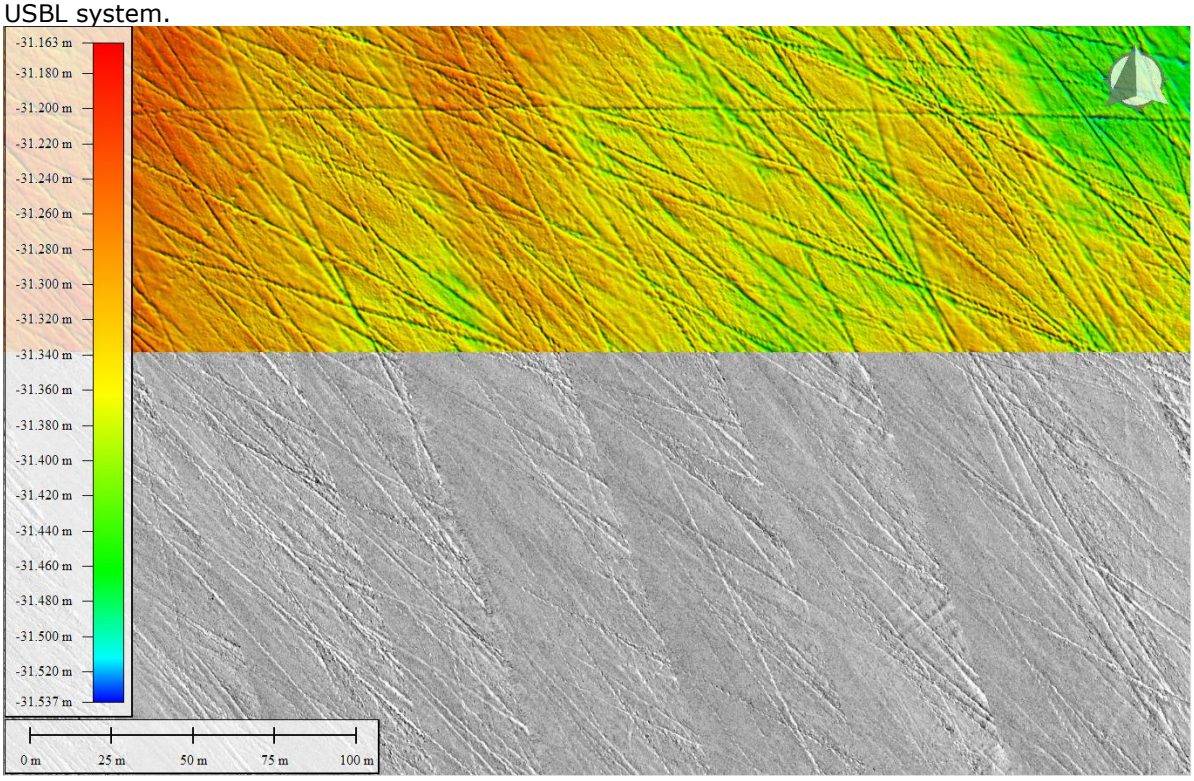

Figure 4-8: Shows the correlation between the SSS data and MBES data in block GL10 using trawl marks.

Thermocline effects are almost removed from the mosaics using the cover-up method. There are few cases nearshore in block GL02 and GL03 where thermoclines are not fully covered. This counts only for minor areas in the nearshore parts and are not affecting the use of the data. See Figure 4-9 for examples of minor thermocline effects in GL02.

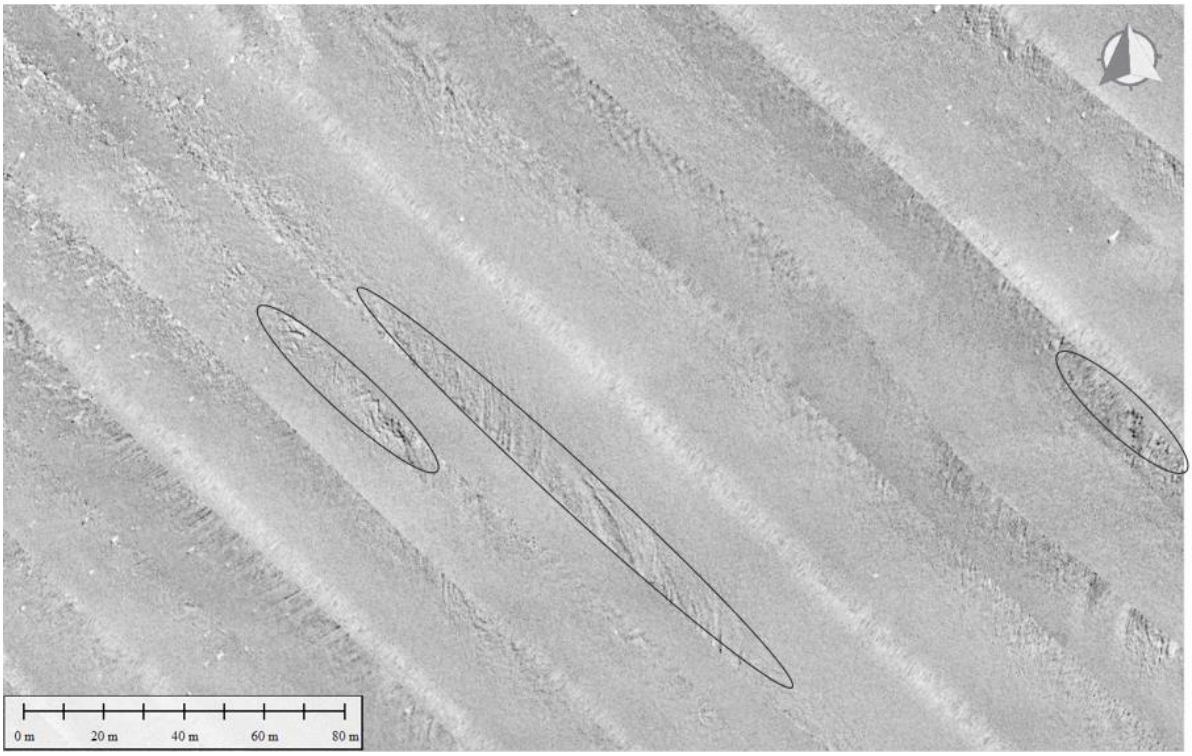

Figure 4-9: Shows a block of GL02 where some thermoclines are not covered up in the HF mosaics.

4.3.3 MAG

Only few lines where resurveyed due to too high altitude or low signal strength (altitude above 5m and signal strength lower then approx. 400). In cases where boulder fields are very dense such as in block GL02 and GL03 the magnetic data can be a bit noisy and create magnetic responses in the total field, as seen in Figure 4-10. These magnetic responses are related to the boulders and most likely not related to any metallic objects. The noise is especially evident when the boulders are observed as ridges crossing the survey corridor. In these areas the noise ratio is calculated to help identifying real signal and potential noise.

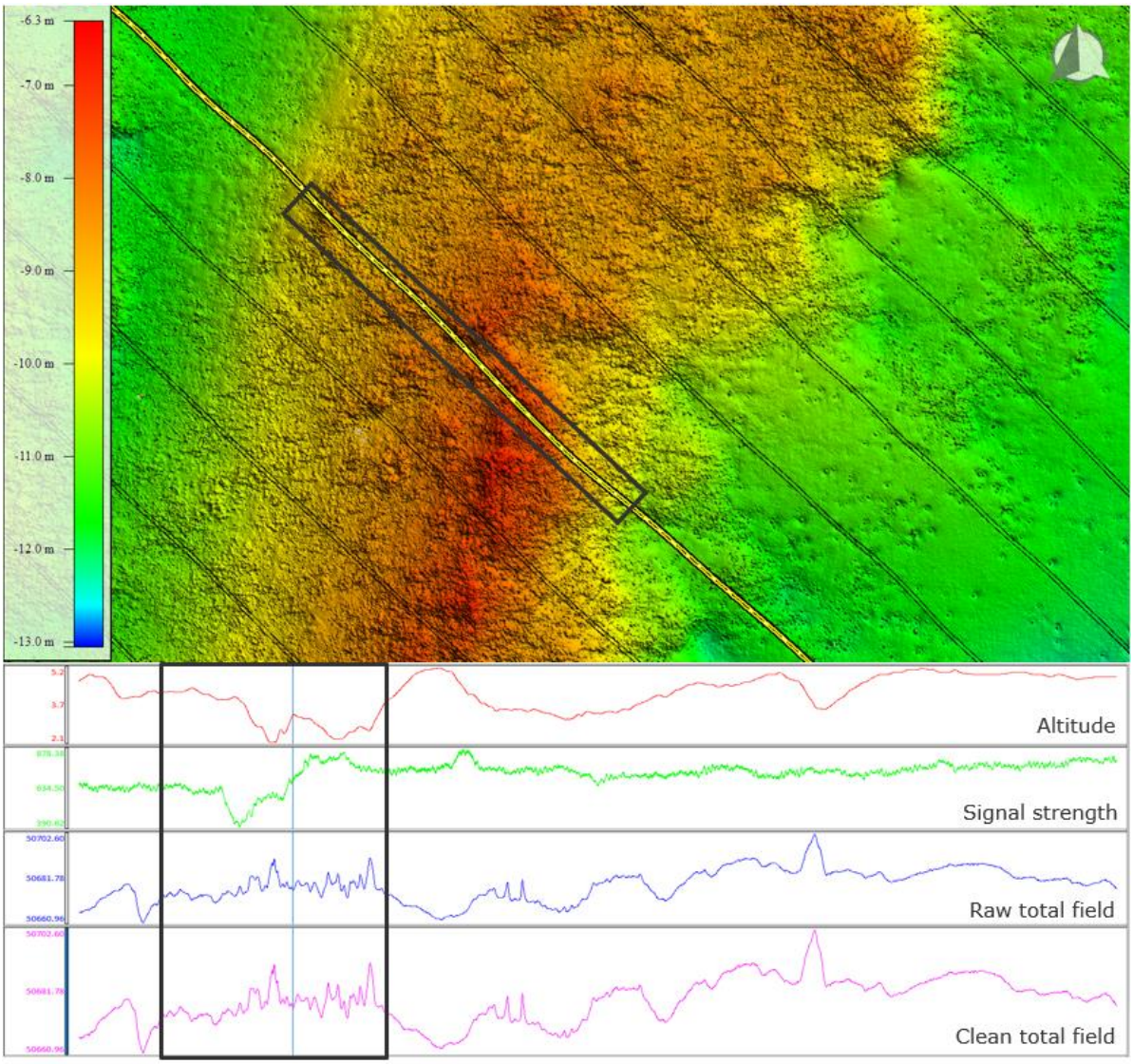

Figure 4-10: Example of how the noise looks like when boulder ridges are crossing the survey corridor and thereby making a response in the magnetic field. The boxes are highlighting the noisy interval.

4.3.4 SBP

The SBP data acquired within the cable corridor has generally very good quality and the depth of interest of minimum 10m has been achieved within entire survey area- except at locations where glacial tills are found close to the seabed. This is due to the fact, that the penetration depth of pinger SBP systems is highly dependent on the local geological conditions. Signal penetration is limited in hard sediments such as tills as well in coarse or highly compacted sands, due to scattering. However, presence of glacial deposits close to the seabed is limited to the southernmost part of the cable corridor and based on understanding of regional and local geological conditions it can be assumed that the lower boundary of the glacial deposits is found below the investigation depth. Figure 4-11-shows variations in penetration depth of SBP data depending on the subsurface conditions along the survey line 20085_MTK_GL_03_C000_SES_20201024_103720_RAW_LF.

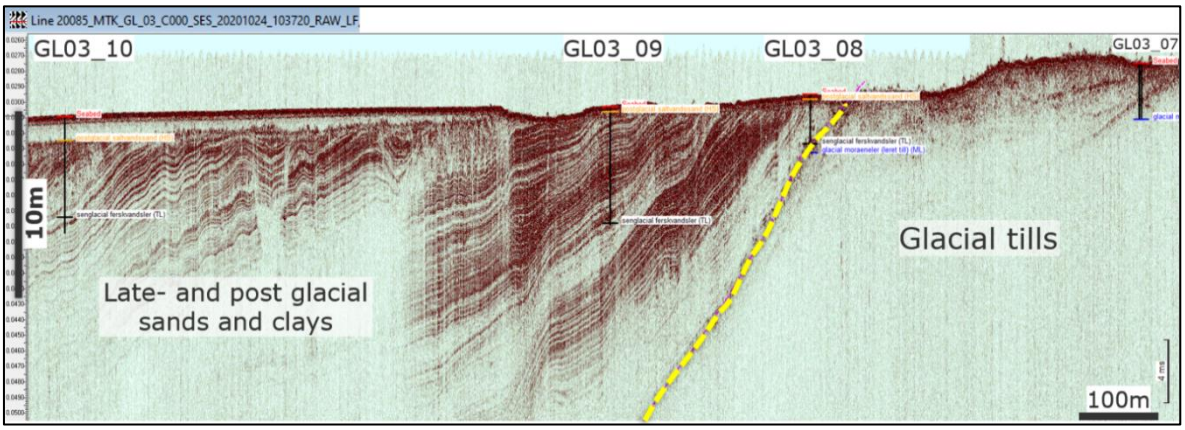

Figure 4-11 Penetration depth of SBP data, an example line 20085_MTK_GL_03_C000_SES_20201024_ _103720_RAW_LF. Penetration depth varies from a few meters within glacial till deposits to more than 20 meters within the very fine grained Late Glacial and Post Glacial units.

The seismic resolution has been evaluated for the SBP-data. The dominant frequency is approx. 8kHz (see amplitude spectrum for a representative survey line 20085_MTK_GL_04_R045_SES_ _20201024_070921_RAW_LF) on the Figure 4-12). With an average velocity of 1600 m/s, the theoretical vertical seismic resolution (λ/4) is ~0.05m. The horizontal resolution is estimated to be better that 1m (approx. ~1m at depth of 10 m below seabed).

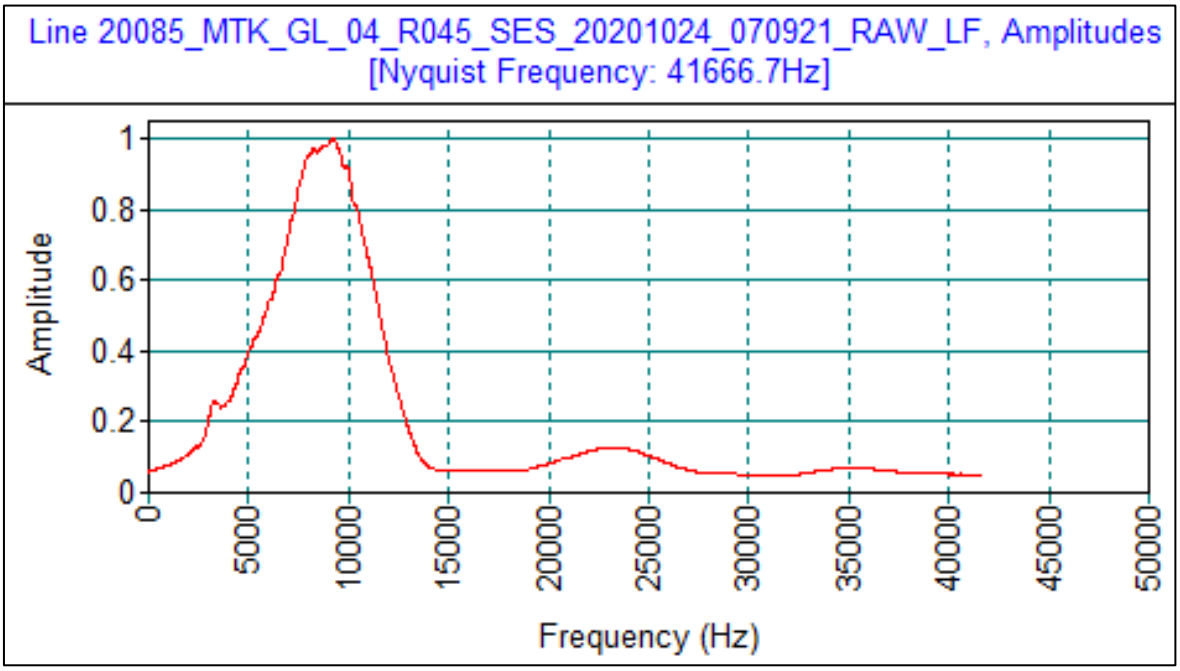

Figure 4-12 Amplitude spectrum for the acquired pinger data showing a dominant frequency of approx. 8 kHz (profile 20085_MTK_GL_04_R045_SES_20201024_070921_RAW_LF).

4.3.5 Lidar

The Lidar data are compared up against the benchmarks and extra control points as described in section 3.4, 5.2 and Appendix 6. The accuracy is within a few millimetres both in X, Y and Z. The point density is not below 20 points/m^2, see Figure 4-13, except for the offshore part but these points will however be rejected when making the terrain model. The standard deviation ranges from 0.01m to 0.16m, the largest standard deviation is related to the steep cliff, buildings and vegetation as expected. The standard deviation can be seen in Figure 4-13.

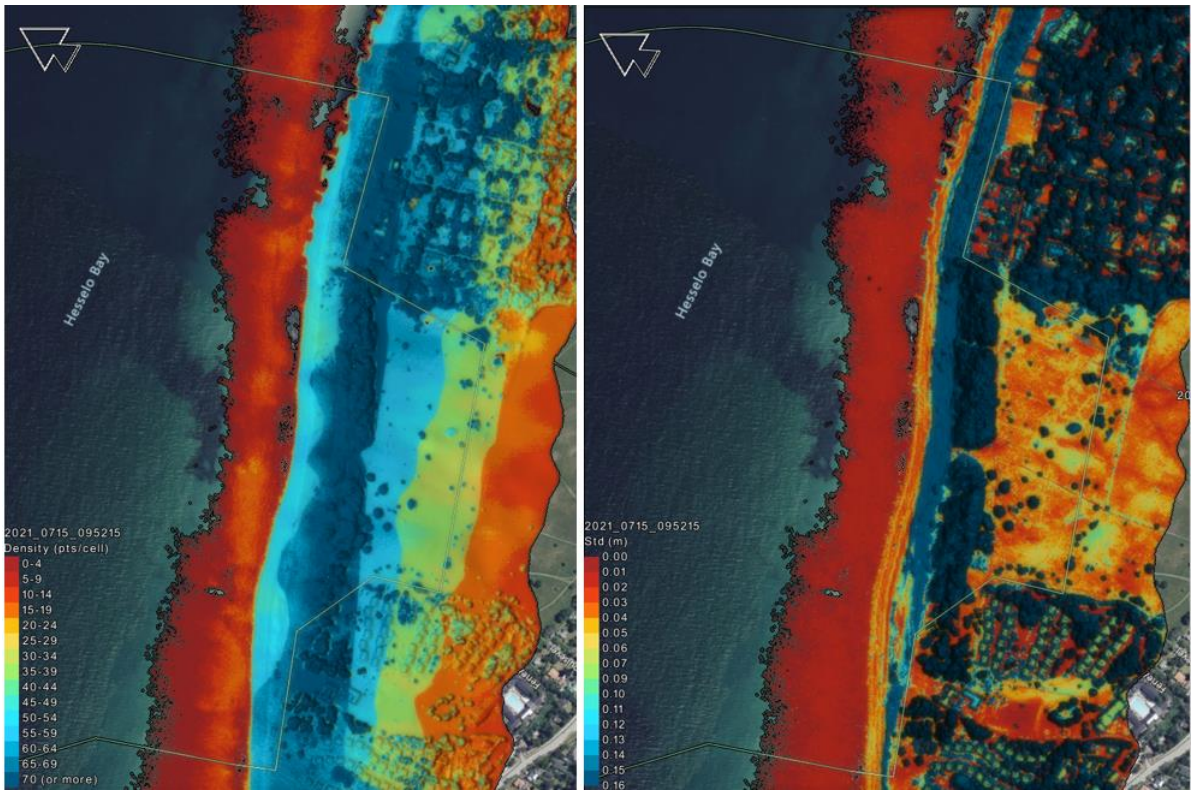

Figure 4-13 Lidar data quality. Left image shows the ping density inside the survey area. Right image shows the standard deviation inside the survey area

5. DATA ACQUISITION

5.1 Survey summary

An overview of the different survey dates is listed in Table 5-1.

Table 5-1 Timeline for the survey, the dates do not include mobilisation and calibration

Task	Periode
WP A	23.10.2020 to 14.11.2020
WP B (Hydrocat)	23.10.2020 to 03.11.2020
WP B (Hydrocat 2)	24.10.2020 to 07.11.2020
WP B (Rambunctious)	26.10.2020 to 30.10.2020
WP B (Lidar Mapping)	15.11.2020 to 15.11.2020
WP C	06.11.2020 to 02.12.2020

5.2 Reference system and positioning

The coordinate reference system is shown in Table 5-2.

Table 5-2: Geodetic parameters for the geophysical data acquisition

Ellipsoid	Parameters
Horizontal Datum	ETRS89
Vertical Reference	DTU18
Spheroid	GRS 1980
Semi-Major Axis	6378137.000
Semi-Minor Axis	6356752.314140
Flattening Factor of the Earth	1/f = 298.257222101
Prime Meridian	Greenwich
Projection parameters	**UTM**
Projection	Universal Transverse Mercator
UTM Zone	UTM 32N
Scale Factor	0.9996
False Northing	0.00 m
False Easting	500 000 m

The positioning is acquired with RTK GPS utilising real-time corrections on all vessels. The GPS data were recorded in the EIVA software "NaviPac" or QINSy which calculated the offset coordinates of the sensors on board the vessel. Furthermore, Sonardyne USBL Scout Plus' system was used to measure the towed equipment such as the Scanfish and TVG frame. At the same time the quality and accuracy of the coordinates could be monitored.

Navigation data from the processing instruments were received by the central navigation computer and applied to the survey with the software package QINSy and NaviPac. During the survey, all navigation data were recorded at 10 Hz rate. Accurate positions and heights for all sensors were calculated and corrections for roll, pitch, and heave at any sensor location were applied during all survey operations. Position and corrections were stored every second.

All bathymetric measurements have been using DGPS RTK system in reliable height mode allowing for direct conversion of echosounder data into depths related to ETRS89 datum.

At the quayside at Hundested Harbour an independent RTK base station (Triumph LS) was established to confirm geodesy parameters. These base stations were used for static check by Mintaka I, Hydrocat and Hydrocat 2. The results can be seen in Table 5-3 to 5-5.

Table 5-3: Verification of Primary GPS for Mintaka I

Measured by	X	Y	Z
Triumph LS	677757.12	6205268.80	40.984
Mintaka I	677757.23	6205268.70	40.983
Standard deviation	0.11	0.10	0.001

Table 5-4: Verification of Primary GPS for Hydrocat 2

Measured by	X	Y	Z
Triumph LS	677769.61	6205666.33	38.632
Hydrocat 2	677769.63	6205666.34	38.646
Standard deviation	0.02	0.01	0.014

Table 5-5: Verification of Primary GPS for Hydrocat

Measured by	X	Y	Z
Triumph LS	677765.69	6205658.80	4.06
Hydrocat	677764.60	6205658.53	3.79
Standard deviation	1.09	0.27	0.26

Whereas another RTK base stations were set up at Ramboll workshop, Helseholmen. Table 5-6 shows the results of the fixpoint for verification of positioning for Rambunctious.

Table 5-6: Verification of Primary GPS for Rambunctious

Measured by	X	Y	Z
Base station (Ramboll)	717812.843	6167763.849	36.496
Rambunctious	717812.847	6167763.867	36.498
Standard deviation	0.004	0.018	0.002

For the airborne lidar survey five control points were established with an GPS antenna to ensure highest accuracy of the acquired data from the airborne mapping. The points were established in areas where full data coverage was achieved. Table 5-7 shows the control points for verification of the lidar data.

Table 5-7: Control points for verification of airborne lidar data

Measured by	X	Y	Z
ALM-1	702679,9	6224593	9,145
ALM-2	702680,1	6224594	9,110
ALM-3	702680,4	6224593	9,147
ALM-4	702680,8	6224591	9,134
ALM-5	702688,8	6224591	9,198

After data acquisition the control points were compared with the final processed Lidar data. The differences between control points and data can be seen in Table 5-8.

Table 5-8: Shows the error between the measured control points and the acquired lidar data

Measured by	X Error [mm]	Y Error [mm]	Z Error [mm]
ALM-1	-3,96	-0,46	4,14
ALM-2	3,53	1,50	4,62
ALM-3	0,43	-0,57	2,86
ALM-4	-0,49	1,13	5,26
ALM-5	-3,20	-1,62	5,82

5.3 Multibeam echosounder (MBES)

Mintaka I & Hydrocat

The bathymetric data were acquired using a Reson SeaBat T50 mounted both Mintaka I and Hydrocat. The T50 system allow normalized backscatter designed for seabed classification and multiple detections for increased target details which was recorded in QINSy. The Backscatter were acquired in time-series mode and embedded in the raw *.db files as intensities. This Reson T50 MBES is capable to form up to 999 beams with a swathe of up to 150° when using the equi distant mode. Combined with its capacity to operate in a frequency range of 200-400 kHz, this system offers state of the art vertical and spatial resolution in the water depth encountered in the working area. For the project the frequencies were between 340kHz and 400kHz depending on water depth in order to optimize data quality with a ping rate up to 50 pings/s.

Data coverage, grid cell sounding hit count and standard deviation was monitored online during the survey. The multibeam data were recorded using QPS QINSy acquisition software, which made it possible to display the recorded DTM online for efficient quality control. Also, during the survey point clouds and DTMs were exported for QC.

Rambunctious

The bathymetric data were acquired using a Norbit iWBMSh mounted on the starboard side on Rambunctious. This system allows normalized backscatter designed for seabed classification and multiple detections for increased target details. The Backscatter were acquired in both Side Scan mode and snippets mode and stored in the raw MBES *.SBD files as intensities. This Norbit iWBMSh MBES is capable to form up to 512 beams and guarantees a swath coverage of up to 210°. Combined with its capacity to operate in a frequency range of 200-700 kHz, this system offers state of the art vertical and spatial resolution in the water depth encountered in the working area.

Also, the acquired MBES from Rambunctious was online QC'd and monitored as for Mintaka I and Hydrocat. The data was on daily basis send to office for further QC before demobilization.

5.4 Side Scan Sonar (SSS)

Mintaka I

The side scan sonar recording was carried out using a towed EdgeTech 4205 side scan sonar recording at low frequency of 300kHz and high frequency of 600kHz. The side scan fish was towed after the vessel and positioning was derived from the USBL system. The range was set to 50m and the depth of towing was approx. 4-6m above seabed. The resolution along track for the high frequency channel is 0.45m whereas for the low frequency channel the along track resolution is 1.0m. The across track resolution is 1.5cm for high frequency and 3cm for low frequency. All data was recorded using Discovery and data was stored as *.xtf and *.jsf format for later processing.

Data was daily exported and QC'd for positioning, thermocline effects, coverage etc. in SonarWiz.

Hydrocat 2

The side scan sonar recording was carried out using a towed EdgeTech 4200 side scan sonar recording at low frequency of 300kHz and high frequency of 600kHz. The side scan fish was towed after the vessel and positioning was derived using manual layback. The range was set to 50m and the depth of towing was approx. 4-6m above seabed. The resolution along track for the high frequency channel is 0.45m whereas for the low frequency channel the along track resolution is 1.0m. The across track resolution is 1.5cm for high frequency and 3cm for low frequency. All data was recorded using Discovery and data was stored as *.xtf and *.jsf format for later processing.

Data was daily exported and QC'd for positioning, thermocline effects, coverage etc. in SonarWiz.

5.5 Sub Bottom Profiler (SBP)

Mintaka I, Hydrocat 2 & Rambunctious

The seismic data were recorded using a pole mounted Innomar SES2000 Standard (SBP). The acquisition frequency of 8 kHz was assessed to produce best results in terms of penetration and resolution. The Innomar's was roll, pitch and heading compensated and was able to work with a ping rate of 60 pings/s. The data were recorded using the Innomar SESWIN control software. Data were uploaded on daily basis for onshore QC as well as quality controlled on the vessel during acquisition to ensure best possible range settings and optimize record length/recording window required penetration and expected seabed morphology. Delay/start time was adjusted to accommodate water depth without compromising vertical resolution in recorded data.

5.6 Magnetometer (MAG)

Mintaka I & Hydrocat

The magnetic survey was performed with two G-882 magnetometers Caesium vapor with depth and altimeter sensors using a Scanfish and later these was attached to a TVG frame. The sample rate during acquisition was set to 10hz which corresponds to a measurement distance of 0.15 - 0.2 m along the lines depending on the survey speed. The noise level during the acquisition was below 1 nT. Maglog acquisition software was used for acquisition where altitude, depth, signal strength and raw total field readings was monitored. The inclination of the magnetometer sensor was calibrated using Geometrics CSAZ for the survey. The calibration showed the best results when applying an inclination angle of 45^{o}. The source was therefore adjusted to this angle. The depth Scale, Depth Bias, Altimeter Scale and Altimeter Bias factors were entered into Maglog to get reliable depth and altimeter values. This was hereafter tested against the multibeam measurements. The magnetometer setup can be seen in Figure 5-1.

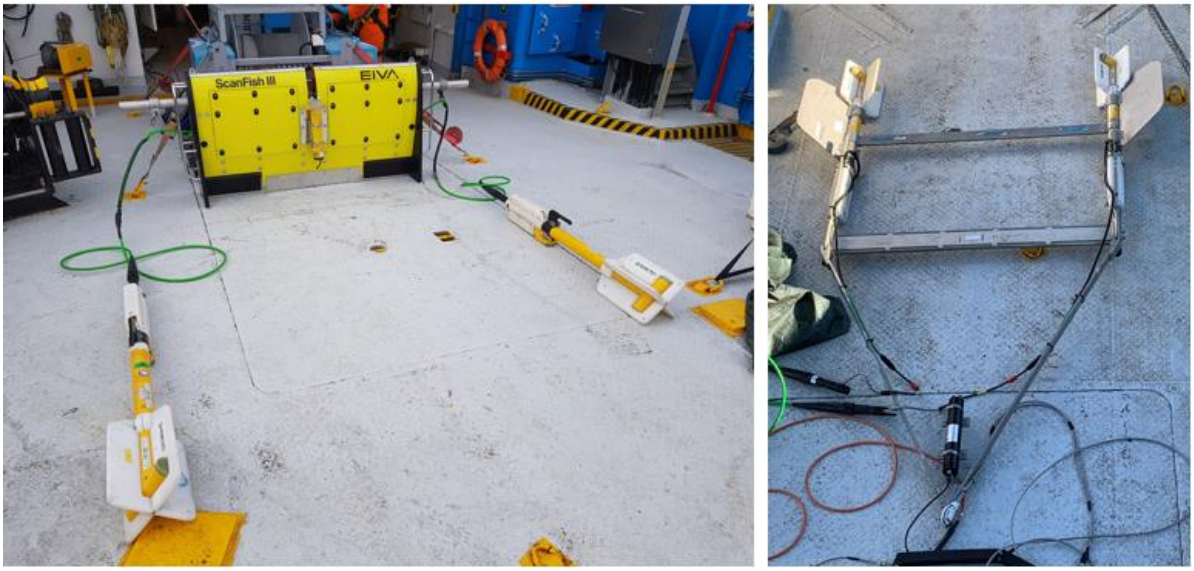

Figure 5-1: Magnetometer setup with two magnetometers on the Scanfish III from EIVA (left) and TVG frame (right) - the examples are from Mintaka I

5.7 Airborne lidar

Laser scanner

For this project a RIEGL VQ480i was used. This scanner has an operating frequency range of 50kHz to 550kHz using a laser wavelength near infrared. Since the operating flying altitude was 312m the frequency was set to 400kHz which means the effective measurement rate was approx. 200.000 measurements/s and with a scan speed of 10-150 scans/s this system allows highly dense and accurate measurements. During the survey the laser scanner was roll, pitch and yaw compensated. With an altitude of 312m and a speed of 70 knots will give a theoretical point density of 50 points/m^2 with this setup.

5.8 Geotechnical investigations

The geotechnical campaign (WP C) is more detailed described in the geotechnical data report – Appendix 1.

6. DESCRIPTION OF DATA PROCESSING

6.1 Multibeam

PosPac was used to process the data from the Applanix POS MV GNSS. This provides highly accurate position and orientation. Here the PP-RTX method is used which is a multi-frequency GNSS positioning technology that combines the high accuracy of reference stations based differential GNSS with the highly productive wide-area coverage of global satellite corrections. Once the navigation was processed the data were then exported as SBET files relative to ETRS89 datum. SBET contains all corrections for altitude, motion and navigation ready to be applied to the bathymetry data.

The multibeam bathymetric data were recorded using the software QINSy and were collected over several parallel run-lines along the cable route corridor. The lines were surveyed with an approximately overlap of 20 %. Besides the main survey lines, some additional infill lines were acquired to ensure full data coverage. The multibeam echosounder data acquired was of very high quality with very low noise. Processing of the raw multibeam echosounder data were performed using the software QPS Qimera and NaviEdit/NaviModel. The processing steps in Qimera comprise the application of sound velocity profiles, applying SBET and RTK correction and filtering of data. Sound velocity profiles were measured regularly during the survey and a linear temporal interpolation was made between each sound velocity profile. The data underwent a preliminary cleaning to remove significant outliers and then a filter was setup to remove erroneous points.

Finally, data were merged together in NaviModel and from here the point cloud soundings in XYZ format and the binned data with 0.25 m, and 1.0 m and 5 m grid cell size in XYZ format were exported. The exported XYZ files were loaded into GlobalMapper where GeoTiffs was generated with sufficient shading to highlight contacts and seabed variations.

The following software packages from QPS and EIVA were utilized to process the bathymetric datasets:

- Qimera – Project file manager and editing of overall survey parameters.
- NaviModel – 3D modelling for visualization and data deliverable generation.

In Figure 6-1 is shown a simplified workflow for the MBES processing.

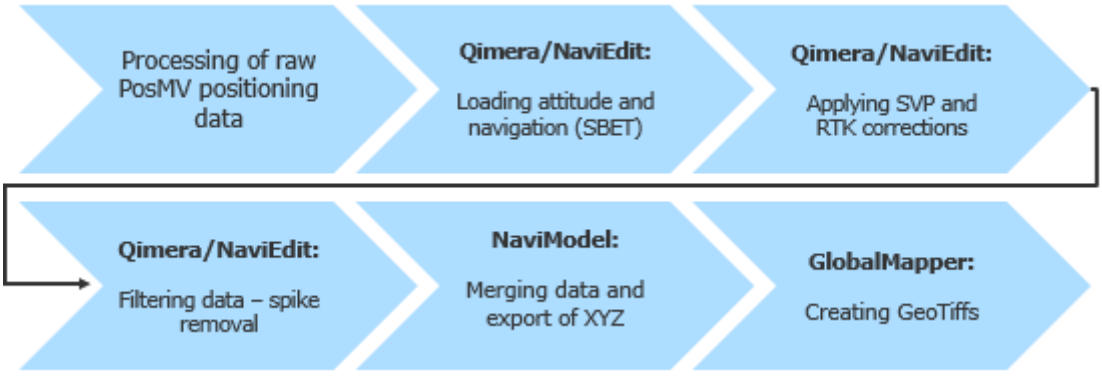

Figure 6-1: Workflow for MBES processing

In few cases the TVU and THU exceeded the IHO special order specifications. These peaks in THU/TVU are caused by lost RTK correction. However, if the RTK correction was lost over longer time the line was either resurveyed or infill was acquired later on. In some areas located offshore near the windfarm site the RTK correction was lost over short time. For these areas the following procedures has been made to improve data quality:

- Two filters were used to fit the area without RTK correction;

- Shift pings to neighbours: the selected track will be shifted to its neighbours by using the best fit algorithm – this applies only for tracks which have two overlapping neighbours.
- Shift pings to neighbours (Inspection Area): this algorithm does the same as above but just applies for pings inside a selected area.

The shifts are applied to the transducer height so the entire ping will be shifted vertically. This will not change the original transducer height the shifts will only be stored in the AutoClean files. In order to verify these corrections the same procedure was made in Qimera using the TU Delft function which do the same shift but using another algorithm. The results from the ping corrections can be seen in Figure 6-2 and 6-3.

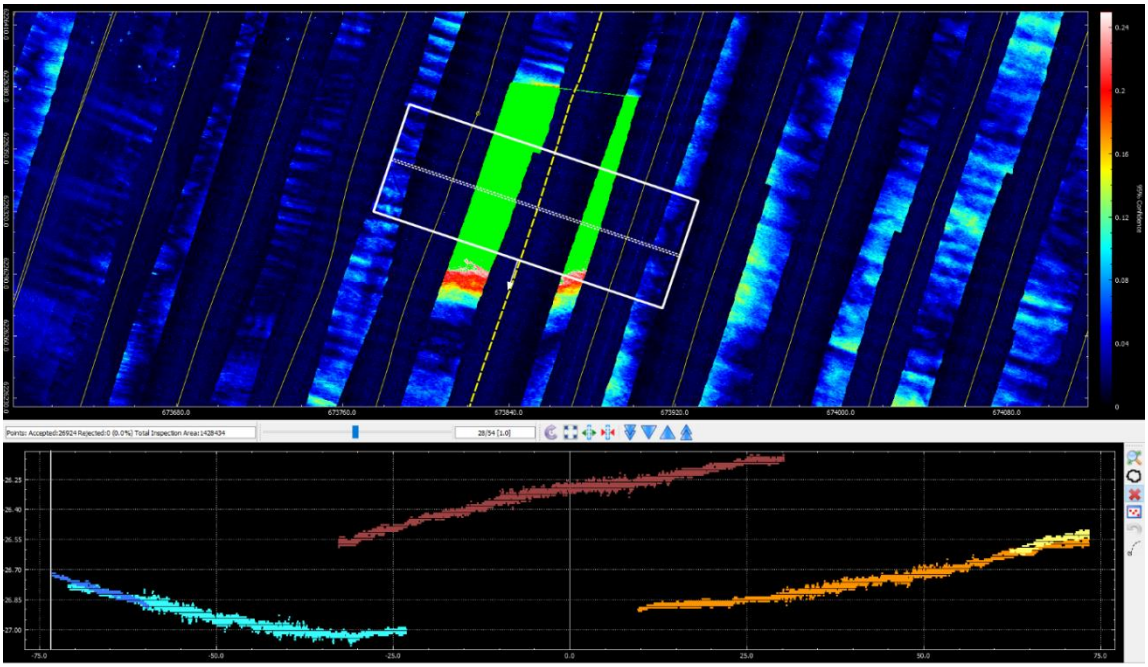

Figure 6-2: MBES grid with missing RTK correction – before shift correction

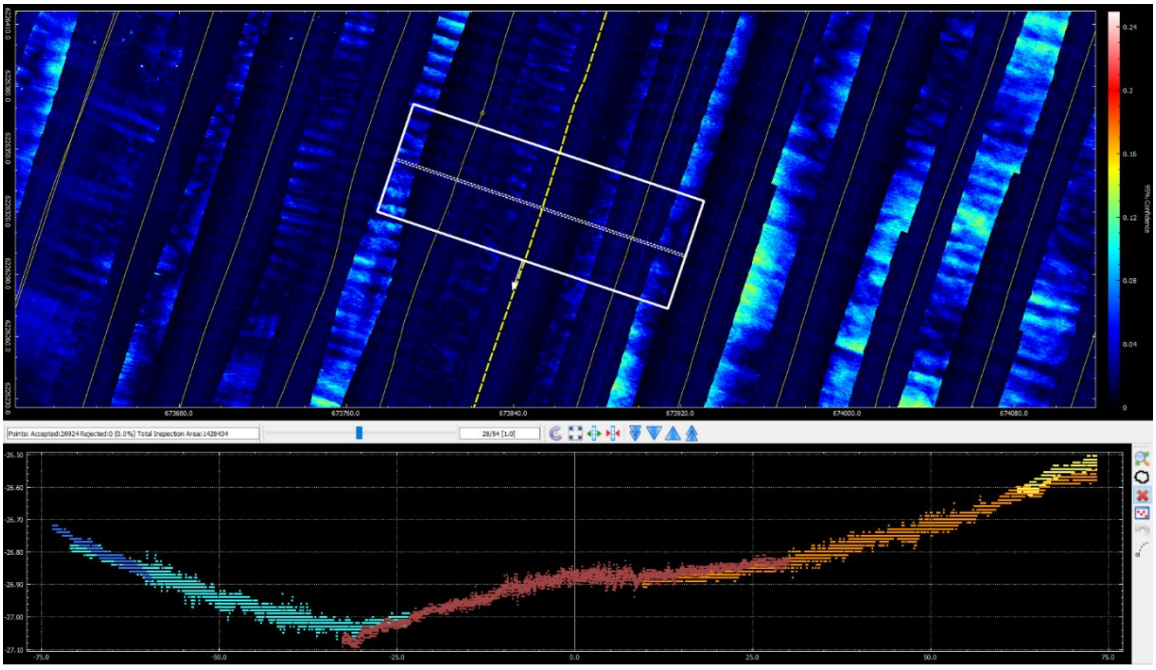

Figure 6-3: MBES grid after shift correction

6.2 Backscatter

Backscatter data was recorded and stored in the raw MBES files (*.db in QPS QINSy and *.SBD in NaviScan). For Mintaka I and Hydrocat the backscatter data was acquired with the Reson T50 and recorded in Time-Series mode. Whereas, for Rambunctious the data was acquired using the Norbit iWBMSh and recorded both in, side scan- and snippets mode. Backscatter data was processed in NaviModel and QPS FM Geocoder Toolbox. The overall processing workflow can be seen in Figure 6-4.

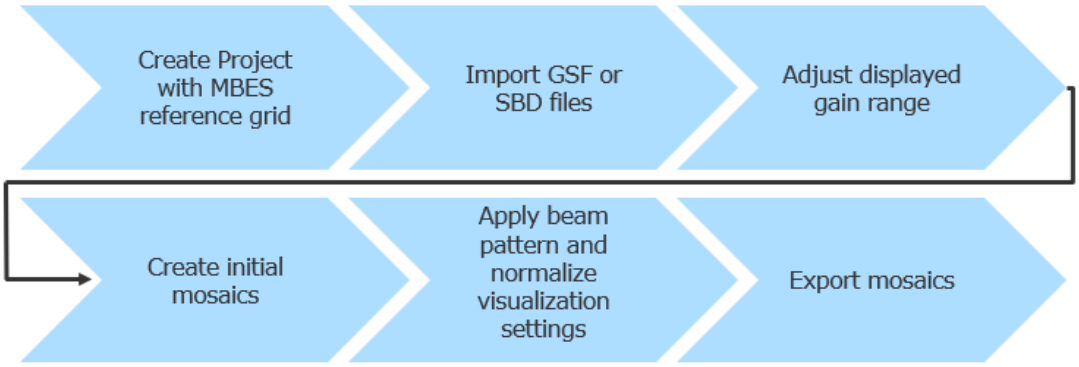

Figure 6-4: Workflow for Backscatter processing

The backscatter was processed using fully processed MBES data.

6.3 Side Scan Sonar

Chesapeake SonarWiz was used to process the raw low and high frequency xtf files. The data were loaded into several separate projects: one for each acquired block (GL01-GL12) which also are divided into one low frequency (LF) and one high frequency (HF). A course made good (CMG) was applied to the heading and a 200 pings smoothing was applied during the import. The data were further smoothed with regards to heading by executing a smoothing filter of 15 pings to ensure no real navigation was lost. The smoothed navigation from the LF was exported and injected into the HF files. Also, the LF navigation data were exported and used to produce track lines.

After the navigation was processed a suitable bottom track was made for all lines, and a bottom track batch was then used. Hereafter, the bottom track was checked on a line-by-line basis to ensure the water column was removed sufficiently.

Based on the slant-range corrected data in both projects an Empirical Gain Normalisation (EGN) was set up to enhance quality and balance of the intensity across all lines. The EGN table was QC'd and to improve the data quality a de-stripe was set up. An extra EGN table was set up in cases where the gain wasn't aligned across survey lines. If, the extra EGN wasn't acceptable a AutoTVG was applied and the EGN was removed from the line. After the gain settings was applied the xtf files was ordered to show the best data on top and to ensure as much nadir coverage as possible.

Some of the processing steps are seen in Figure 6-5.

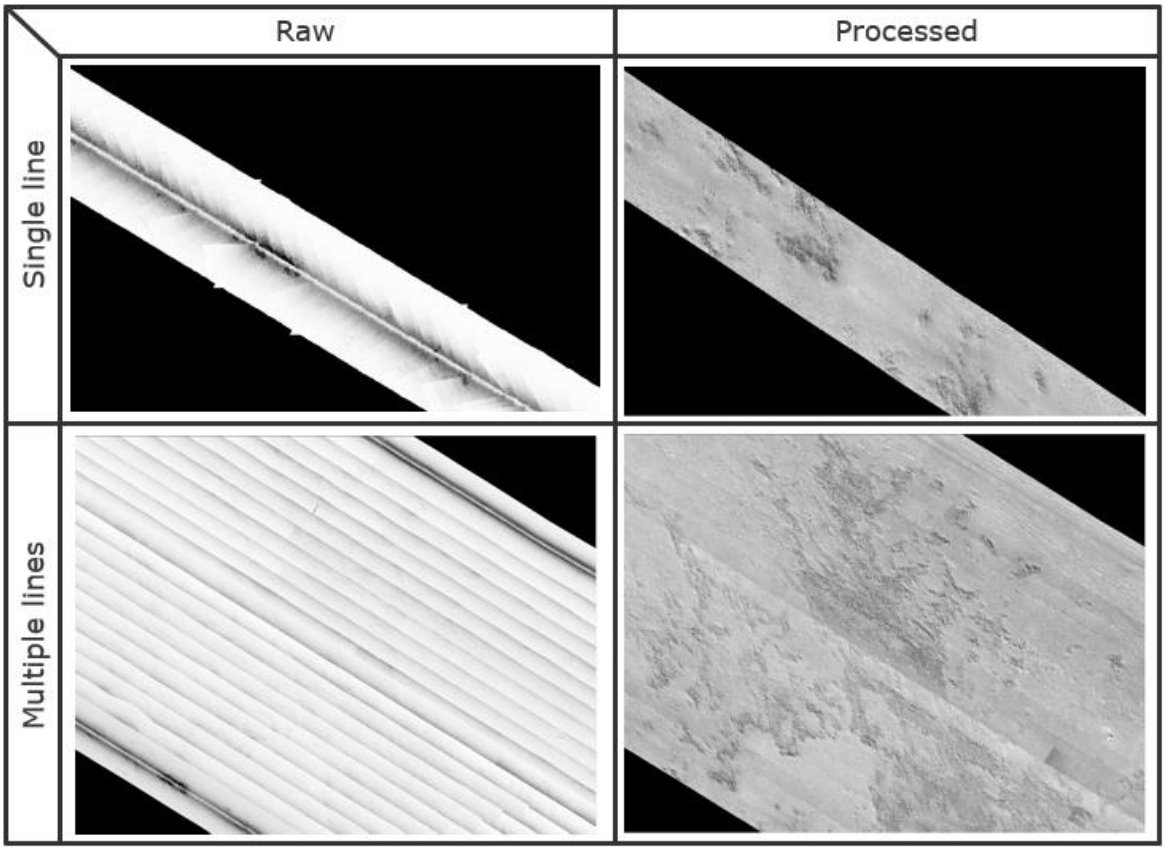

Figure 6-5: Shows processing steps on singles and multiple lines

Once the mosaics were exported on a block-by-block basis in cell size of 20x20cm. Contact picking was hereafter performed in SonarWiz in waterfall view using the contact manager.

6.4 Sub Bottom Profiler

The SBP data has been acquired with the Innomar SES-2000 Standard. The raw data was recorded in RAW- or SES3 formats and converted to SGY with the Innomar SESConvert software.

The quality of data has been controlled in real time with the Innomar's system control software. The first processing steps included applying signal gain, automatic bottom track as well as corrections for vessel movements: heave-roll-pitch, tide/swell and sound velocity. The SBP data has been subsequently imported into a Kingdom project for quality assessment. In case of any issues the lines have been flagged and rerun.

The data processing and QA/QC workflow included following steps and has been summarised on the diagram shown on the Figure 6-6:

- Processing applied during data acquisition:
  - Bottom track
  - Signal gain
  - Corrections for vessel movements: heave-roll-pitch, tide/swell and sound velocity
- File conversion to the SGY-format
- SBP data import into the Kingdom project
- Quality control including:
  - Navigation/positioning
  - Heave corrections
  - Correlation with the preliminary MBES data
  - General data quality assessment
- Mapping of reflectors

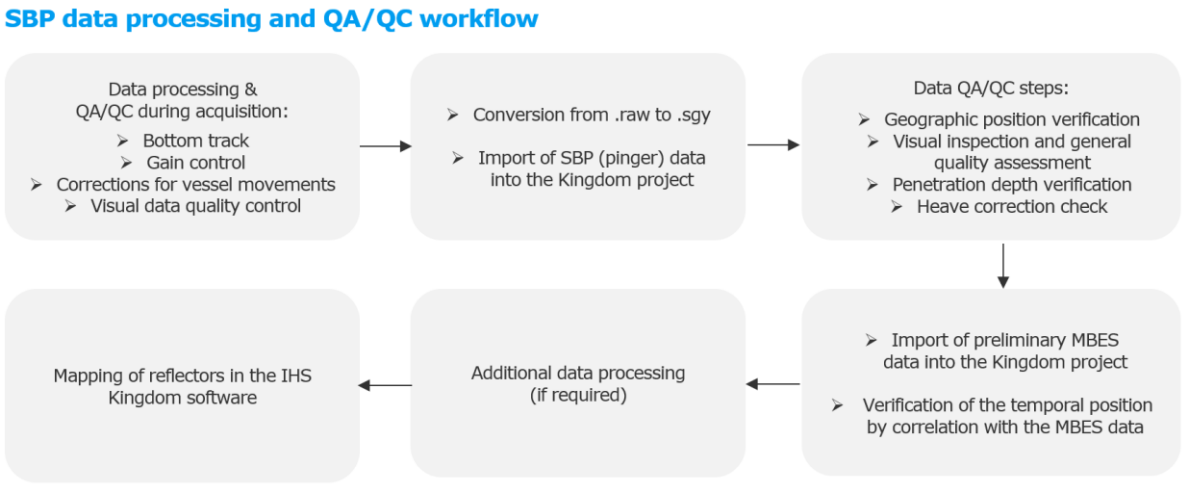

Figure 6-6 Data processing and QA/AC workflow for the sub-bottom profiler data.

Applying additional filters was not necessary as it did not increase data quality.

6.5 Magnetometer

The magnetometer data were processed in Geosoft's Oasis Montaj. The navigation was applied to the raw magnetometer data during acquisition. The navigation was filtered and interpolated in areas where USBL positions were lost. The raw ASCII files were imported into Oasis Montaj for processing where scripts were used to automate the processing and QC tasks. The processing was carried out on a line-by-line basis.

The raw navigation data were checked for gaps and a non-linear filter applied to remove high frequency noise. Spikes were removed and interpolated to create smooth tracks. Sensor offsets were applied using the processed navigation to create X and Y channels for each of the two magnetometers. Altitude was checked for height above seabed not to exceed the specifications and spikes were removed from the channel. The raw total field was despiked and cleaned. Hereafter, a series of non-linear filters and B-spline filter were applied to the total field to remove non-magnetic noise and to derive the background field. Then the background field was removed from the clean total field to obtain the residual field to highlight anomalies. Some of the processing steps are seen in Figure 6-7.

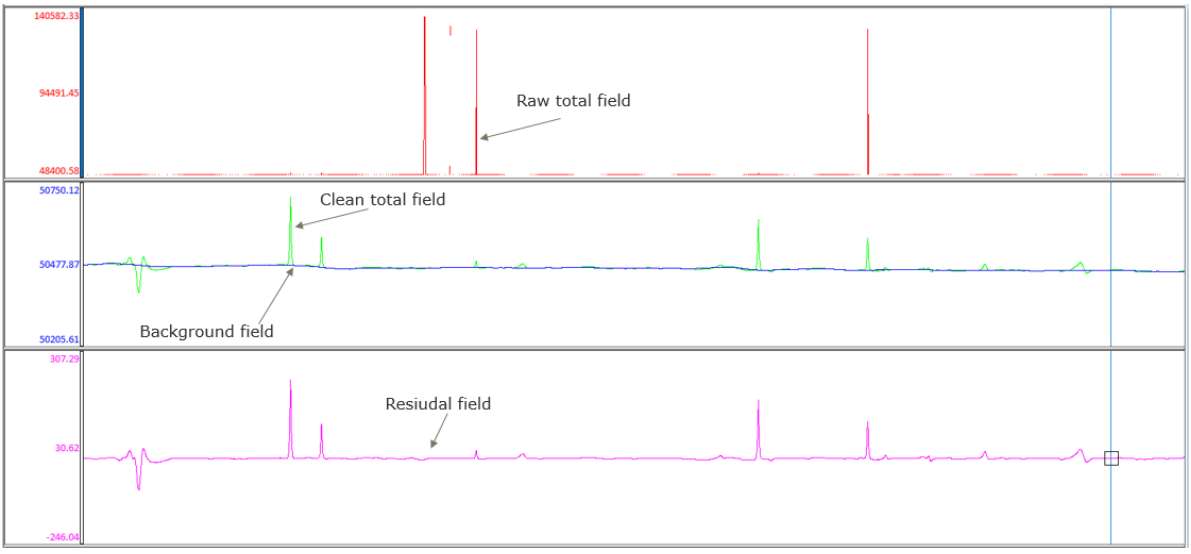

Figure 6-7: Shows the processing steps in Oasis Montaj going from raw total field to the final residual field

The anomalies are picked from the residual field channel and was automated using the pick-from-profile function in Oasis Montaj. Using this function all anomalies down to 5nT are detected. See more about target picking in section 8.8.3.

6.6 Airborne lidar

All GPS/INS data were processed in Applanix MMS suite and correlated with base stations from the national net. The parameters were checked to ensure precise positioning and orientation. If the trajectory data was of good quality, the data were exported as a trajectory data POS file which was used to process the lidar and camera data.

The lidar data was correlated with the positioning and orientation data using the Riegl program, RiProcess. Here, the point cloud data was getting filtered and georeferenced for every line acquired. All lines were analysed and corrected for misalignments in RiPrecision.

The control points from section 5.2 are used as reference points to ensure no torsion of the point cloud data. The control points are used in RiPrecision to twist the data and correct for any potential offsets. Figure 6-8 shows the processing steps for lidar and camera data.

No correction has been made on the point cloud along the X,Y and Z axis, as the accuracy is well within parameters. Overlap beyond +/- 30 degrees have been cut away.

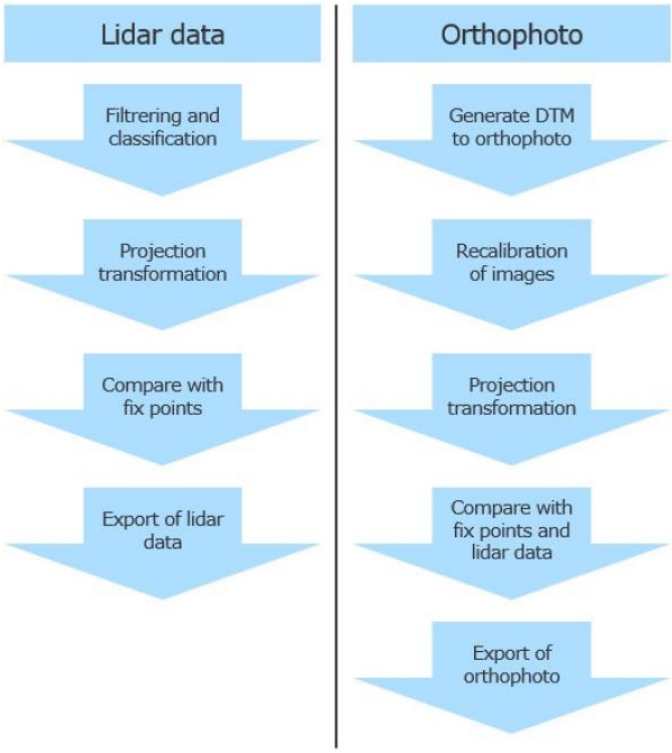

Figure 6-8: Shows the processing work flow for lidar data and orthophoto

For quality control the following was checked:

- Accuracy of the point cloud and the GSD of the images (orthophoto) have been crosschecked.
- Hit count for point cloud
- Coverage across the survey corridor
- Image orientation file crosschecked with images
- Images have undergone sampling to determine correct quality

6.6.1 Benchmarks

Three geodetic benchmark points at the landfall area near Gilleleje was established. The benchmarks were measured with the receiver, Trimble MPS856 and each position were measured 2 times with a duration of 300 seconds. All three points are located north of Tinkerup Standvej near the Dancenter at the parking lot in Gilleleje. All three benchmarks are located in an area with full data coverage from the lidar survey. The positions of the three benchmarks can be seen in Figure 6-9.

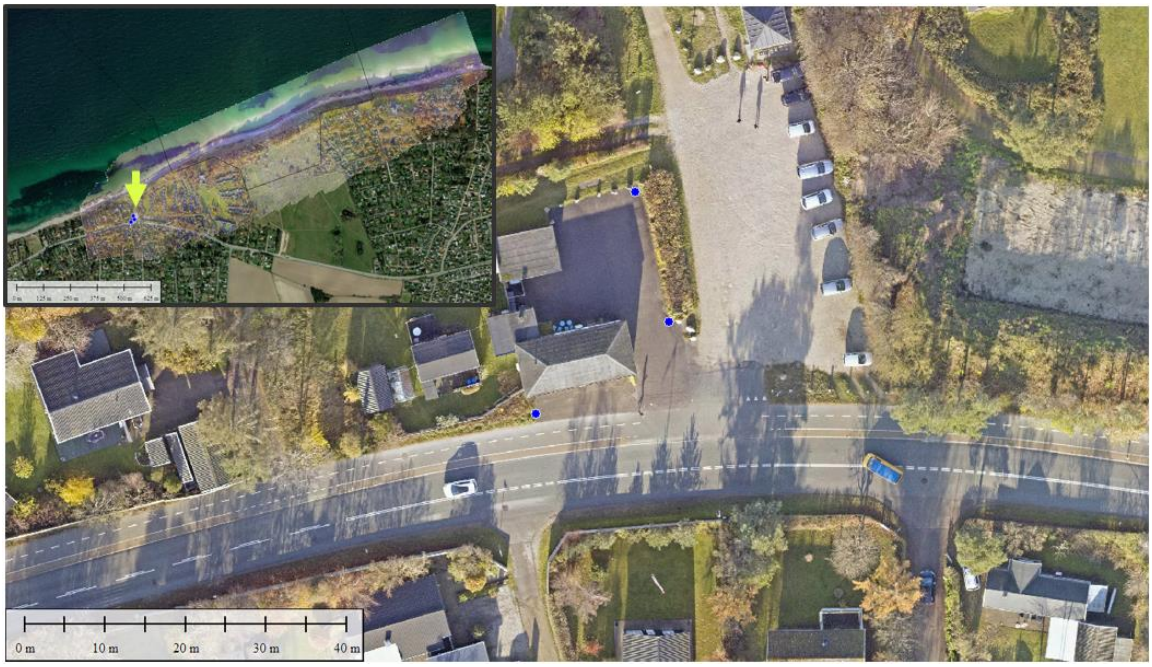

Figure 6-9 shows the positions of the three geodetic benchmarks (blue dots) located at the parking lot next to Dancenter in Gilleleje

For all positions both UTM coordinates, Cartesian coordinates and Geographic coordinates including elevation in relation to DTU18 and DVR90 was measured. Table 6-1 shows the UTM coordinates for the three benchmark positions. The benchmarks are further described in Appendix 4

Table 6-1 shows the results from when the Benchmarks was measured in. The results are shown as UTM coordinates

Name	Easting	Northing	Orthometric height (DTU18/DVR90)
Benchmark 01	702652.941	6224591.284	9.142m/9.251m
Benchmark 02	702669.457	6224602.686	8.886m/8.778m
Benchmark 03	702665.210	6224618.787	8.825m/8.717m

7. GEOLOGICAL DESK STUDY SUMMARY

The Hesselø OWF cable corridor is situated in the southern Kattegat. The area has been previously investigated in relation to i.a. establishing the adjacent Anholt OWF and exploration for raw marine materials. Based on the available data a desk study presenting geological framework for the region has been prepared by GEUS /1/. A short summary of geological development from the latest glaciation is included in the following paragraph of this report. For more details regarding geological history of the southern Kattegat, refer to /1/.

Both the Hesselø OWF and the cable corridor are located within the Sorgenfrei-Tornquist zone, where numerous extensional and strike-slip faults run generally in the NW-SE direction. The Sorgenfrei-Tornquist zone is an active tectonic zone and earthquake activity is still being observed. Reactivation along the existing basement fractures has been pointed out as one of geotechnical challenges in the study prepared by GEUS /1/. The Figure 7-1 shows location of major faults within the study area.

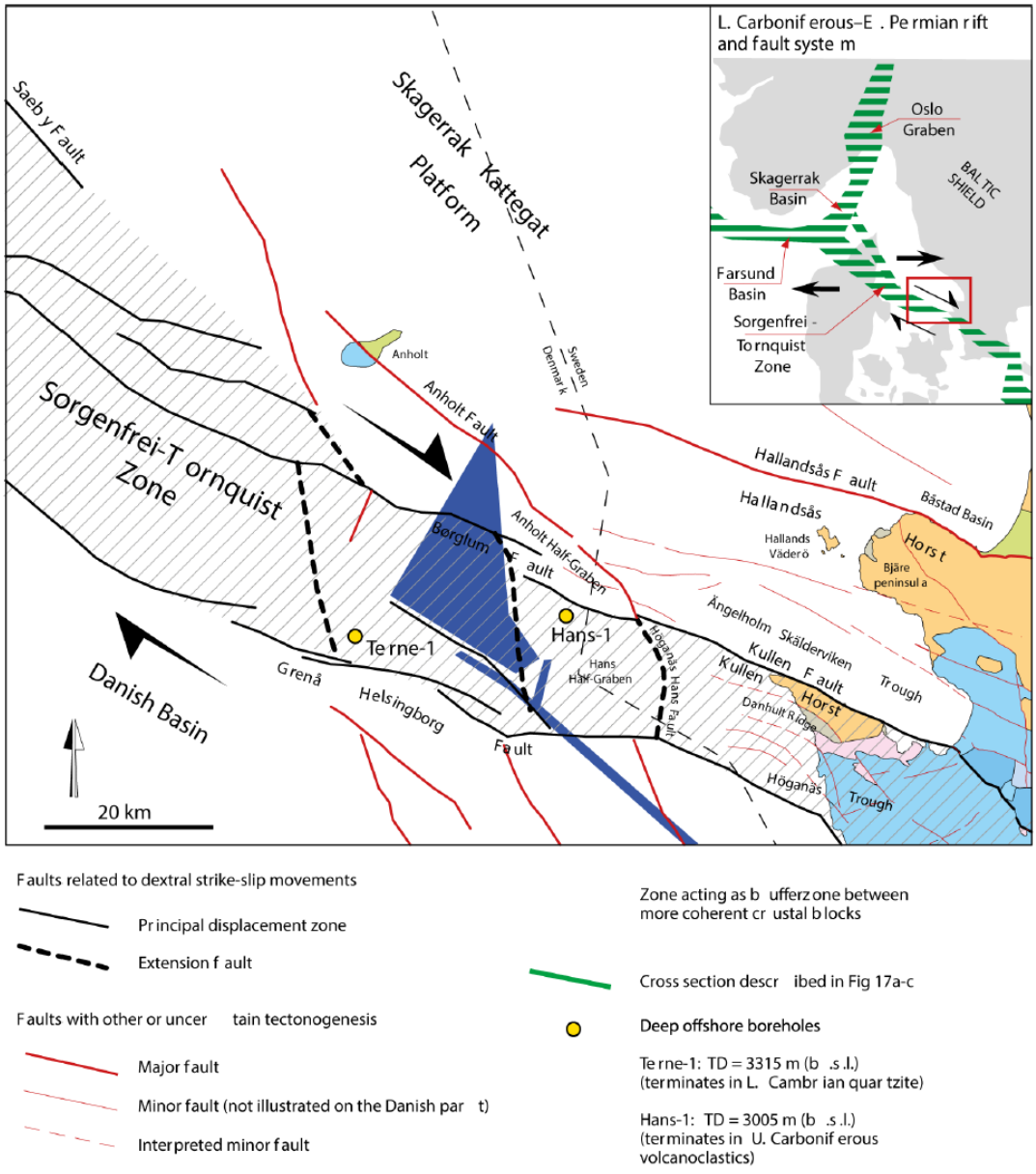

Figure 7-1 Tectonic framework for the southern Kattegat: location of major faults forming part of the Sorgenfrei-Tornquist Zone within the study area, from /1/.

The top pre-Quaternary surface is found at relatively large depths below the seabed and significantly below the expected investigation depth of pinger data, hence, the pre-Quaternary succession will not be discussed in this report.

The Quaternary sediment cover in the Kattegat region is thick and composed of Eemian and Weichselian glacial and interglacial deposits overlain by successions of Late Weichselian glaciomarine and Holocene marine sediments /2/.

During the deglaciation of the region following the Weichselian glacial maximum (approx. 22 ka BP), major melting phases were interrupted by stillstands and re-advances of the ice margin until approximately 17 ka BP, when the ice sheet had gradually retreated from the area /3/.

After the gradual retreat of the ice sheet the region was subjected to isostatic depression that led to relatively high sea level despite of eustatic sea level being at low. The area was inundated and became part of a relatively open towards the northwest marine basin were glaciomarine conditions prevailed /3/. A thick succession of Late Glacial glaciomarine sediments dominated by fine-grained clays can be found on top of glacial tills. The southernmost part of the Hesselø OWF area and the associated cable corridor are located in the marginal part of the southern Kattegat late glacial glaciomarine basin deposition area /1/.

A global eustatic sea level rise followed the period of deglaciation. However, the faster glacio-isostatic rebound of the crust resulted in a fall of the relative sea level in the Kattegat and Baltic Sea. The initial Late Weichselian highstand was therefore followed by a forced regression and significant erosion of the Late Glacial deposits. Within the study area the upper boundary of the Late Glacial glaciomarine succession is marked as a pronounced erosional unconformity /3//1/.

When the eustatic sea-level surpassed the isostatic rebound, the relative sea level begun to rise – which in Kattegat was dated to about 11.4 ka BP /3/. This regional marine inundation marks the beginning of the Littorina transgression, and the increasing relative sea level resulted in, amongst other changes, alterations to the hydrographical conditions of the Kattegat region and led to deposition of marine muds/gyttja in the deeper parts of the Kattegat /1/.

During the early Holocene, at the beginning of the marine transgression a tidally dominated estuary with fine grained infill and large tidal mouth bars and banks developed just south-west from the Hesselø OWF cable corridor (Figure 7-2) /1//2/.

The Hesselø OWF area has been submerged most of the time after the last deglaciation, but in the lowstand period around 10.5 ka BP only partly, and lowstand sediments can be found. Already in the initial phase of the Holocene transgression the Hesselø OWF area was again fully submerged. The cable corridor area has a longer transgression history with postglacial marine sediments being very thin or absent in its southernmost part.

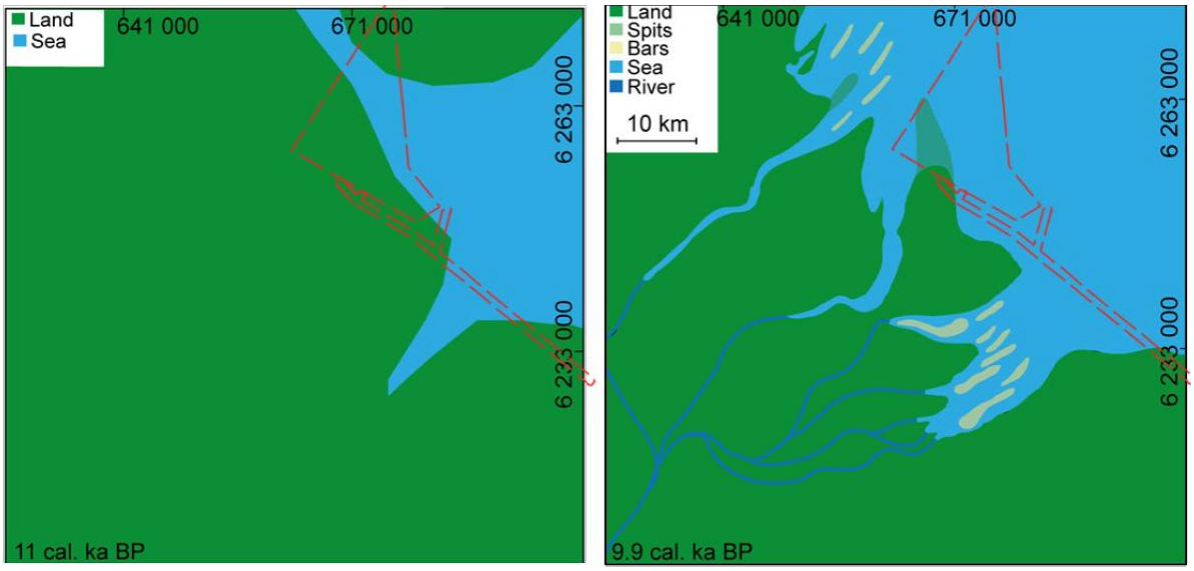

Figure 7-2 Paleogeography of the study area during the Early Holocene lowstand (11 ka BP) and early transgression (9.9 ka BP) showing the coastal environment during the early Holocene in the southern Kattegat. Note several estuaries and spits as well as numerous bars existing just south-west and north-west from the Hesselø OWF site and cable corridor areas. Figure from /1/.

As a result of previous studies, the Quaternary succession has been divided into three main geological units: PG (Post Glacial), LG (Late Glacial) and PG (Post Glacial). A short summary of the seismic facies units is presented in the Table 7-1. This study will adopt the unit classification.

Table 7-1 Geological unit division of the Quaternary succession based on previous studies /1/.

Unit		Age	Lithology	Description/ depositional environment
GL Glacial		Weichselian	Glacial till	In the southernmost part of the southern Kattegat glacial sediments are represented by tills from the Weichselian glaciation.
LG Late Glacial		Late Weichselian	Clays with dropstones, might include thin layers of coarser sediments, silt to sand. Generally weakly laminated to structureless.	Late Weichselian highstand sediments deposited in glaciomarine environment during the local highstand caused by depression from the Weichselian ice sheet. Found both in the basin areas as well as in the deeply eroded channels and reaching significant thicknesses of up to 75m /1/. As the highstand was followed by a regression and significant erosion of the LG deposits marked as a pronounced erosional unconformity.
PG Post Glacial	PG I	Early Holocene	Medium- to coarse grained sand, may contain cobbles and pebbles. Fining upwards.	Lowstand sediments deposited during the early transgression in the Kattegat and interpreted as marine coastal deposits or erosional channels fill.
	PG II	Holocene	Interlayered medium and coarse-grained sand layers and laminated silt to clay	Estuarine and coastal deposits deposited after the eustatic sea-level rise surpasses the diminishing isostatic rebound (a transgressive systems tract).
	PG III	Holocene (most recent)	Structureless clay to fine sand	High stand sediments deposited in a marine basin after the latest Littorina transgression

A chronostratigraphical chart for the region of southern Kattegat /1/ is shown on the following Figure 7-3.

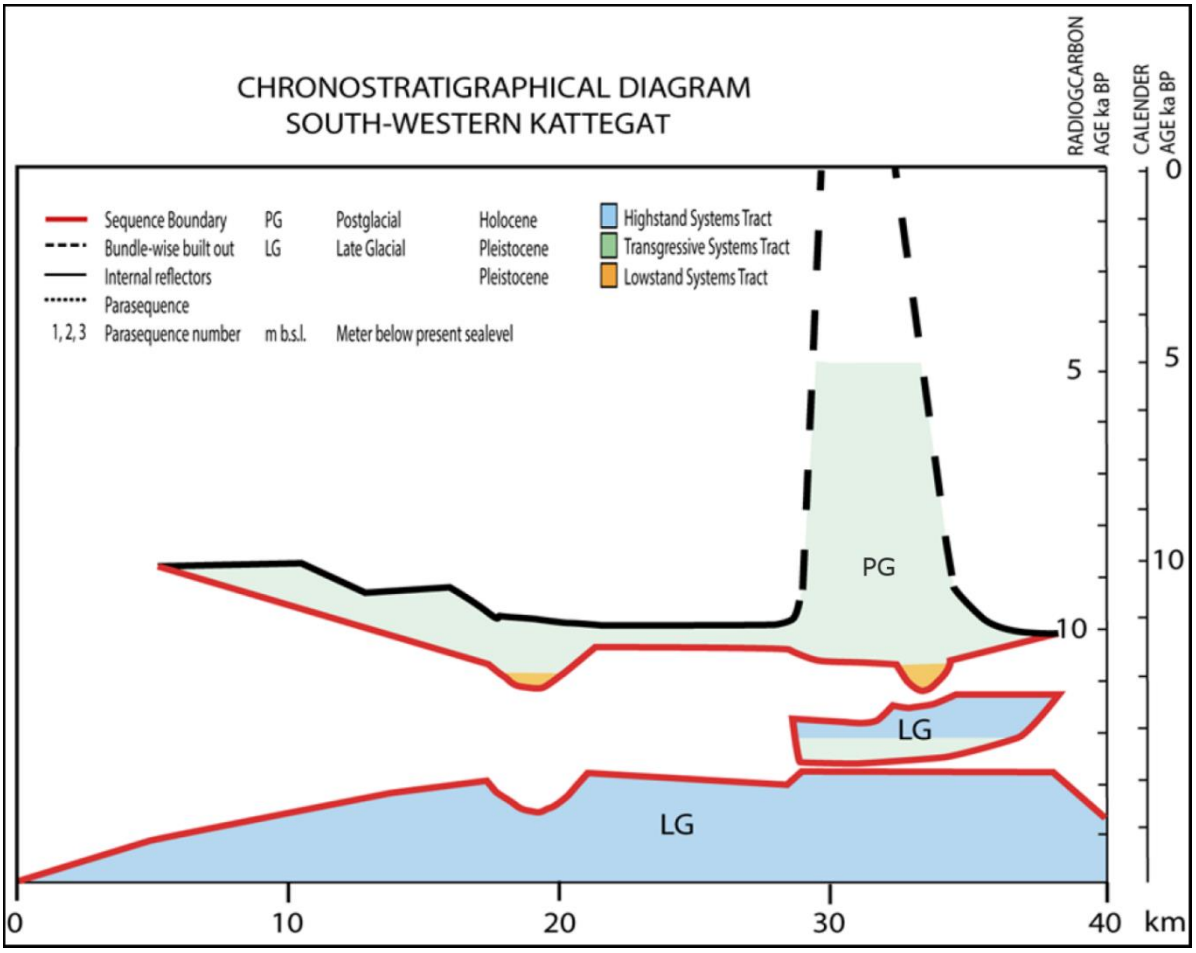

Figure 7-3 Chronostratigraphical chart for the region of southern Kattegat, from GEUS /1/.

8. DATA INTERPRETATION

A short presentation of the general results from the survey is presented in the sections below. For detailed results, please see the digital deliverables and charts and the KP route analysis. The charts include MBES 25 cm gridded surface with 0.5 m contours, seabed geology, highlighted boulder fields with targets and magnetic anomalies. Also, cross-section with interpreted horizons from sub-bottom data are included the CPT/Vibrocore information. The charts can be found in Appendix 2. Whereas a detailed KP start to end analysis can be found in Appendix 3.

8.1 Bathymetry

Overall, the requirements were met in relation to 16 pings/m^2 only in few places in the dense boulder fields were affected by shadow effects as seen in section 4.3.1. The TVU and THU specifications are within the IHO special order requirements only minor RTK dropouts caused some higher values in the TPU as explained in section 6.1. The bathymetry data from Hesselø cable route survey shows that the cable route water depths are ranging between 0.9m to 34m according to DTU18. The bathymetric data can be seen in Figure 8-1 and cross-sections in Figure 8-2.

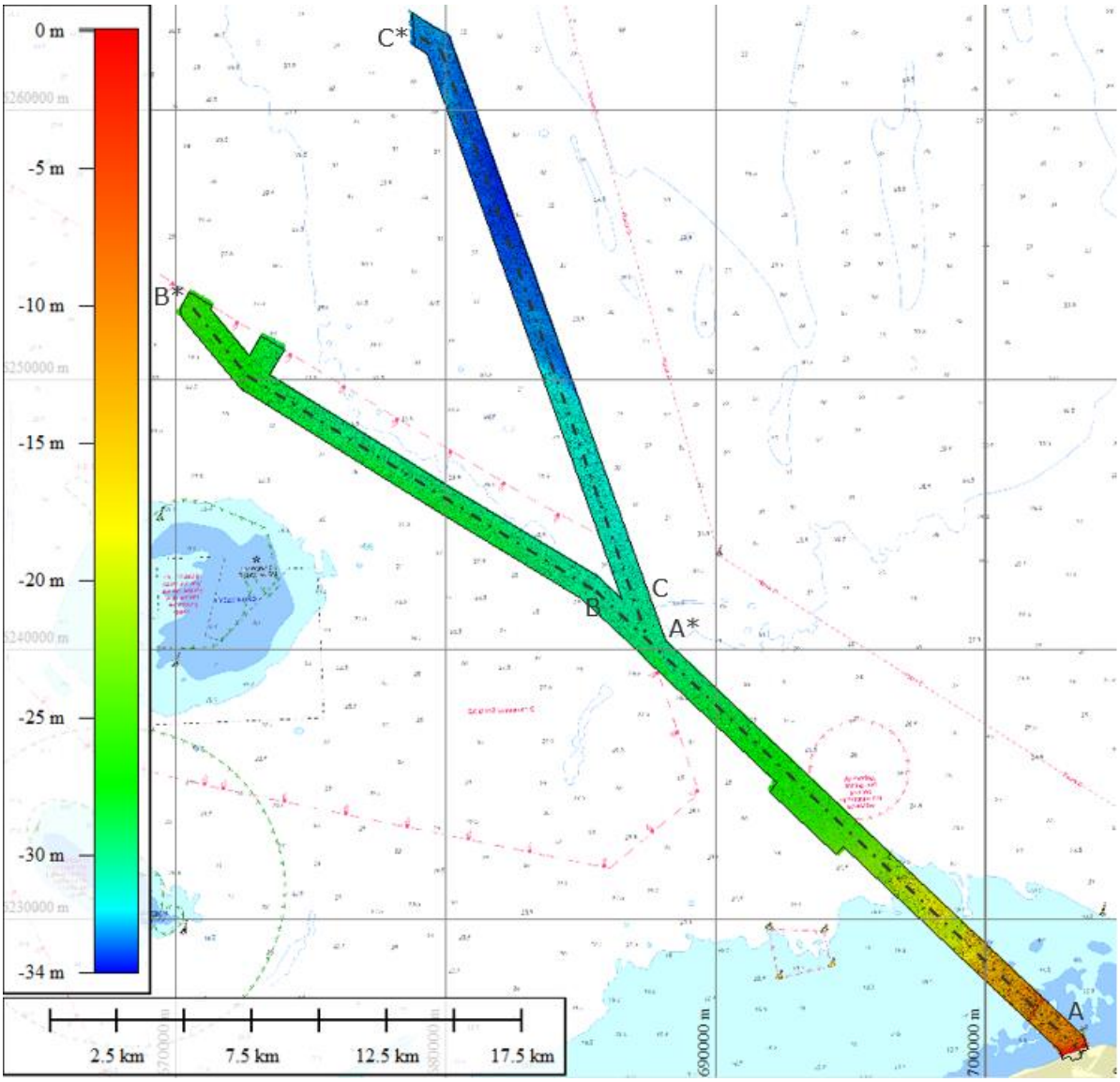

Figure 8-1: Bathymetry showing the water depth for the cable route

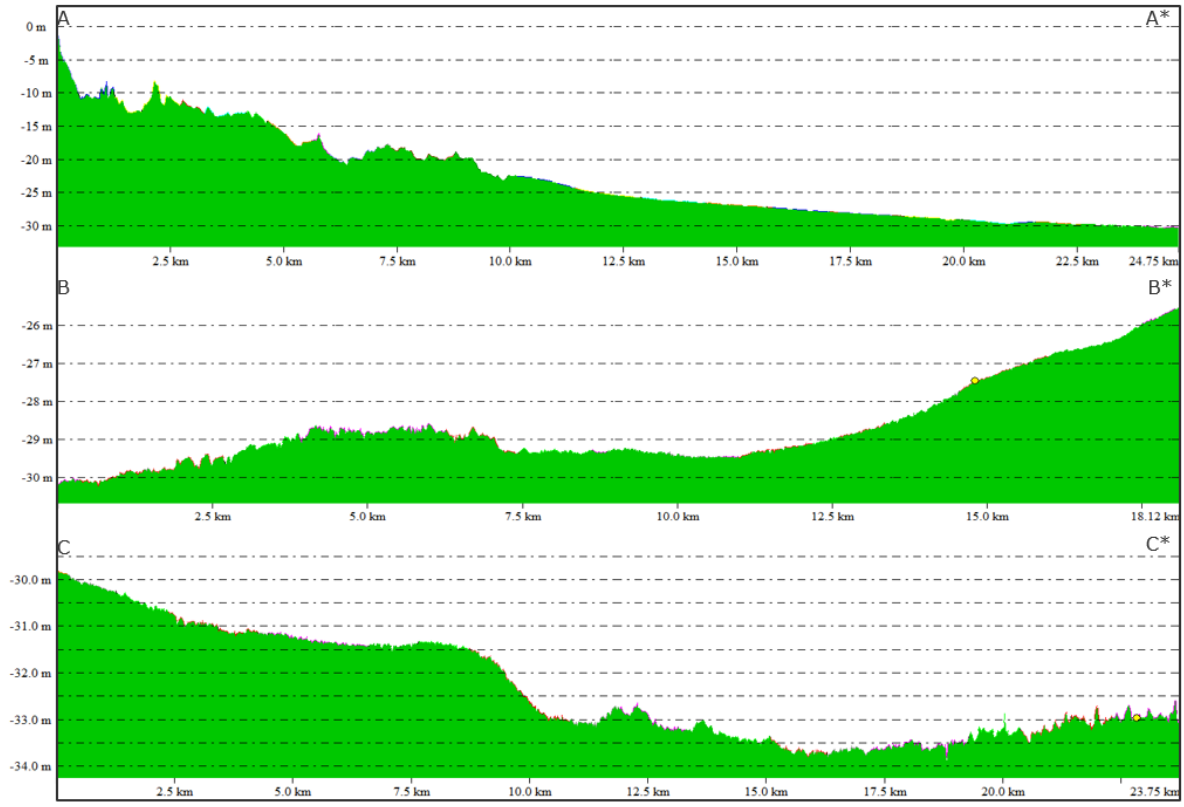

Figure 8-2: Cross-sections of the bathymetry along the cable route

From the bathymetry data the slope along the cable route reveals that the seabed surface is quite flat, and slopes do not exceed approx. 12-15 degrees. The most significant slopes can be found towards landfall. The slope can be seen in Figure 8-3. The most conspicuous slopes are related to the dense boulder fields in the nearshore parts where in some cases the boulders are forming stone reefs as illustrated in Figure 8-4.

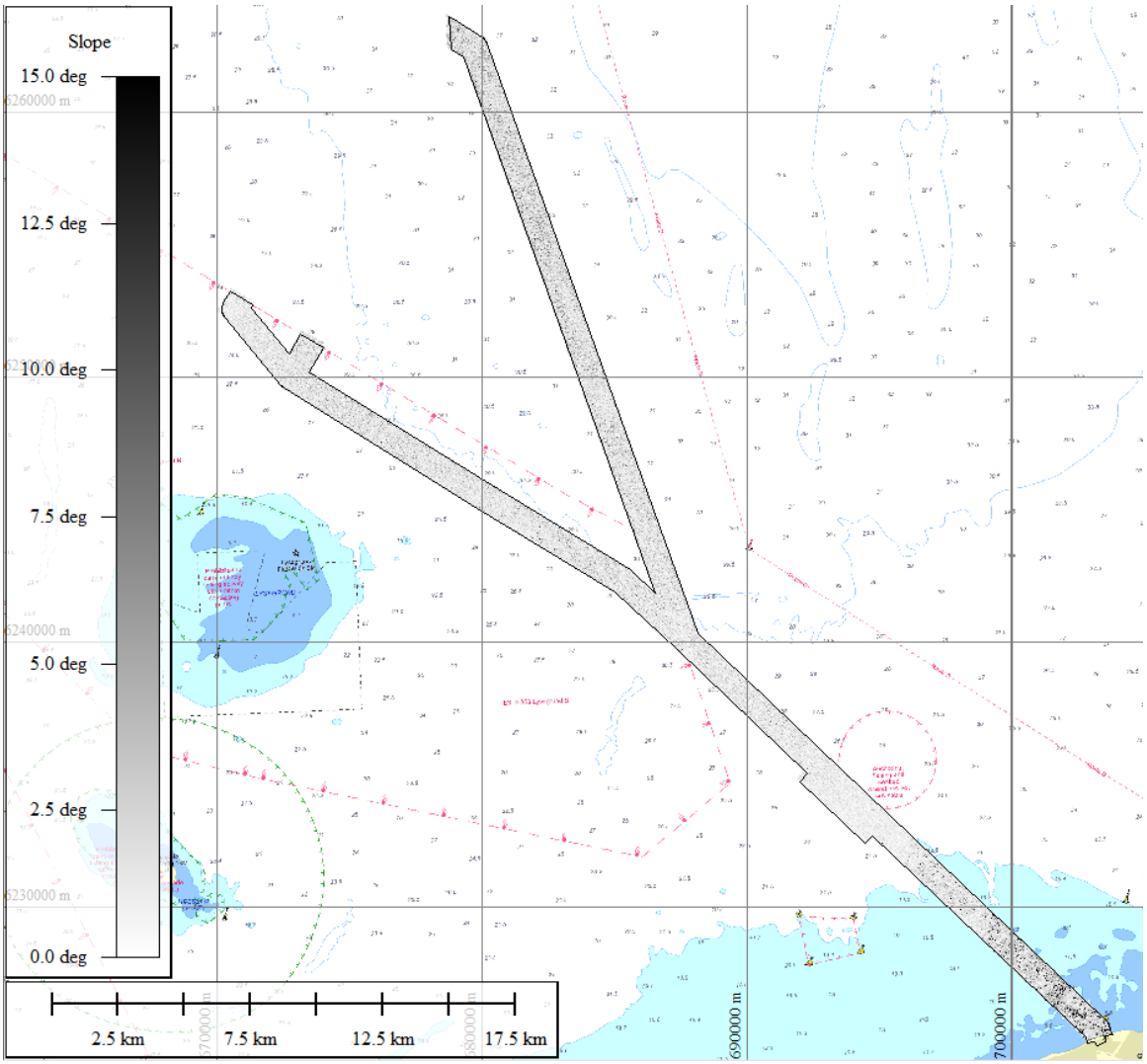

Figure 8-3: Bathymetry grid showing the slope in degrees along the cable route. Slope values calculated for from 0.25x0.25m bathymetry data.

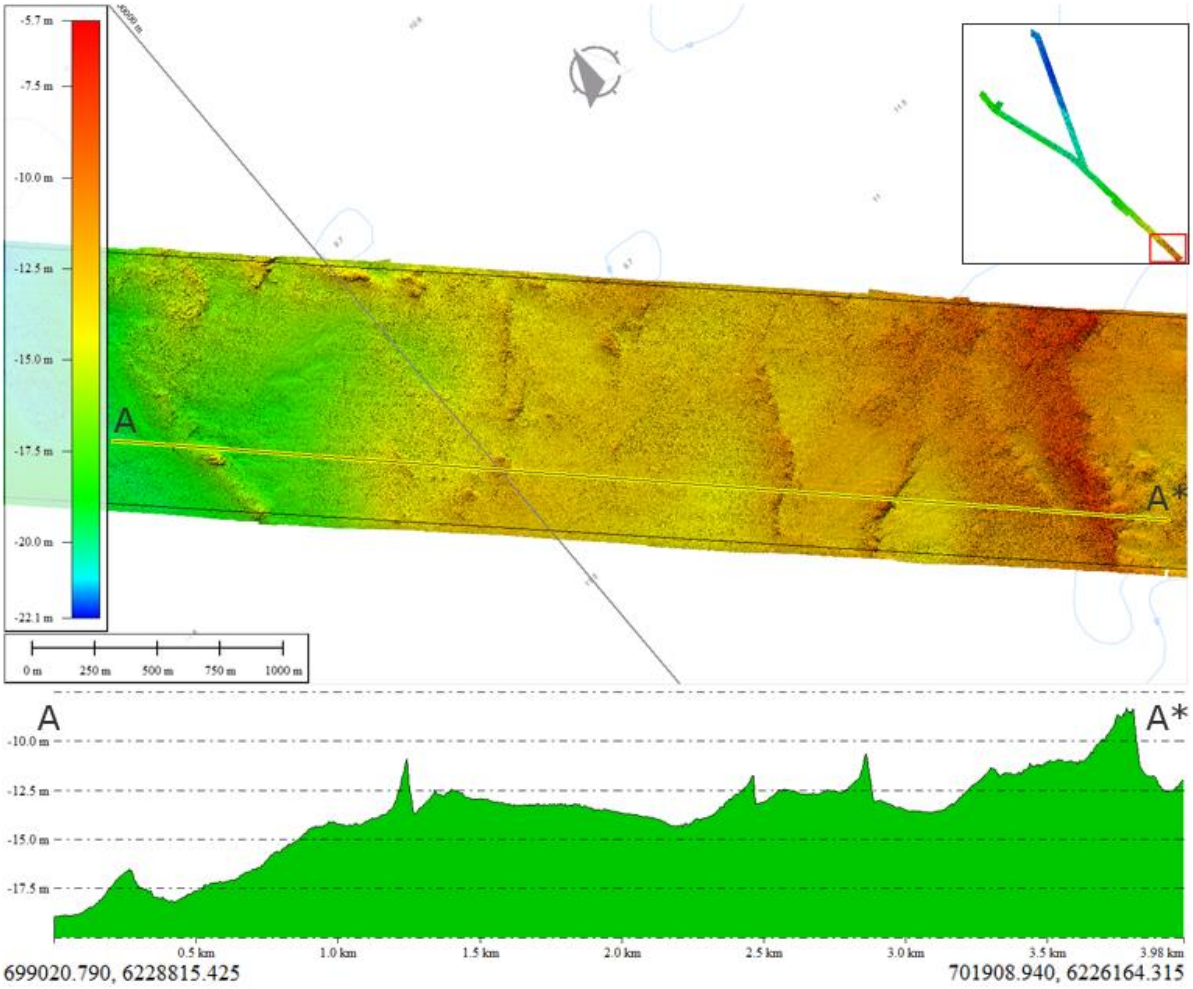

Figure 8-4: Cross-section of the seabed across the highs build up by the dense boulder fields and thereby decreasing the water depths and creates the steepest slopes along the cable corridor

A sound velocity probe was deployed at least every 6 hours which ended up in total 71 SVP casts acquired by Mintaka I, Hydrocat and Rambunctious. These SVP profiles are merged together and an average sound velocity of 1486 m/s for the water is determined within the period 21-10-2020 to 15-11-2020. The average of each SVP cast can be seen in Figure 8-5.

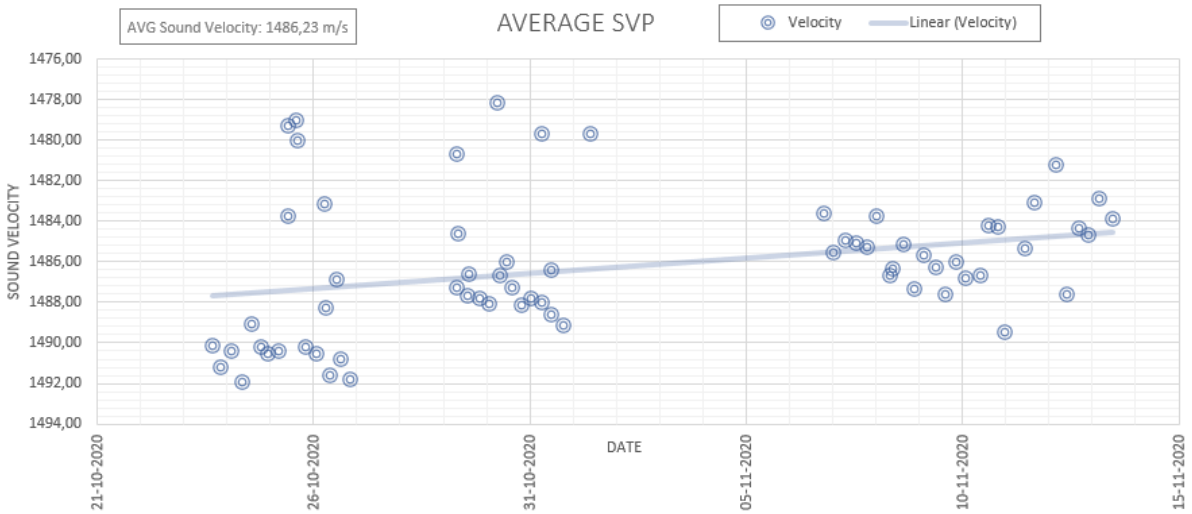

Figure 8-5: Average sound velocity for each SVP cast along the corridor

8.2 Backscatter

The backscatter is used to assist the low frequency side scan sonar mosaics during interpretation of the seabed geology and substrate types. Therefore, the backscatter mosaic is normalised to the side scan mosaics meaning that the dark colour is high intensity (hard soil) and brighter colours are low intensity (soft soil). Figure 8-6 shows the backscatter mosaic along the cable route.

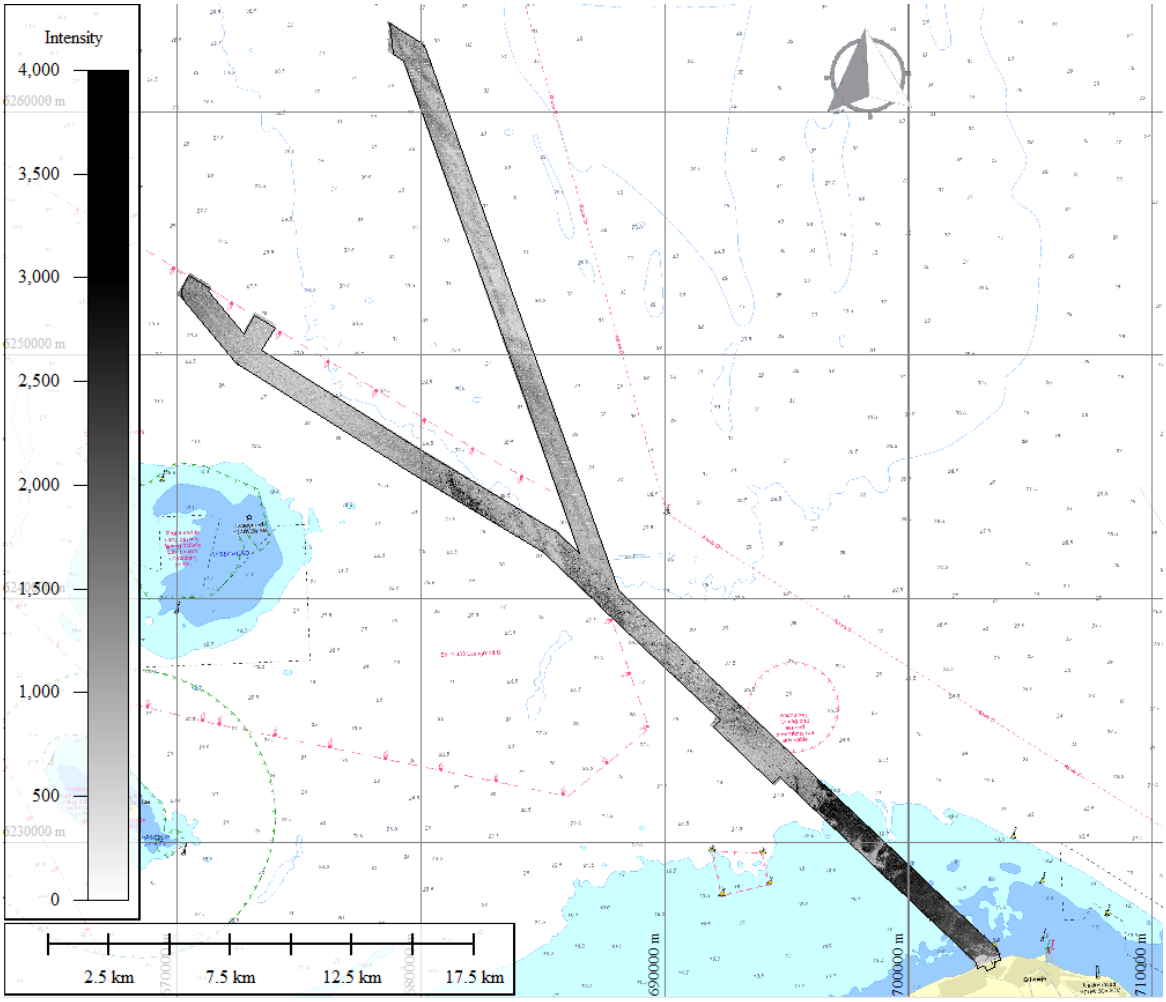

Figure 8-6: Backscatter intensities along the cable corridor. Bright colours are low intensity (soft, fine grained seabed deposits), while darker colours are high intensity (harder and coarser grained sediments)

It can be seen that the harder seabed geology conditions are located nearshore in block GL01, GL02 and GL03. Otherwise, the intensity of the seabed is quite uniform except of one minor area located more offshore in GL05 and GL06. The seabed substrate type and seabed geology are further described in section 8.4, 8.5 and 8.6.

8.3 Side Scan Sonar

The side scan sonar data is of good quality and coverage for seabed characterization and contact identification. The acquired low frequency (300 kHz) is used for seabed interpretation whereas the high frequency (600 kHz) provides the resolution for imagery of seabed contacts. The provided mosaics have the cell size of 20x20cm. In some cases, between overlapping survey blocks smaller gain differences can be seen, these differences are mostly related to different intensity responses to changes in altitude. This is mostly evident in the high frequency data which are requiring more user corrections and cannot be entirely corrected even when using the EGN table and the AGC (static gain settings). Figure 8-7 shows the low frequency mosaics along

the survey corridor. The two boxes in Figure 8-7 highlights some of the areas with the most significant seabed changes in reflectivity, these boxes seen in Figure 8-8.

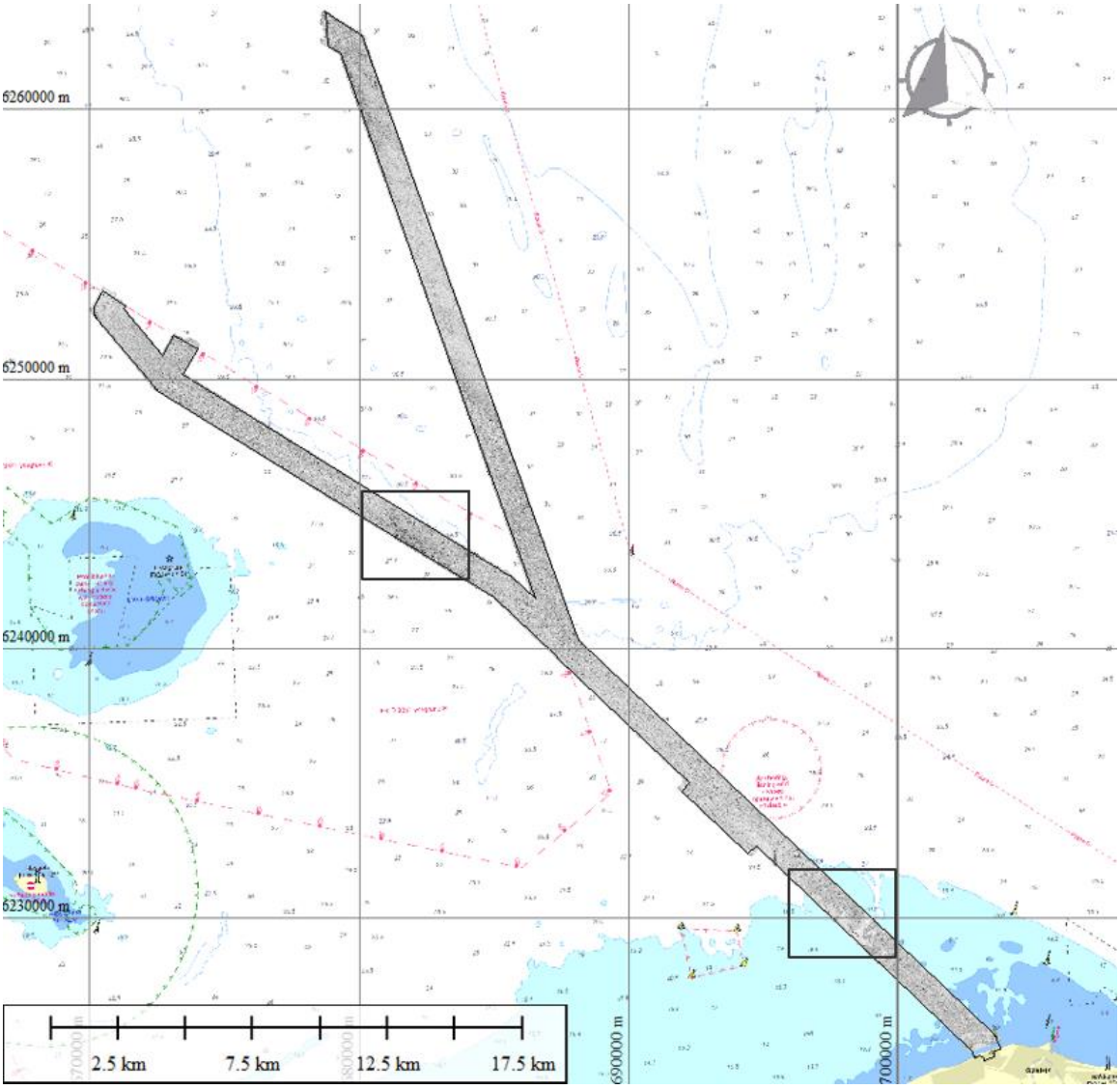

Figure 8-7: Shows the low frequency side scan sonar mosaic along the cable corridor. Darker reflectivities indicates coarse sediments and bright reflectivities indicates fine-grain sediments. The two boxes highlight some areas with significant seabed changes

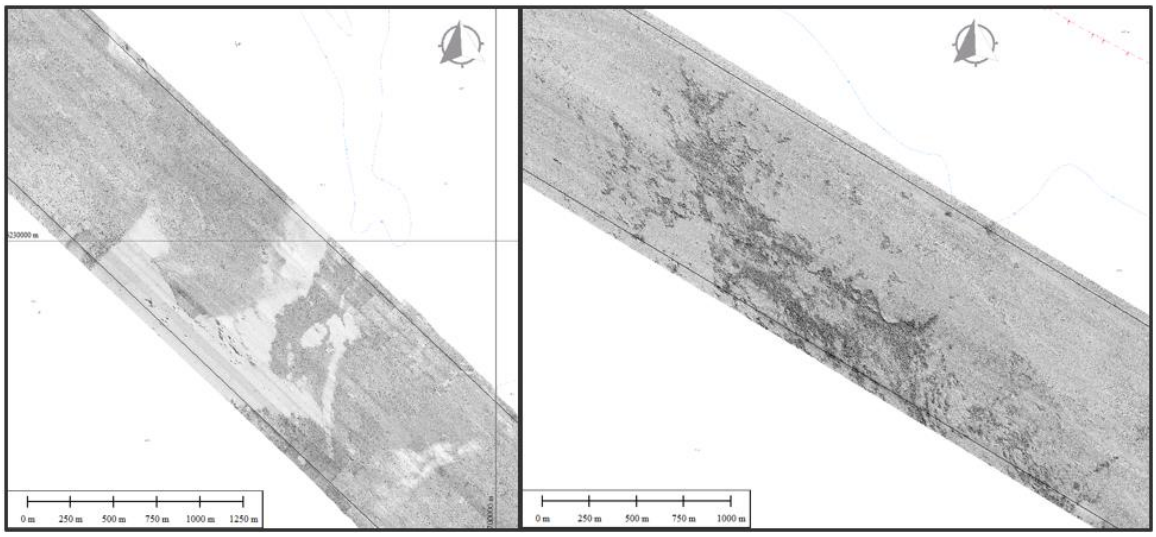

Figure 8-8: Examples of significant changes in seabed reflectivity. The image to the right is from the offshore parts in block GL05 and GL06. The image to the left is from the more nearshore parts in block GL02 and GL03.

The most significant changes in reflectivity in the side scan sonar are located in GL01, GL02 and GL03. Otherwise, the reflectivity is quite uniform meaning no larger changes in seabed sediments except for a minor area in GL05 and GL06. In areas affected by thermoclines data is either trimmed or stacked in order to have best data on top. In cases of the navigation processing can't compensate for motion effects a minor static gain was applied. The seabed substrate type and seabed geology are further described in section 8.4 and 8.5.

8.4 Seabed surface geology

An integrated seabed surface geology interpretation for the Hesselø ECR corridor is derived from a palette of all acquired and related geophysical datasets. The interpreted results are an outcome from raw or processed bathymetry, backscatter, side-scan sonar, grab samples, vibrocores and finally cross correlated with sub bottom profiler. The classification of seabed substrate types in section 8.5 and seabed surface features in section 8.6, rely closely on the same observations as found in the data for seabed surface geology.

The following seabed sediment classes have been identified in the interpretation of the seabed surface geology (classification reference: *Seabed sediment map 2014*, GEUS):

- **Till/diamicton:** Mixed sediment type of glacial origin. Often covered by a thin layer of sand, gravel, boulder and/or sandy mud washed out of the till.
- **Gravel and coarse sand:** Mixed sediments of more than 0.50 m thickness. Lag sediments covering till, meltwater deposits or fossil coastal deposits.
- **Sand:** Homogeneous layer of loose, well-sorted sand.
- **Muddy sand:** A mixed sediment type composed of variable content of sand and mud. Deposited at the rim of basins or as a thin cover layer in erosion areas.
- **Quaternary clay and silt:** Marine, meltwater or lake deposits of clay. Often laminated with sand/silt and/or peat layers, in some cases covered by few cm of lag sediments (sand, gravel or pebbles).

The classification expresses the sediment type of the upper 0.50 m of the seabed. Each sediment class is defined based on the specific grain size distribution. However, till is a mixed sediment of clay, sand and gravel. The interpreted seabed sediment is configured so there is full coverage within the ECR corridor.

Sediment description and grain size distribution of grab samples and vibrocores, collected at locations along the corridor, have been used to ground truth the reflectivity from the side scan sonar and backscatter intensity, and derive the seabed surface geology, including the seabed sediment classes. Results from vibrocores have only been included if there has been a subsample

analysed at/or close to the seabed surface (max 50 cm in depth). Figure 8-9 shows an overview of the derived seabed sediments for the ECR corridor with landfall at Gilbjerg Hoved near Gilleleje. The predominant seabed surface geology along the corridor is *Sand* and *Muddy sand*, although the area is characterised by the outcrop of glacial *Till* and quaternary *Clay* at the seabed. The outcrops are primarily located in the southern part of the corridor.
The *Muddy sand* (or gyttja) is primarily a constitute of clay, silt, fine sand and with shell fragments. The colour is olive grey to dark grey. The *Sand* is fine to medium, clayey, silty and organic with shell fragments. The colour ranges from dark olive grey to dark grey.

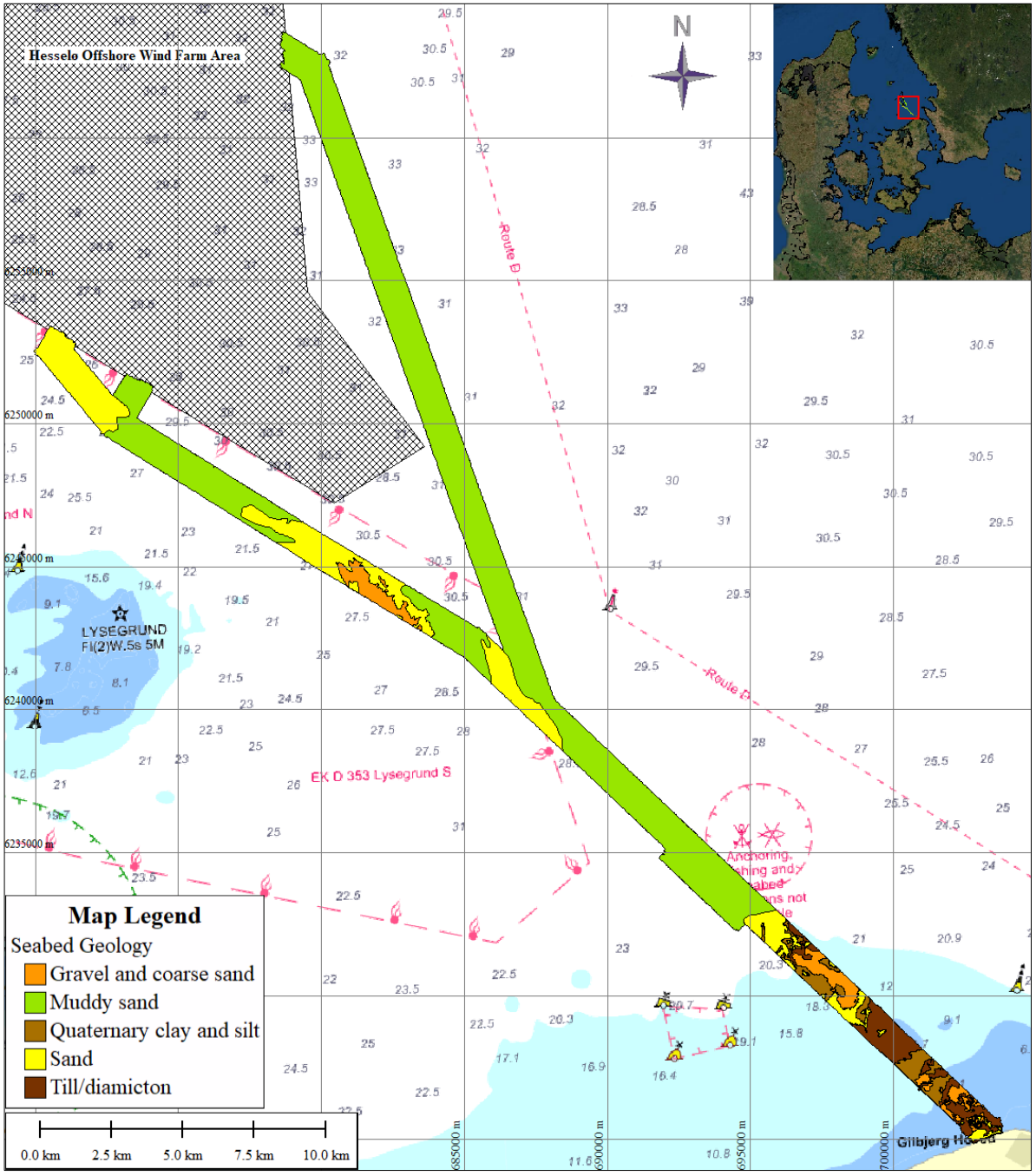

Figure 8-9: Overview of the interpreted seabed surface geology alongside the ECR corridor from Gilbjerg Hoved in the south to the OWF area in the north. Nearshore seabed geology is a mix of clay and till, whereas offshore seabed geology is manly sand or muddy sand.

Figures 8-10, 8-11 and 8-12, highlights three areas with sharp variations in seabed sediments. In figure 8-10, close to the landfall, three seabed samples (two grab samples and one vibrocore) are classified as *Sand*, two seabed samples denotes *Gravel* and one vibrocores *Till*. One can see a clear delineation between the different areas as described by the seabed samples. Backscatter show relative low intensities in areas interpreted as *Sand* and high intensities for areas with *Gravel* or *Till*, figure 8-10(B). The side-scan sonar reflectivity gives same alteration with bright areas of low reflectivity corresponding to *Sand* and darker areas equal to *Gravel* or *Till*, figure 8-10(D). The distinction between *Gravel* and *Till* is related to the grain size distribution and utilising bathymetry, figure 8-10(C). Areas with very high densities of boulders is more likely to be *Till*. This observance is finally cross correlated with results from the interpretation of sub bottom profiler data.

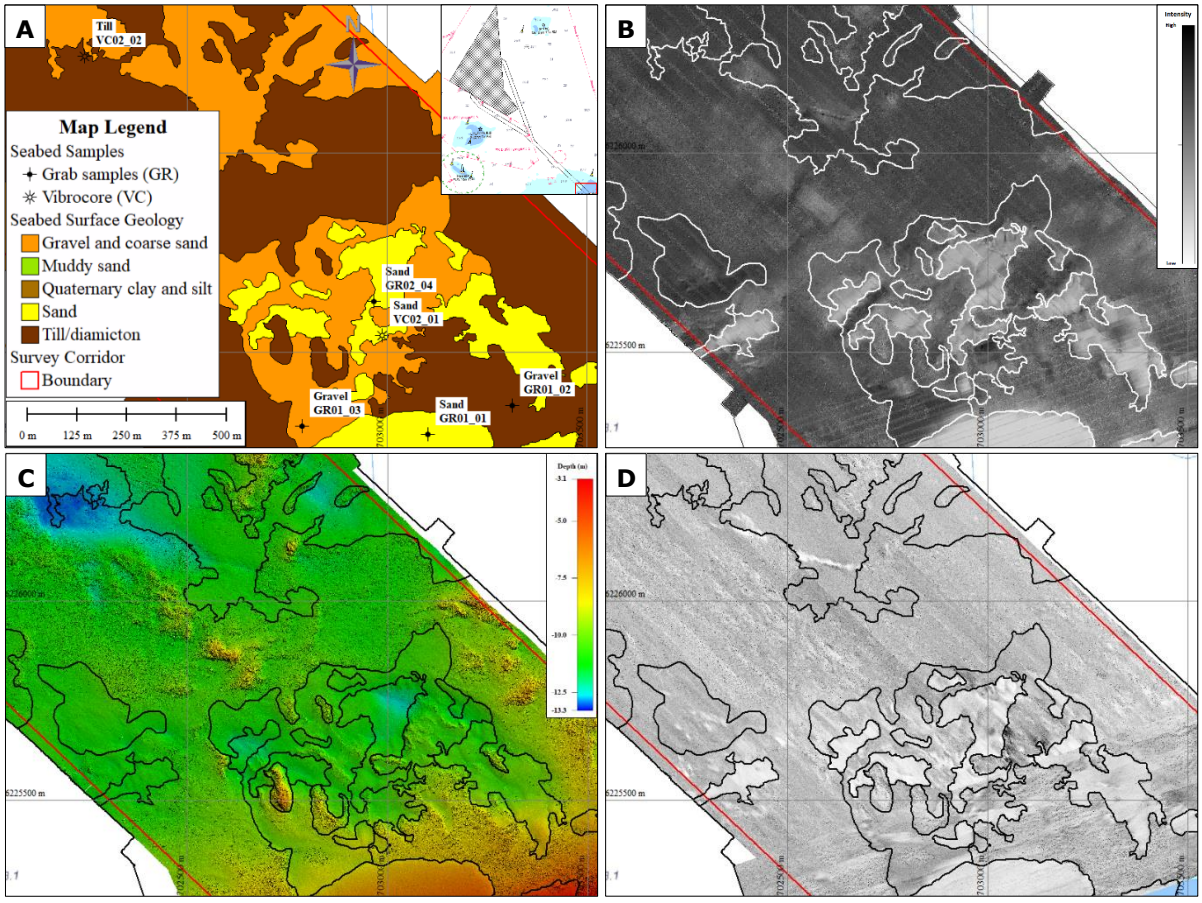

Figure 8-10: Showing the southern part of block 2 and the landfall area located in block 1. (A) Grab samples and vibrocores and the accompanying interpreted seabed sediment, (B) Backscatter intensities, (C) Bathymetry and (D) Low frequency side-scan sonar reflectivity.

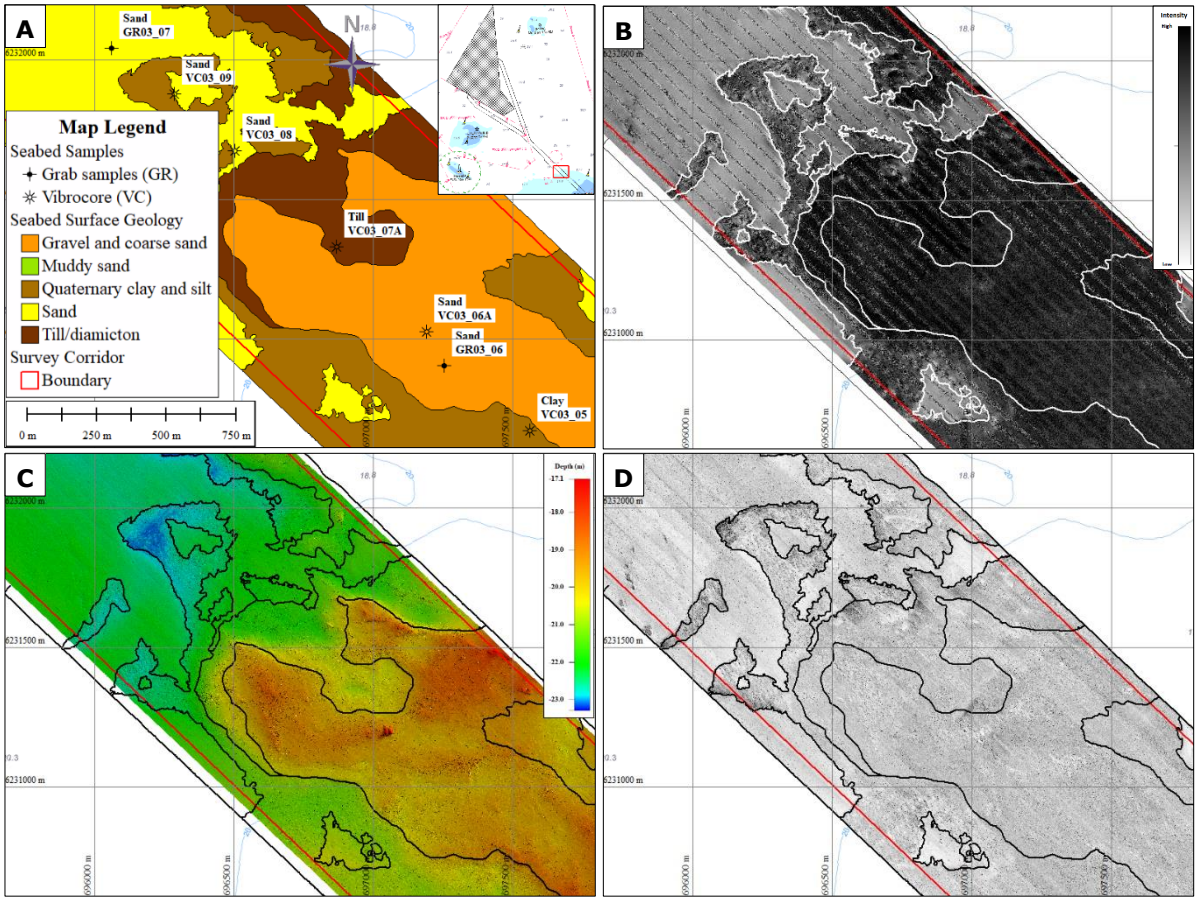

Figure 8-11: Figures showing the northern part of block 3, on the border between the nearshore and offshore part of the corridor. (A) Grab samples and vibrocores and the accompanying interpreted seabed sediment, (B) Backscatter intensities, (C) Bathymetry and (D) Low frequency side-scan sonar reflectivity.

Another example of seabed sediment classification is seen in figure 8-11, located further north in block 3. Seven seabed samples have been collected in this area with seabed sediment analysed as either *Sand*, *Clay* or *Till*. The same intensity and reflectivity patterns are observed compared to figure 8-10. The only variation for this area is the presence of clay. A small subtle change in backscatter is observed. The relative intensity for clay is between *Sand* (low intensity) and *Gravel/Till* (high intensity).
The large area interpreted as *Gravel* in the middle of figure 8-11(A) with two seabed samples indicating *Sand*, is a result of vast amount of large grain size particles and numerous boulders.

The offshore part of the corridor as seen in figure 8-12 is located inside block 5 and the start of block 6. Here seabed sediments changes from *Muddy sand* to *Sand* and *Gravel*. The gravelly area is a mixed sediment of till, coarse sand, slightly clayey and organic with shell fragments. Outside the gravel zone, the reflectivity is quite uniform meaning that there are no major sediment changes on the seabed.
The bathymetry data (figure 8-12(C)) is quite plane indicating that the areas are not affected be high energy systems, hence no areas with ripples or other natural surface morphology.

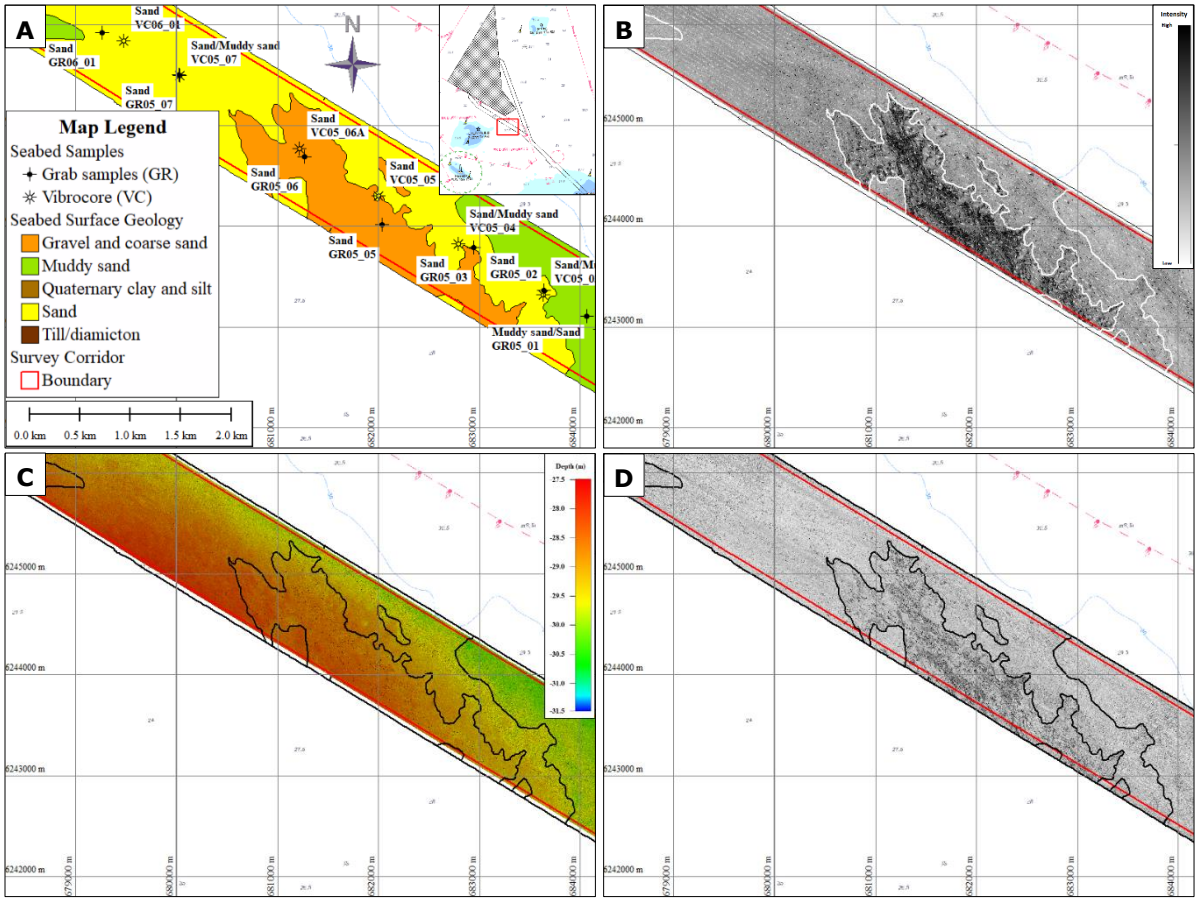

Figure 8-12: Figures showing an area of block 5 and the start of block 6 of the corridor. (A) Grab samples and vibrocores and the accompanying interpreted seabed sediment, (B) Backscatter intensities, (C) Bathymetry and (D) Low frequency side-scan sonar reflectivity.

8.5 Seabed substrate type

The integrated interpretation for classification of seabed substrate types, are closely following the same methodical as for the interpretation of seabed surface geology in section 8.4. The seabed substrate is divided into the following seabed substrate types, cf. the Danish Råstof-bekendtgørelsen (BEK no. 1680 of 17/12/2018, Phase IB):

- Substrate type 1 - Sand, silt and mud
- Substrate type 2 - Sand, gravel and pebbles
- Substrate type 3 - Sand, gravel and pebbles, and larger stones
- Substrate type 4 - Stony areas and stone reefs with 25-100% of larger stones

The seabed substrate types 1 to 4 is subdivided into seven substrate classes, and their definition is described in table 8-1.

Table 8-1 Seabed substrate types

Type	Description of seabed substrate types	Grain Size*
1a	Fine/medium sand, silty, soft bottom	0.06-2.0 mm
1b	Fine/medium sand, solid sandy bottom	0.06-2.0 mm
1c	Clay bottom	0.06-2.0 mm
2a	Medium/coarse sand, gravel and pebbles – few larger stones	2-20 mm + larger stones
2b	Medium/coarse sand, gravel and pebbles – seabed cover of larger stones 1% to 10%	2-100 mm + larger stones
3	Coarse sand, gravel and pebbles – seabed cover of larger stones 10% to 25%	2-100 mm + larger stones
4	Stony areas and stone reefs - seabed cover of larger stones 25% to 100%	2-100 mm + larger stones

* Larger stones: 10 cm and upwards

Figure 8-13 shows an overview of the interpreted seabed substrate types for the ECR corridor. The predominant seabed substrate along the corridor is of type 1 – either *sandy soft bottom (1a)* or *solid sandy bottom (1b)*. The area located in the southern part of the corridor (nearshore), is characterised by coarse sand, gravel and large amount of pebbles/stone at the seabed. Here the seabed substrate is varying between type 1 to 4.

Particle grain size distribution from sieve analysis and the amount of glow loss measured in the laboratory for the seabed samples, provide information on how to classify areas on the seabed. Figures 8-14 and 8-15, focus on areas with greater variations in the seabed. In figure 8-14, close to the landfall, areas with relative low backscatter intensities and bright colours in the side-scan sonar reflectivity together with no apparent boulders in the bathymetry and fine to medium grain size plus very little grow loss, are interpreted as *solid sandy bottom – substrate type 1b*.
When moving into darker colours in the backscatter and side-scan data, typical grain size distribution in the laboratory, moves from fine to medium to coarse particles. Together with information on the number of larger stones and boulders from the bathymetry, a further subdivision of the seabed substrate is necessary according to table 8-1. This detailed subdivision is seen in figure 8-14(A) and 8-15(A), as areas with light oranges, darker orange and black colours.
To distinguish between *solid sandy bottom* and *sandy soft bottom*, a closer inspection into the amount of glow loss and the presence of clayey-silty particles is needed. There is no exact and clear dissection in the laboratory results on glow loss and grain size distribution, but roughly with numbers of glow loss over 3% and with more than 30% grain size distribution below 0.063mm,

indicate a shift from solid to soft seabed substrate. This division follows close with the interpreted data from the sub bottom profiler.

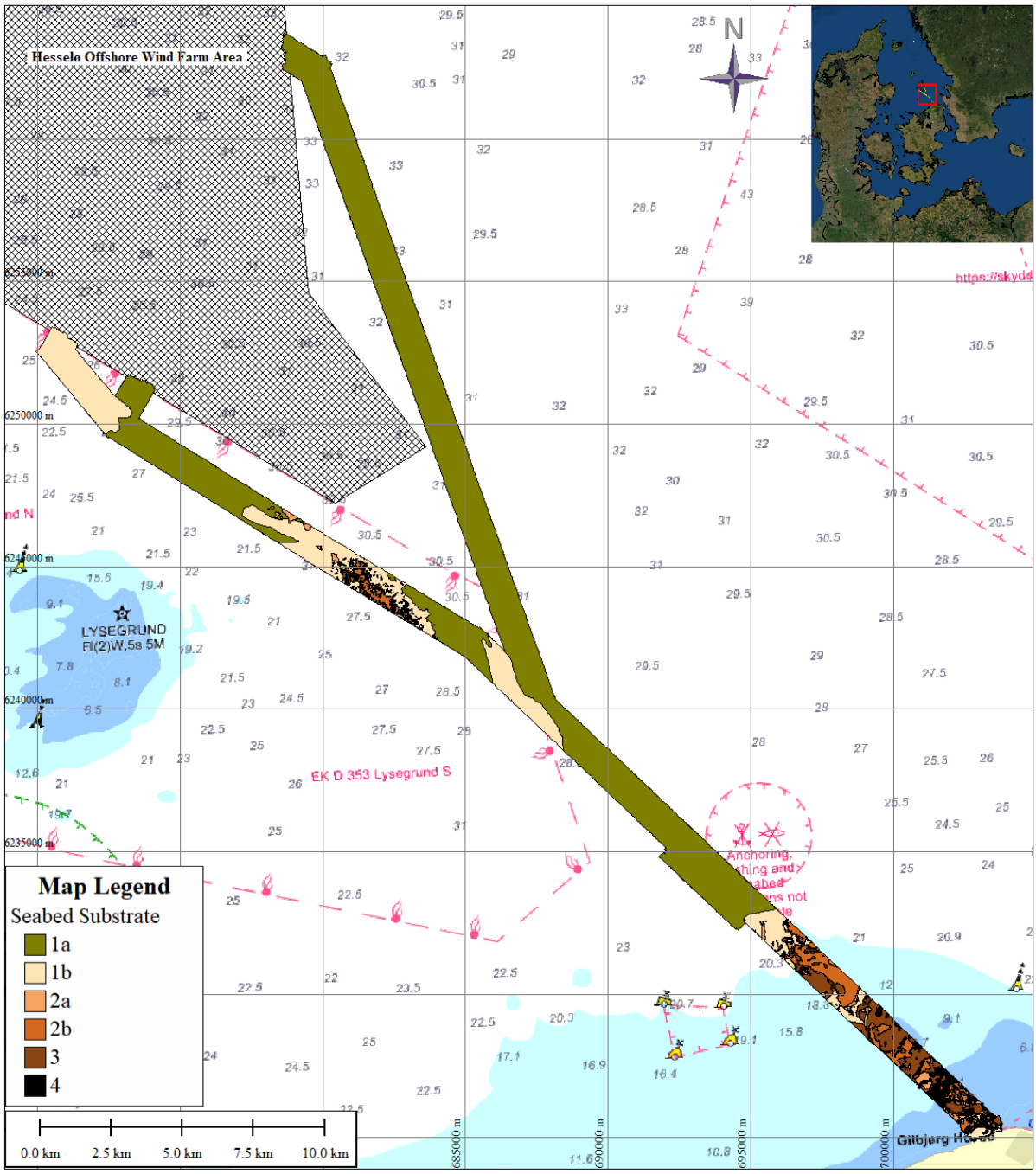

Figure 8-13: Overview of the interpreted seabed substrate types alongside the ECR corridor from Gilbjerg Hoved in the south to the OWF area in the north. Nearshore seabed substrate is a mix of type 1 to 4, whereas offshore seabed substrate is manly type 1.

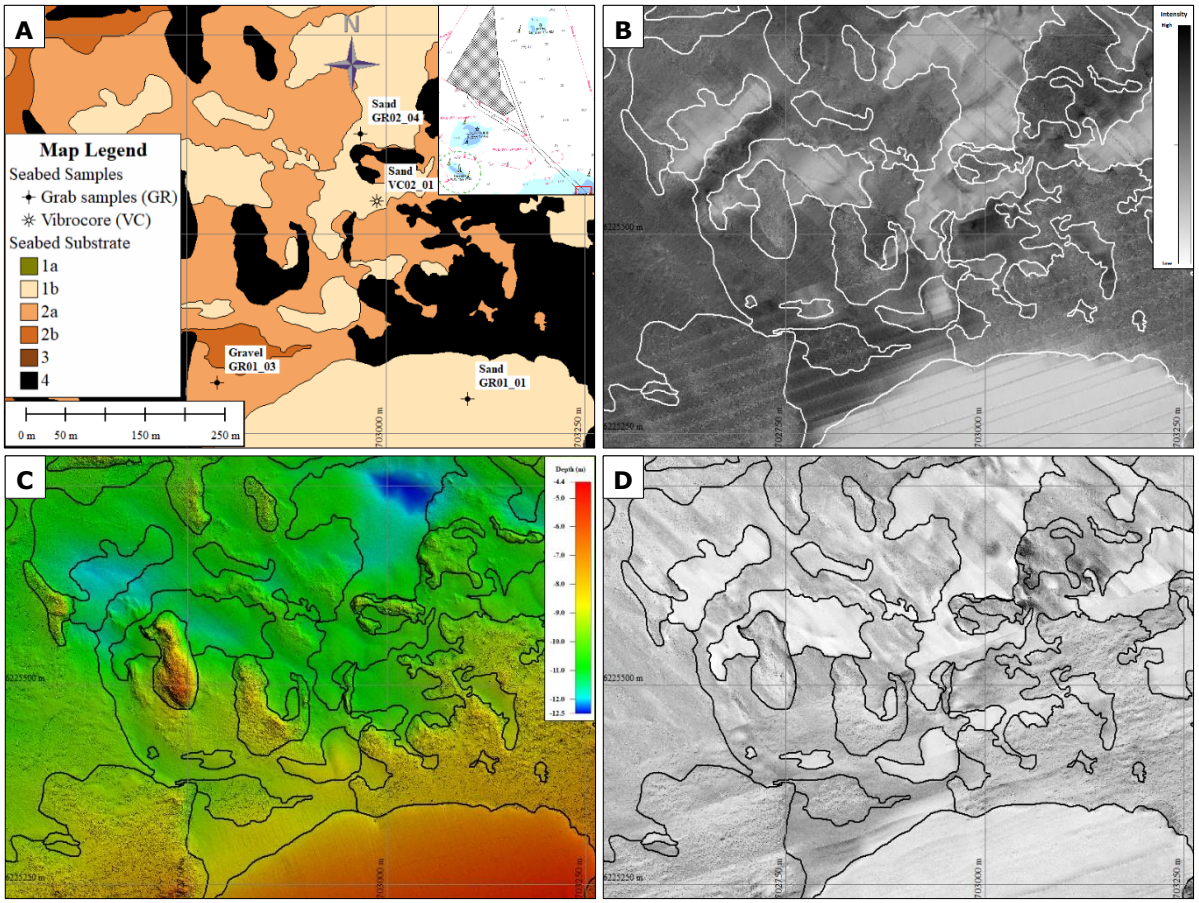

Figure 8-14: Example of seabed substrate types in the southern part of block 2 and block 1.

Figure 8-15: Example of seabed substrate types in the southern part of block 3.

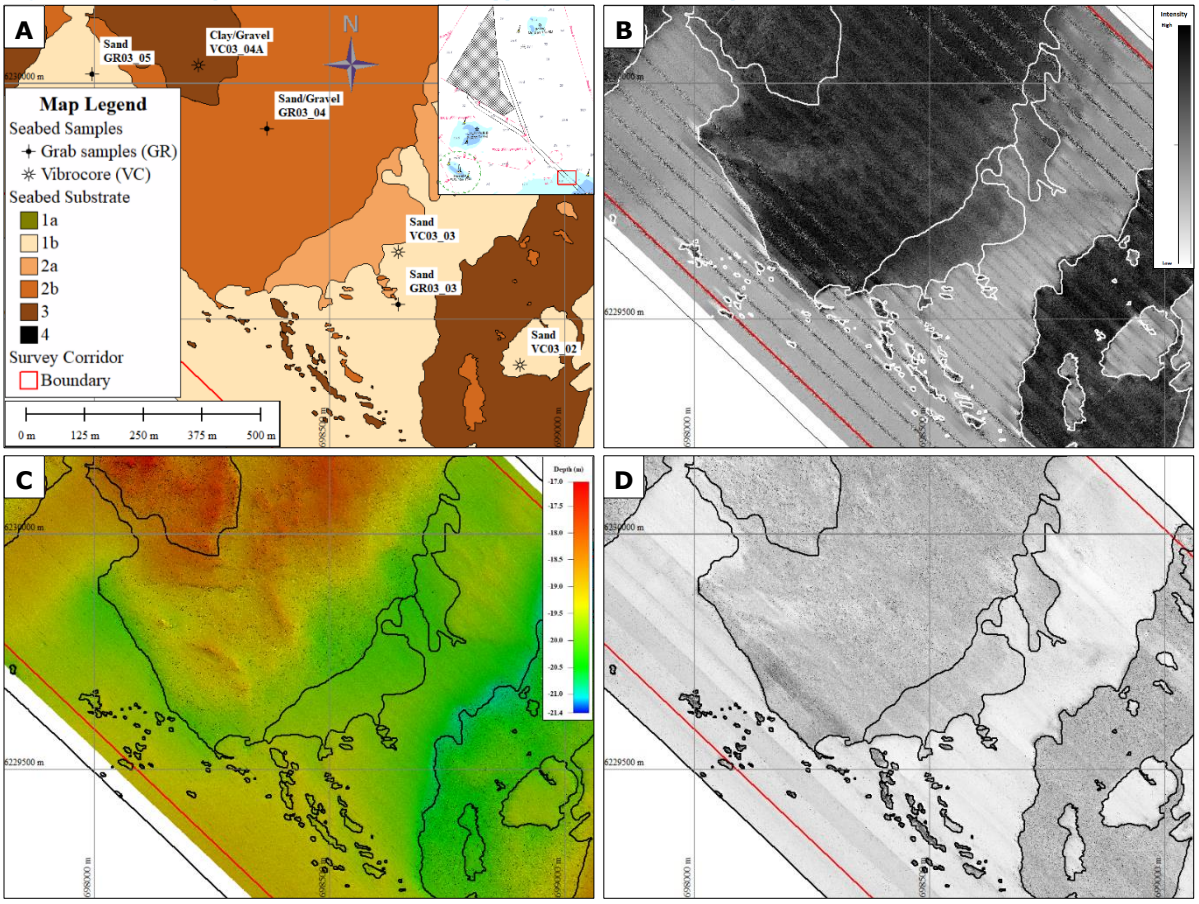

8.6 Seabed surface features

Observed and interpreted seabed surface features along the ECR corridor are listed here:

- Boulder field, Numerous
- Boulder field, Intermediate Density
- Boulder field, High Density
- Trawl mark area
- Anchor scars
- Pock marks
- Scour marks
- Positive/ridge-like feature
- Micro-depression
- Other

The feature classes do not include seabed forms and morphology such as *ripples, mega-ripples* and *sand waves*, since none have been observed in the available dataset.
The interpreted seabed surface features are mostly observed in the bathymetry data, but some features are also visible in side-scan sonar data and in the backscatter dataset. The following figures (figure 8-16 to figure 8-19) are examples of interpreted *point, lines* and *area features*.

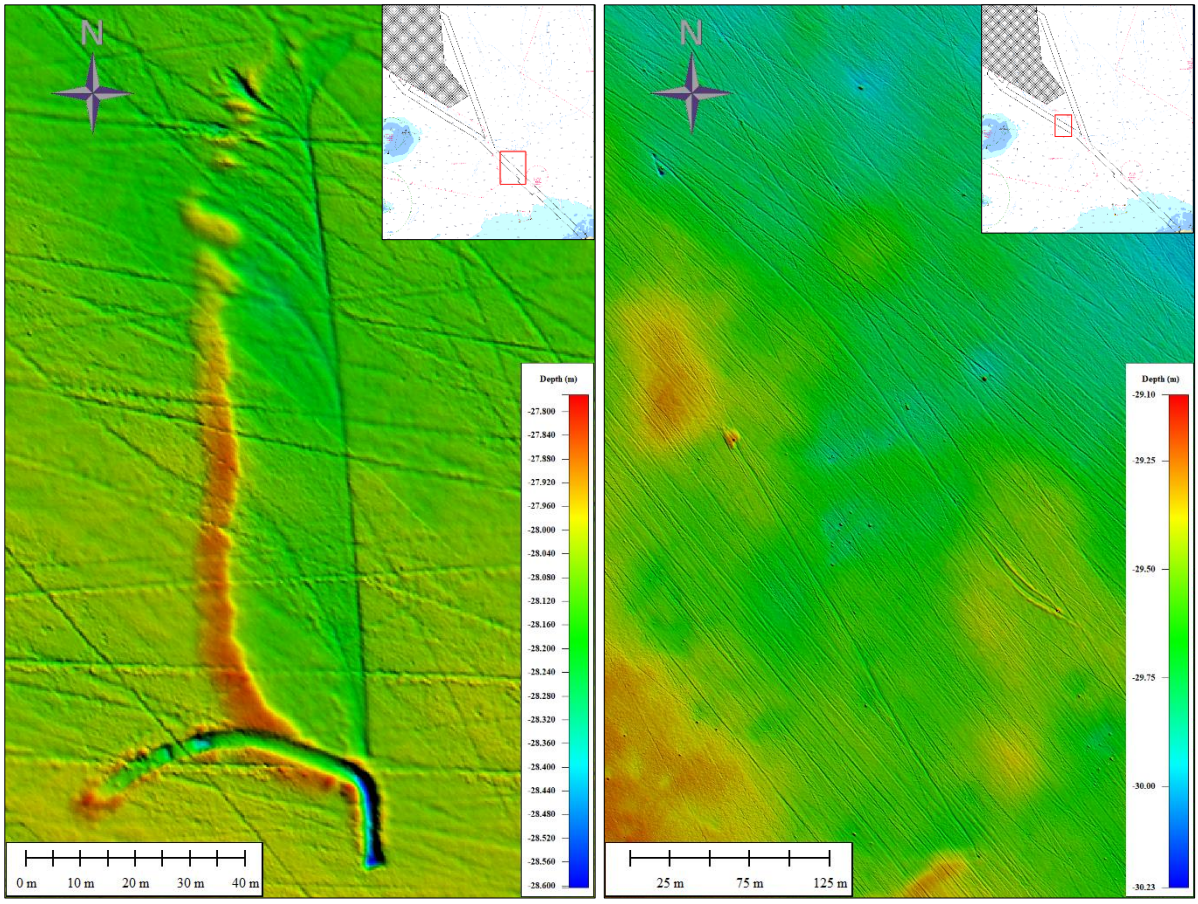

Figure 8-16: Examples of interpreted anchor scars and resulting scour marks along the ECR corridor. Background "lines" are interpreted trawl marks.

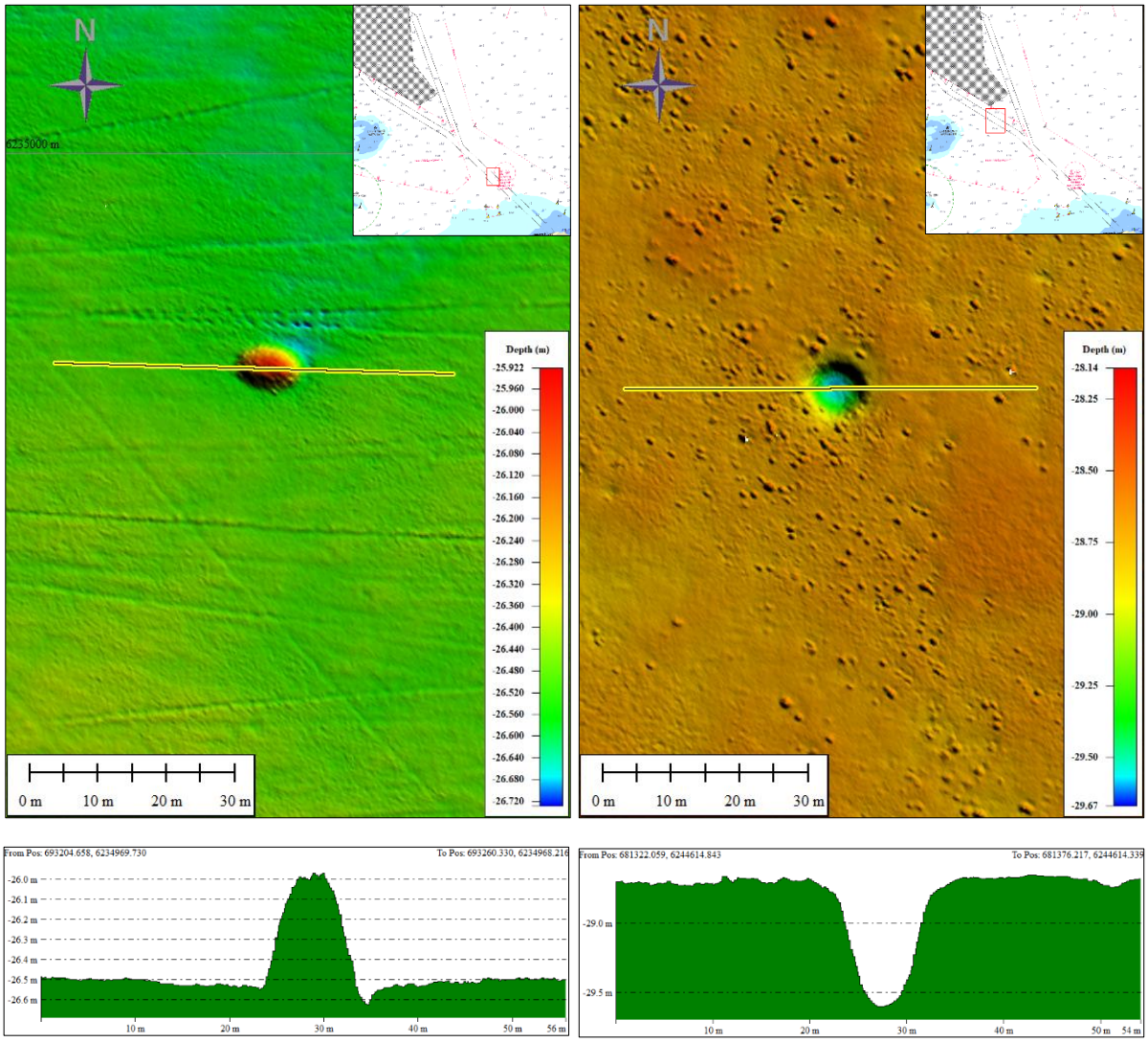

Figure 8-17: Examples of interpreted point features with depth profiles along the ECR corridor; (left) 60 cm high positive/ridge-like feature and (right) 90 cm deep micro-depression.

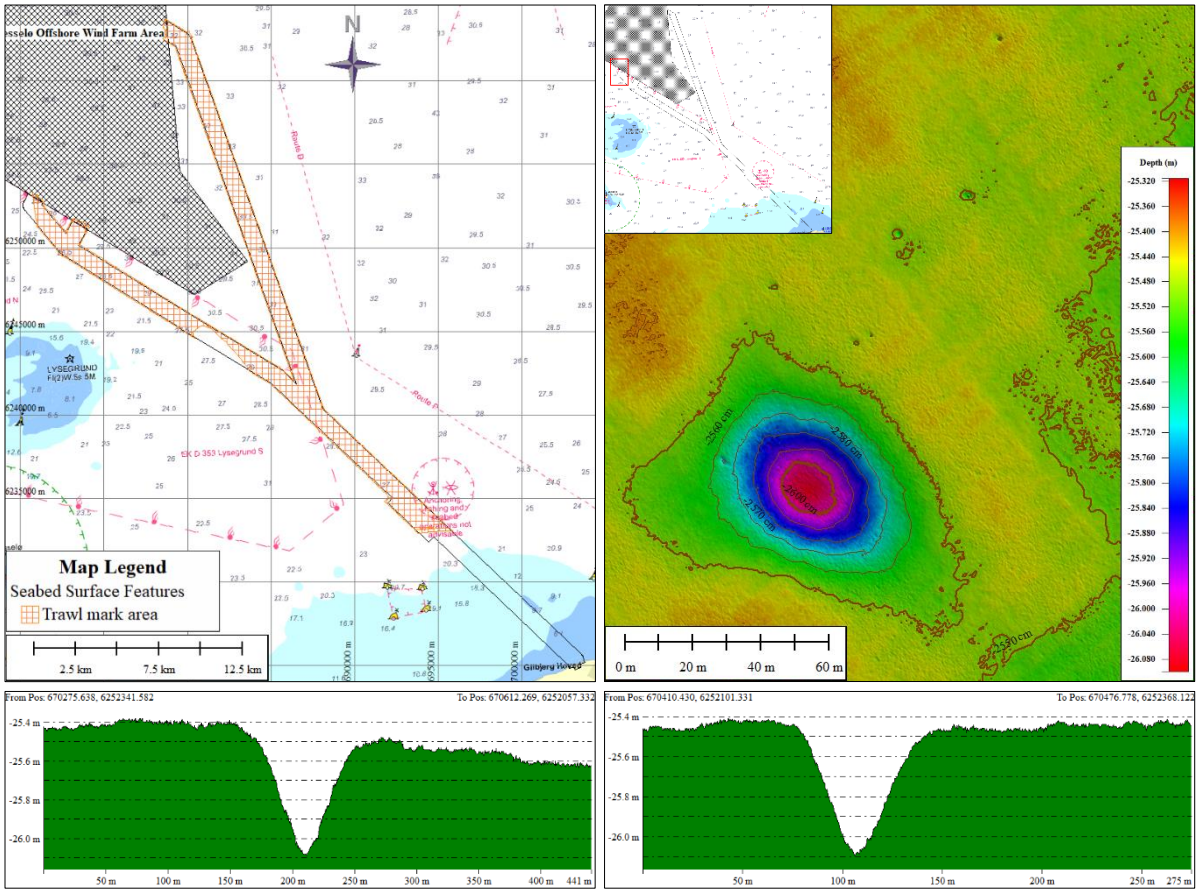

Figure 8-18: Examples of interpreted area features; (top left) Trawl mark areas. There are registered trawl marks in most of the offshore area along the corridor. (top right) 4000 m² large and 65 cm deep pock mark. (bottom left) West to East depth profile for the pock mark and (bottom right) south to north depth profile.

The most conspicuous features are the dense boulder fields towards land in block GL01 to GL03 where boulders built up reefs and a less dense field in GL05 and GL06. Further offshore in block GL03 including the remaining offshore blocks high density of trawl marks appears on the seabed only interrupted by anchor drag marks or depression. In GL12 a couple of north-south going positive ridge-like features appears on the bathymetry deviating with approx. 0.5m from the plane seabed, seen in figure 8-19.

In figure 8-20, three examples of the different types of interpreted boulder fields are seen. Low-density areas (*numerous* boulders interpreted), *intermediate-density* areas and *high-density* areas are interpreted.

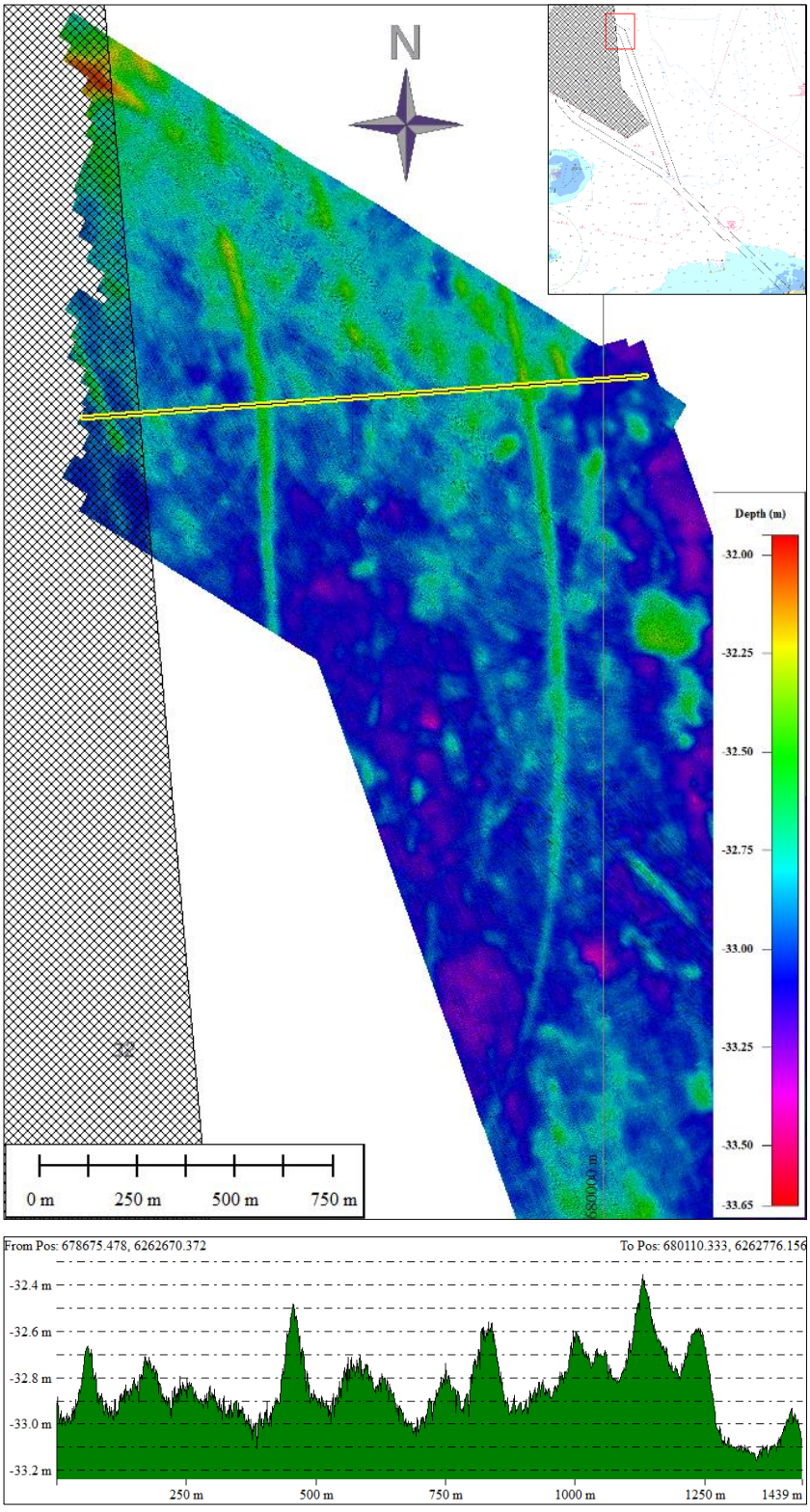

Figure 8-19: Figure showing special line- and area features observed in block 11 and 12 in the northern part of the ECR corridor. Up to 2.3 km long, 60 m wide and 50 cm heigh. No apparent traces are found in side-scan sonar or backscatter data.

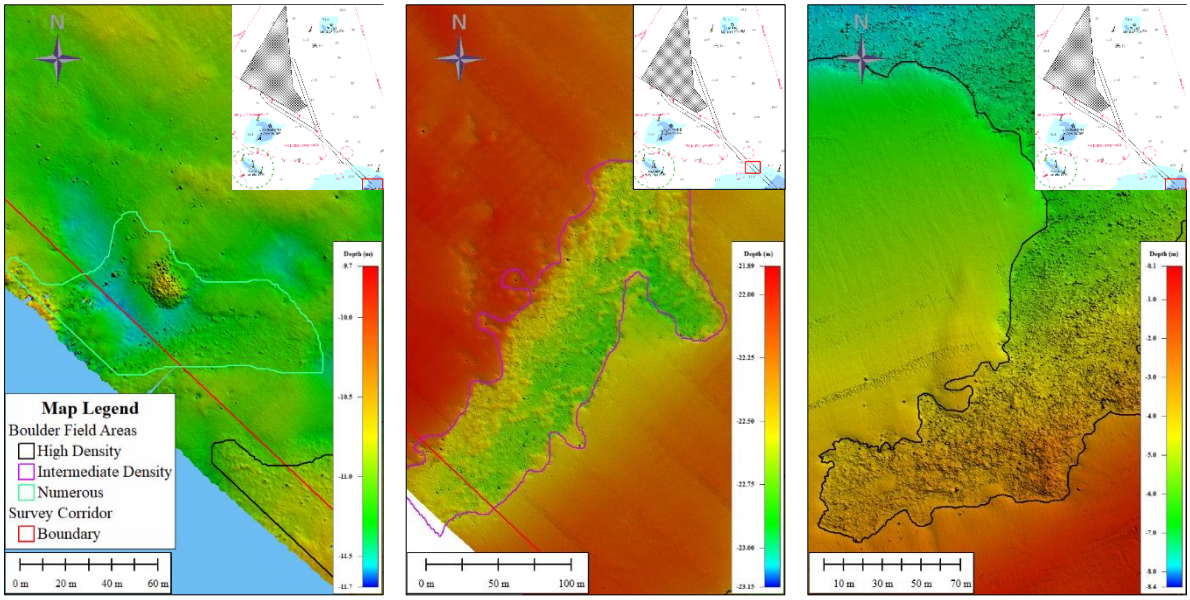

Figure 8-20: Examples of type of interpreted boulder fields; (left) Numerous boulders interpreted. (middle) Intermediate density of boulders. (right) High density of boulders interpreted.

An automatic boulder picking has been performed on the MBES data in Qimera and quality controlled in NaviModel. The algorithm uses the plane of each cell of the 25 cm bathymetry to define boulders with a minimum threshold of 30 cm. In total 89785 boulders were detected mainly located in the boulder fields towards land and a minor boulder field further offshore near the OWF site. From the automated pick the XY positions for each boulder was used to generate a density map, where the cable route was divided into 25x25m, 50x50m and 100x100m cells to highlight boulder fields and the density. For each cell the number of boulders is counted. An example of the 25x25m cell boulder field along the cable route located nearshore towards land in block GL03 can be seen in Figure 8.21.

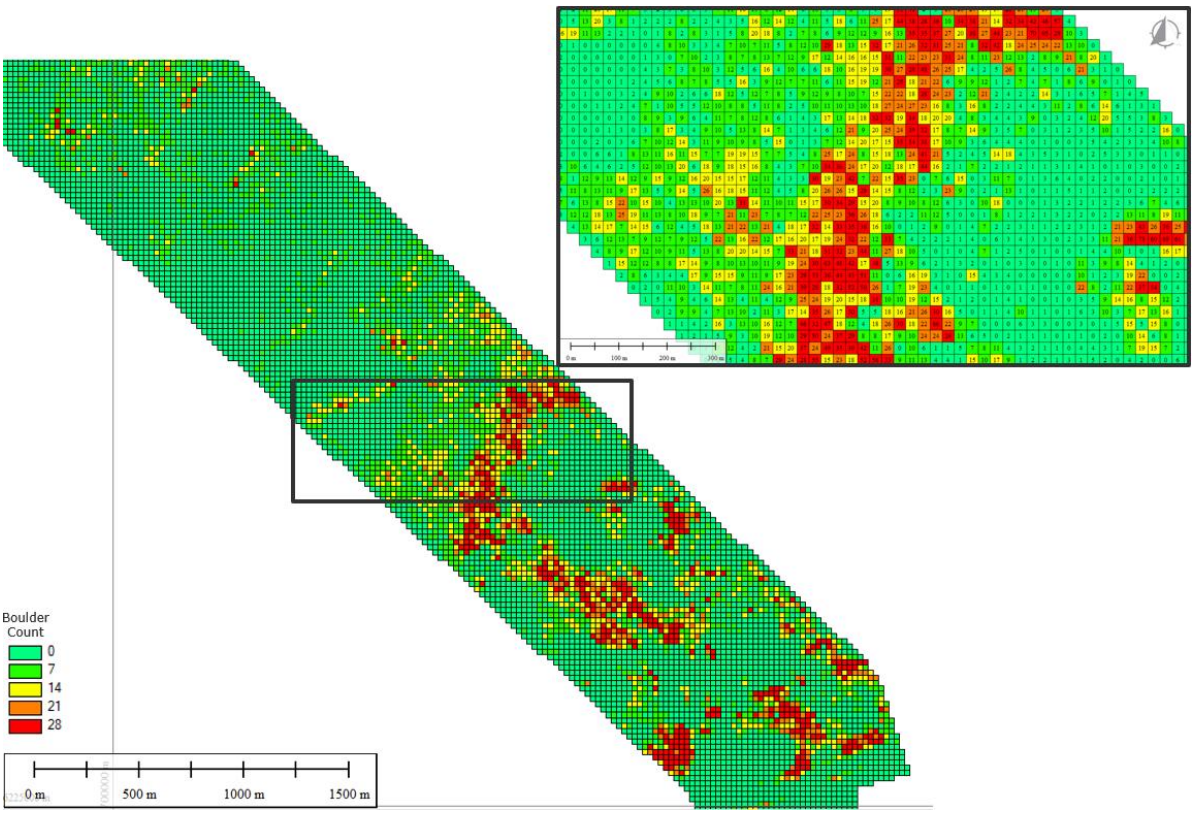

Figure 8-21. Boulder field classification chart. Grid cell size is 25 m x 25 m. Colours represent number of boulders within a cell.

An example of the 100x100m cell boulder field can be seen in Figure 8-22. These cells are defined as described in Table 8-2.

Table 8-2 Boulder zone definition

< 40 boulders (ø>0.5m)	Not a boulder zone (Numerous boulders)
40 – 80 boulders (ø>0.5m)	Boulder zone type 1: Intermediate boulder density
> 80 boulders (ø>0.5m)	Boulder zone type 2: High boulder density

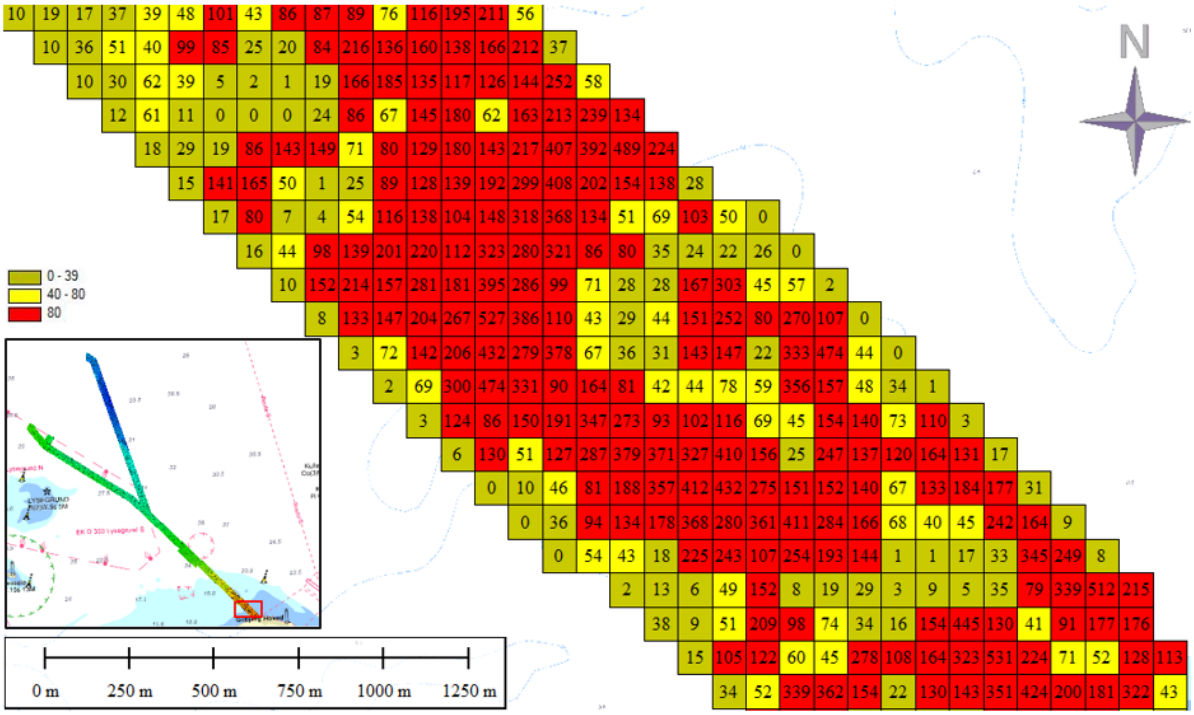

Figure 8-22 Example of the 100x100m cell boulder zones. Green indicates below 40 boulders per 100x100m, yellow indicates between 40-80 boulders and red indicates more than 80 boulders per zone

In addition to the square cells, polygons delimiting boulder areas have been produced and provided as part of the digital data package (the polygons representing the boulder fields are included in the geodatabase, the SEABED features dataset, divided using criteria in Table 8-2). However, it should be underlined that the square cells are a great tool to use to identify high density boulder areas.

Boulder area polygons are mapped along the cable route using the 25x25m cells after the automated polygons are derived from the 25x25m cells the boulder areas are aligned with the MBES 25 cm grid in order to highlight the exact boulder field. Figure 8-23 shows an example of the boulder area polygon above the 25x25m boulder polygon cells. The example is from the nearshore part close to landfall where the boulder fields are of high density.

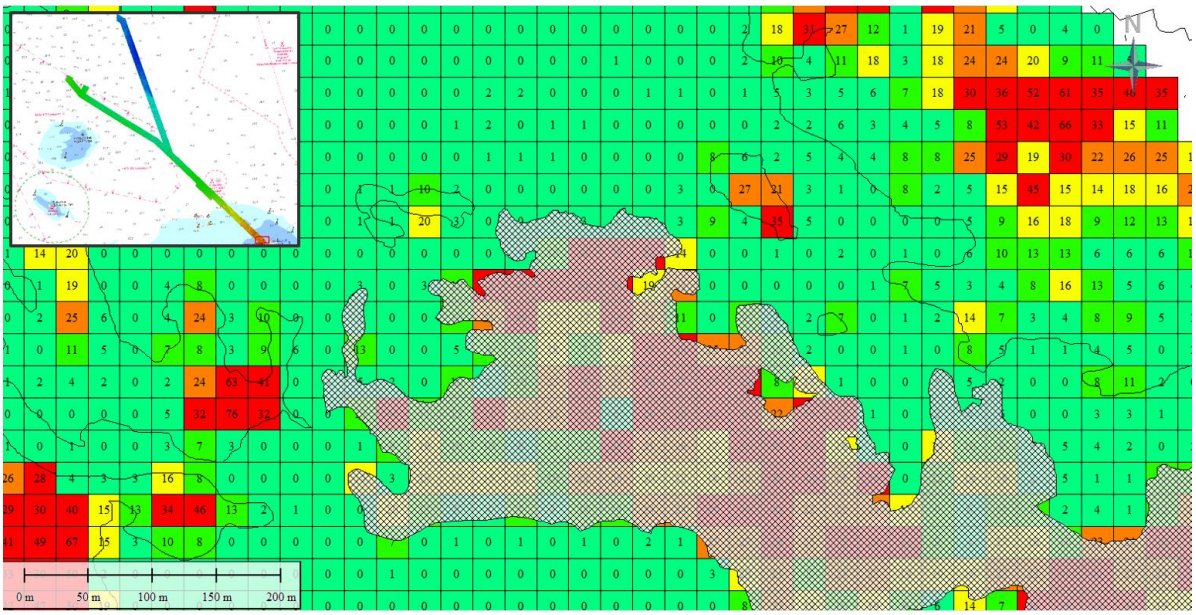

Figure 8-23 An example of the boulder field area polygon above the 25x25m boulder field cells. The hatched area indicates a high-density boulder field derived from the 25x25m boulder cells and adjusted using the 25cm MBES grid

Also, a XY file is created which is the direct export from Qimera, this file includes information of each detected boulder in terms of width, length and height. The distribution of boulders sorted by height, width and length can be seen in below histograms in Figure 8-24 to Figure 8-26.

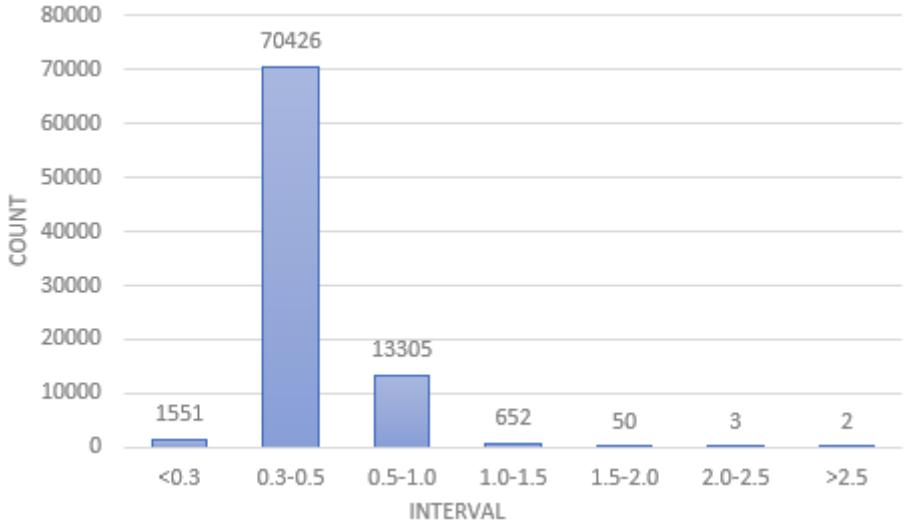

Figure 8-24 Automated boulder picking sorted by Height (Interval is in meters)

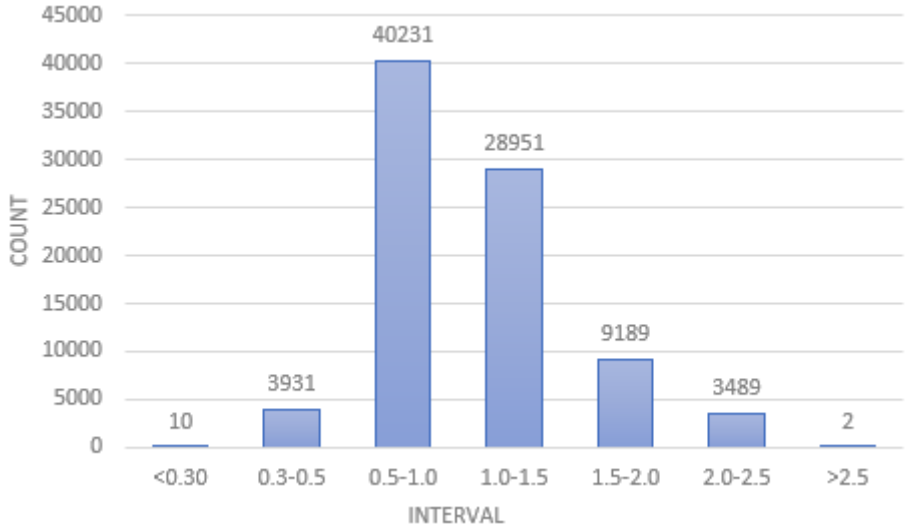

Figure 8-25 Automated boulder picking sorted by Width (Interval is in meters)

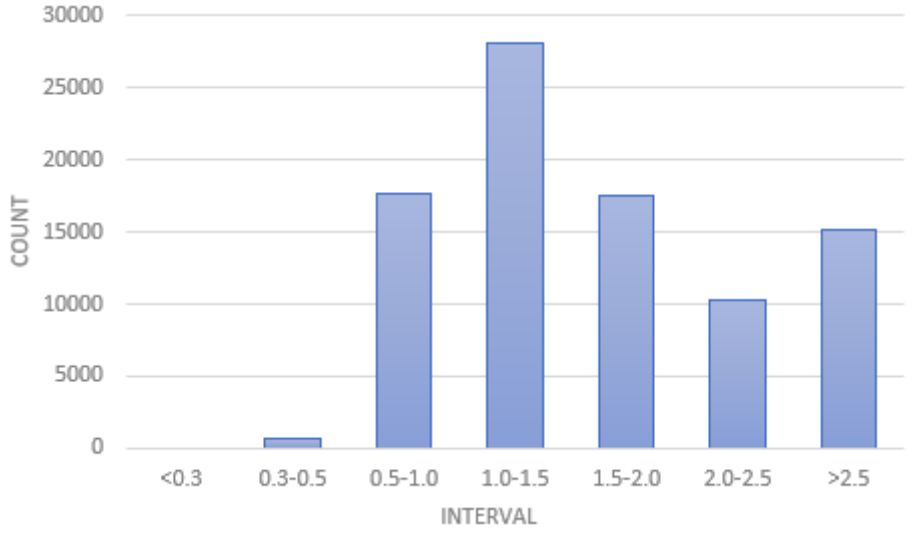

Figure 8-26 Automated boulder picking sorted by Length (Interval is in meters)

8.7 Subsurface geology

Interpretation of the recorded Innomar sub-bottom profiler (SBP) data has been performed with a spacing of approximately 45 m in the whole survey area. Vibrocores, boreholes, cone penetration tests as well as grab sampling results have been used to support the interpretation. An overview over vibrocore locations is presented on the Figure 8-27.

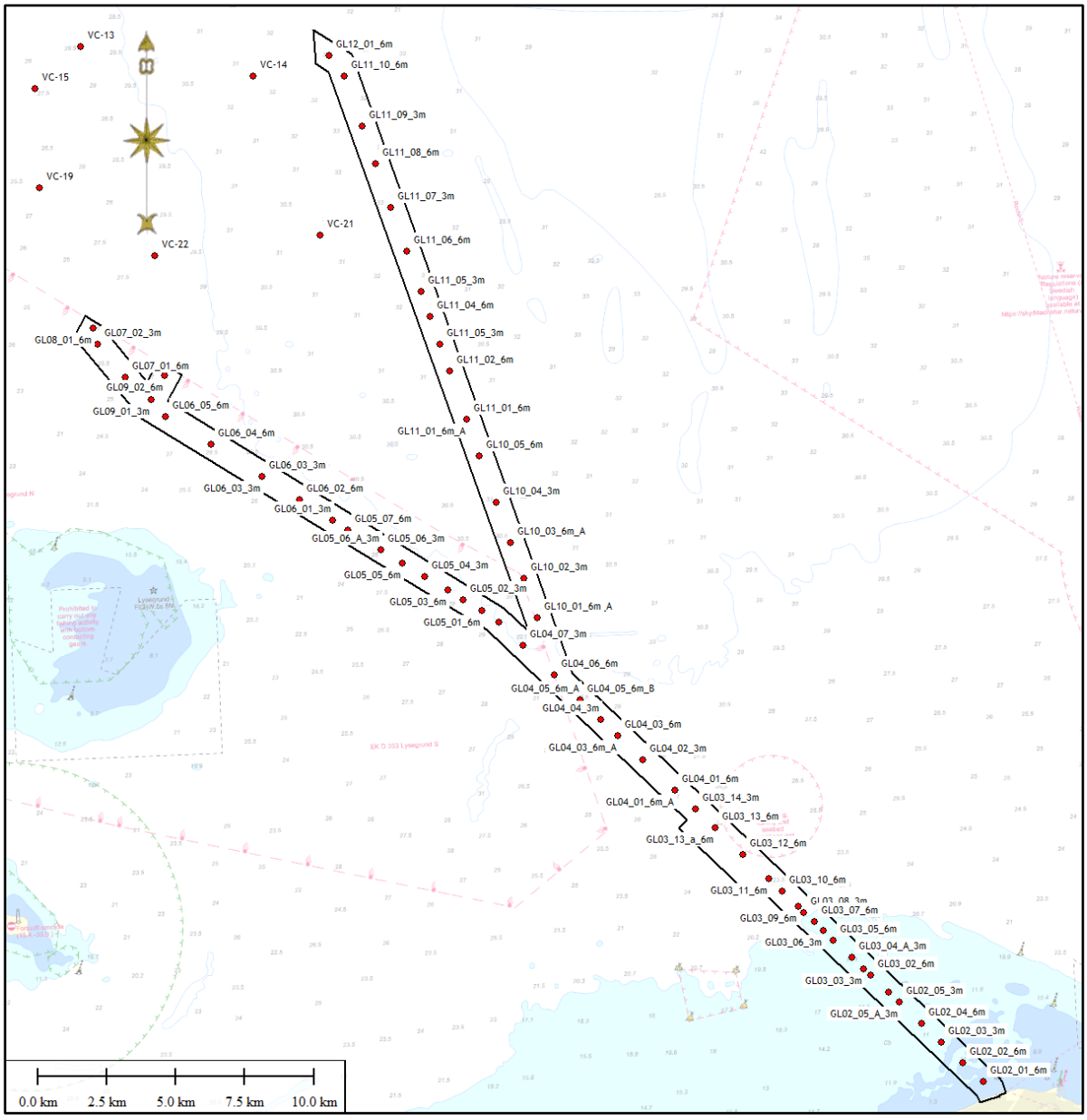

Figure 8-27 Overview over vibrocore positions along the cable corridor.

8.7.1 Integrated data interpretation

The process of producing a final ground model for the Hesselø OWF cable corridor included:

- Review of the existing geological information in order to establish a regional and local geological understanding of the area as well as soil unit classification.
- Import of the acquired SBP and MBES data into the Kingdom project.
- Import of the geotechnical data acquired into Kingdom. This data included soil unit boundaries as well as CPT logs: Cone tip resistance (qc), Sleeve friction (fs) and Pore pressure (u2) and Friction ratio (Rf). Subsequently, the soil unit boundaries were verified against the seismic data. Locations where misalignment between geophysical and geotechnical data had been found were discussed at early stage of the project during several internal interface meetings. As a result, most of the conflicts have been resolved.

- Import of the seabed sediment classification based on the side scan sonar, backscatter and multibeam data and into the Kingdom project. The imported seabed geology classification is reconciled with grab sampling and vibrocore results (for details see paragraph 8.5 Seabed Surface Geology). Subsequently, the seabed classification has been verified against the SBP data and, were necessary, updated in order to align with the interpreted geological soil units outcropping the seabed. It can be concluded that, except at very few locations, the correlation between the seismic and geotechnical data as well as seabed geology classification based on SSS and grab sampling results is good.

- Data interpretation. The choice of seismic reflectors to interpret has been decided based on the soil units defined in the BH/CPT locations as well as understanding of the local geological conditions and the existing sequence stratigraphic geomodel developed for the southern Kattegat region in the previous studies /1/. In addition, while interpreting the boundaries, potential hazards such as shallow gas have been mapped.

- Gridding of the interpreted horizons in 5x5m resolution and export of surfaces representing relevant soil unit boundaries (both relative to vertical datum and in depth below the seabed) as well as thickness maps generated by simple subtraction of grids.

A workflow illustrating the integrated data interpretation approach is shown on the following Figure 8-28.

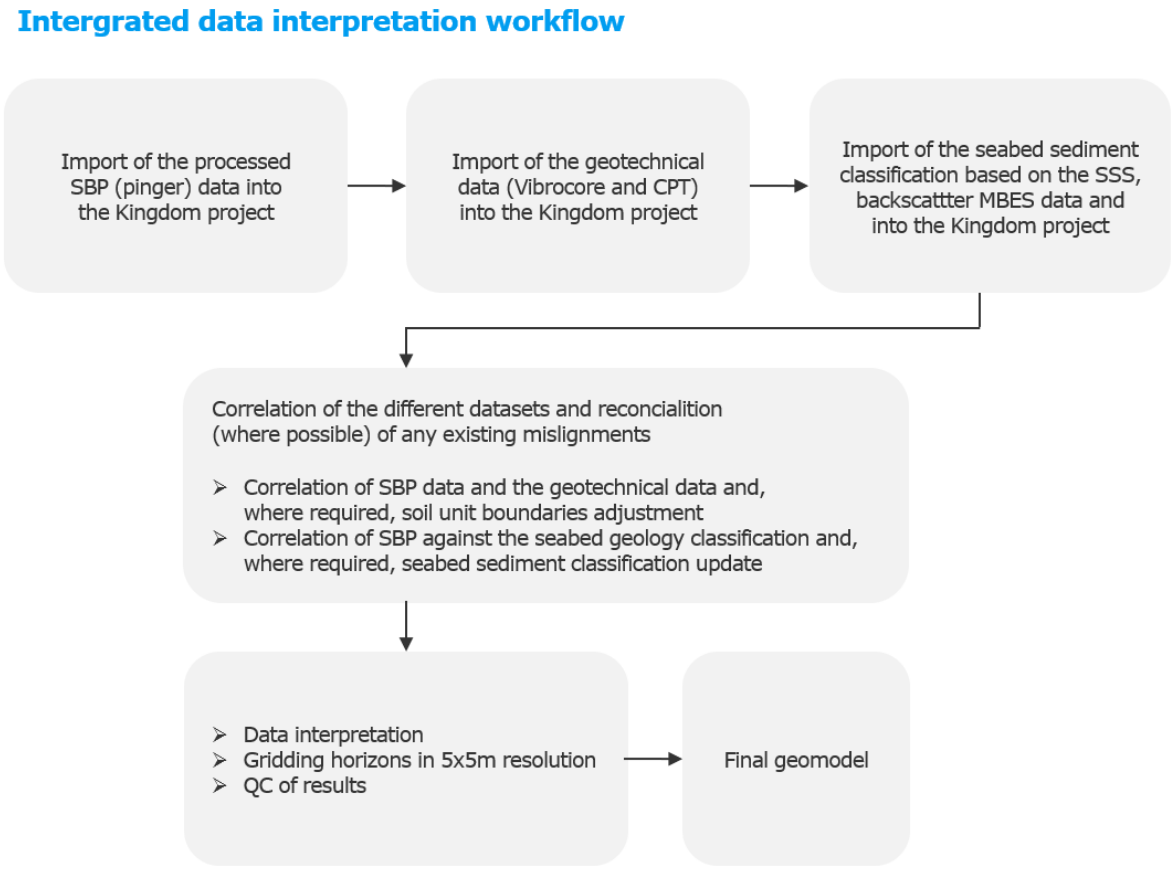

Figure 8-28 Workflow illustrating the integrated data interpretation approach

8.7.2 Time-Depth Conversion

No sonic logs (Vp) have been recorded during the survey campaign and therefore seismic velocities could not have been precisely defined. Velocities within the sedimentary succession in the southern Kattegat has been assessed during previous studies. At the site M0060B – a deep drilling located just north from the study area (for details, refer to /1/), geophysical well logging

was completed in 2013 as part of the Ocean Drilling Program (IODP). Seismic velocities measured for the Late- and Post Glacial vary at this location between 1530 and 1660 m/s (see Table T14, p.122 in /1/).

Based on the results of the previous studies /1/ an average velocity of 1600 m/s (typical for shallow marine sediments) has been used to convert depths to the geological unit boundaries to two-way-time for the sedimentary column. For the water column, seismic velocity of 1485 m/s was used to convert MBES data to two-way-time, which corresponds to the average velocity measured with the sound velocity probe during the survey campaign (see Figure 8-5 in this report).

Figure 8-29 shows correlation between MBES data, geotechnical soil unit boundaries and SBP data at an example location GL04_01_A, survey line 20085_MTK_GL_04_C000_SES_20201024_053005_RAW_LF. The selected velocity values resulted in a good correlation between the different datasets.

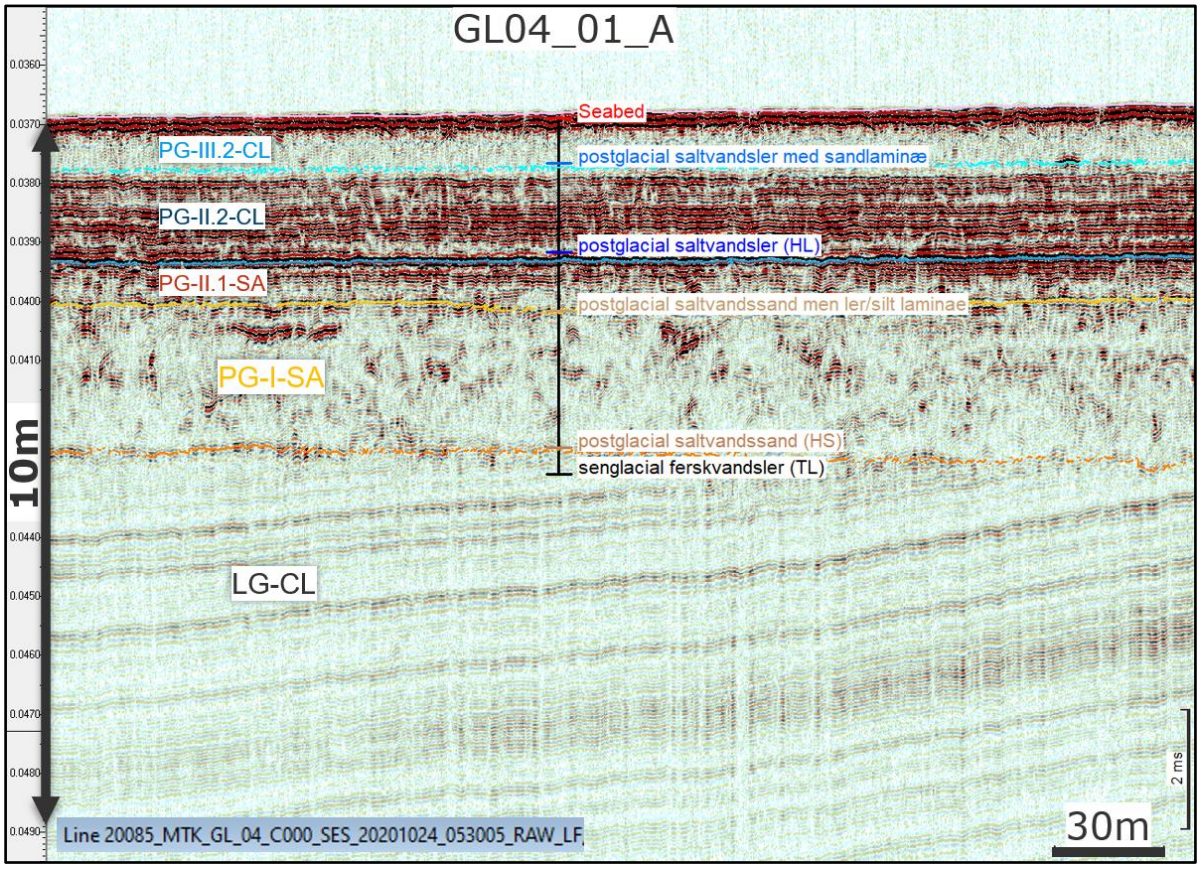

Figure 8-29 Correlation between MBES data, geotechnical soil unit boundaries and SBP data at an example location GL04_01_A, survey line 20085_MTK_GL_04_C000_SES_20201024_053005_RAW_LF

8.7.3 Results and description of the geological units mapped

As mentioned earlier in this report (see Chapter 7), this study adopts GEUS' division of the Quaternary sediment succession into geological units that are described below. A summary of the interpreted horizons is shown in the Table 8-2.

8.7.3.1 Glacial deposits (GL)

Glacial sediments have been penetrated at 7 locations in the southernmost part of the cable route (GL02_02, GL02_03, GL02_05, GL03_01, GL03_04, GL03_06, GL03_07) and at 3 locations along the western arm of the cable route (GL05_04, GL05_06, GL06_02).

Within the OWF Hesselø cable corridor glacial deposits are generally represented by clay tills and sand tills formed out of the ground moraine material of glaciers and ice sheets. In the vibrocore GL_02 glacial tills are interbedded with glacial meltwater deposits (meltwater clays).

The lithological composition as well as geotechnical parameters vary significantly within the till packages. In the vibrocore GL05_04, where glacial tills are found at depths between 0.2 m and 3.3 m below the seabed, the till has been described as very sandy and weak, while at the location GL05_06 the till also contains sand but has normal strength in the uppermost part and it becomes weaker with depth.

The seismic signal is strongly attenuated when penetrating into the glacial deposits and it is therefore not possible to precisely indicate the lower limit or the lateral boundaries between the different glacial packages. Hence, the glacial succession has not been subdivided further and the unit GL includes all glacial deposits.

On the acquired SBP data, the unit is characterised by chaotic internal reflection pattern or lack of internal reflectors, as shown on the Figure 8-30. The seismic recordings did not penetrate to the lower boundary of the glacial deposits what makes it impossible to assess the total thickness of this unit.

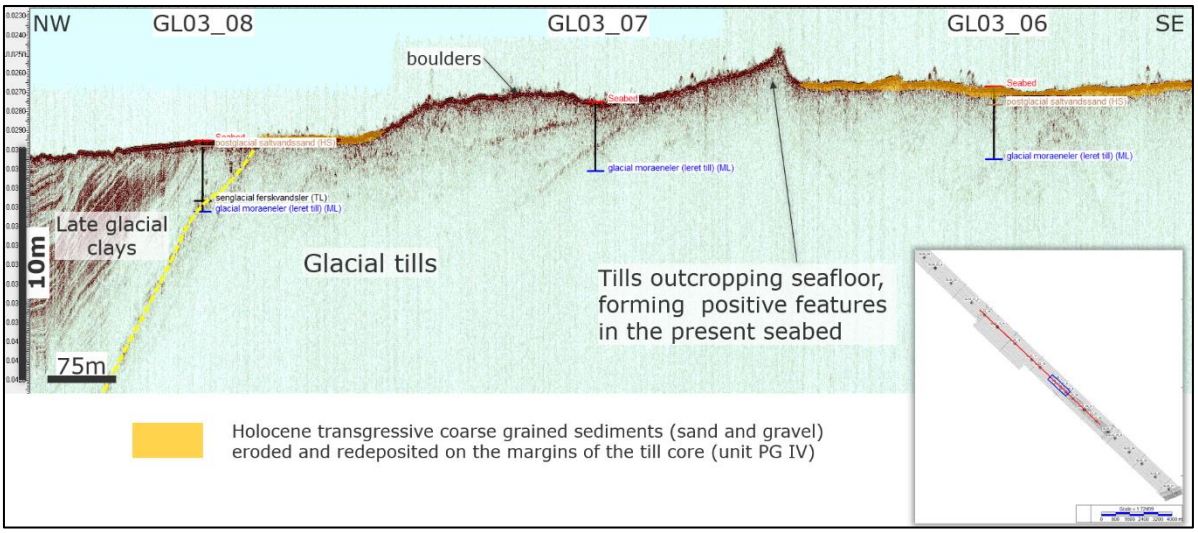

Figure 8-30 Seismic character of the glacial deposits (GL), line 20085_MTK_GL_03_C000_SES_ _20201024_103720_RAW_LF. Note that parts of the ridges composed of harder material form positive features at the present seabed, and the fact that presence of glacial tills at the seabed can be associated with presence of boulders clearly seen on the SBP data.

Two major ice marginal ridges cross the cable corridor area just south from the Hesselø OWF site as well as its southernmost part /1/ (see Figure 8-31). As described by GEUS, the interpretation of retreating ice marginal ridges is supported by the seabed surface sediment map where the ridges in general consist of till, often superimposed by a thin layer of Holocene transgressive sand and gravel, coastal sediments eroded and redeposited on the margins of the till core /1/ (see Figure 8-31).

The extent of glacial deposits along the cable corridor supports the previous studies and can be correlated to the presence of the ice marginal ridges, as indicated in /1/. Figure 8-31 shows areas of the cable Hesselø OWF cable corridor where the glacial deposits have been found close to the seabed, while Figure 8-32 shows depth to the top of the till deposits in the western arm of the cable route (Figure 8-32, left) and in the southern part of the corridor (Figure 8-32, right).

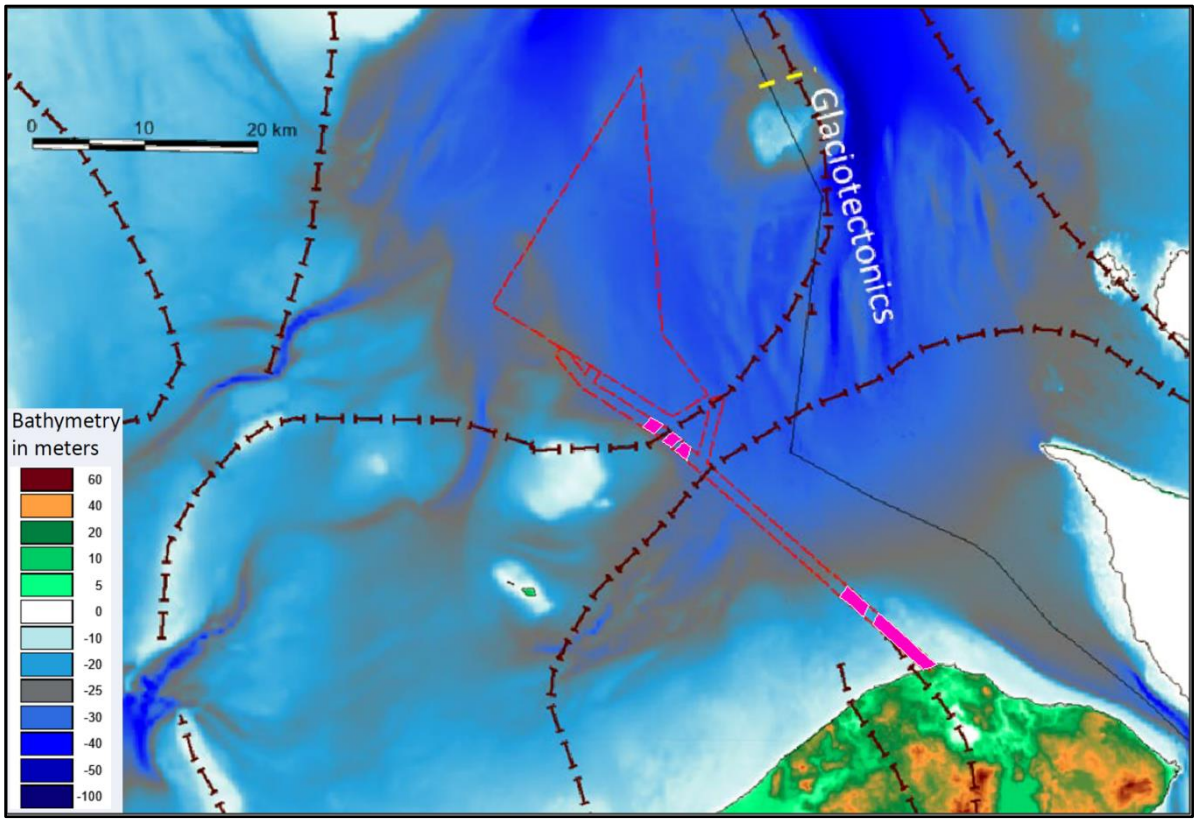

Figure 8-31 Distribution of the glacial deposits (GL) along the cable corridor. The areas where glacial sediments have been identified close to the seabed are marked with pink. Ice marginal ridges interpreted in the previous studies in the southern Kattegat region are marked with black, as in /1/. In the background – bathymetry from Emodnet. Figure modified after /1/.

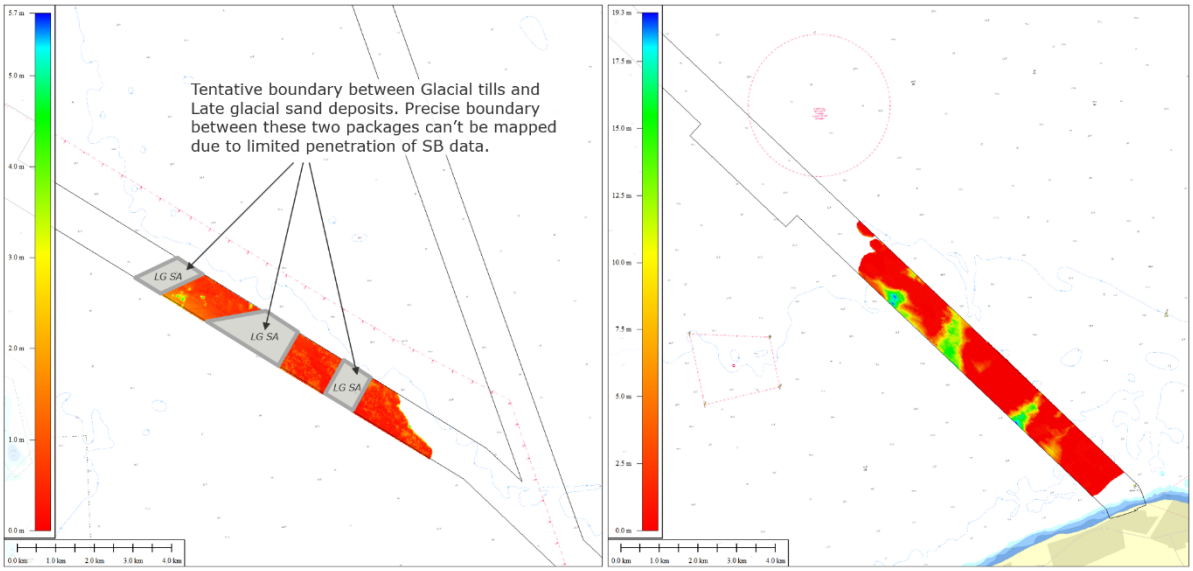

Figure 8-32 Depth in meters below seabed to the top of the Glacial succession (GL).

8.7.3.2 Late Glacial deposits (LG)

Late Glacial sediments are widespread in the southern Kattegat and are found both in the basin areas as well as in the deeply eroded channels. Accordingly, this unit has been penetrated at many locations throughout the entire cable corridor. In the southernmost part (along block GL02 and GL03) it forms laterally limited channel infills within the glacial succession (see Figure 8-33), while towards the north (north from the location GL03_08) both, thickness and lateral extent of the succession increase significantly, as shown on the Figure 8-30.

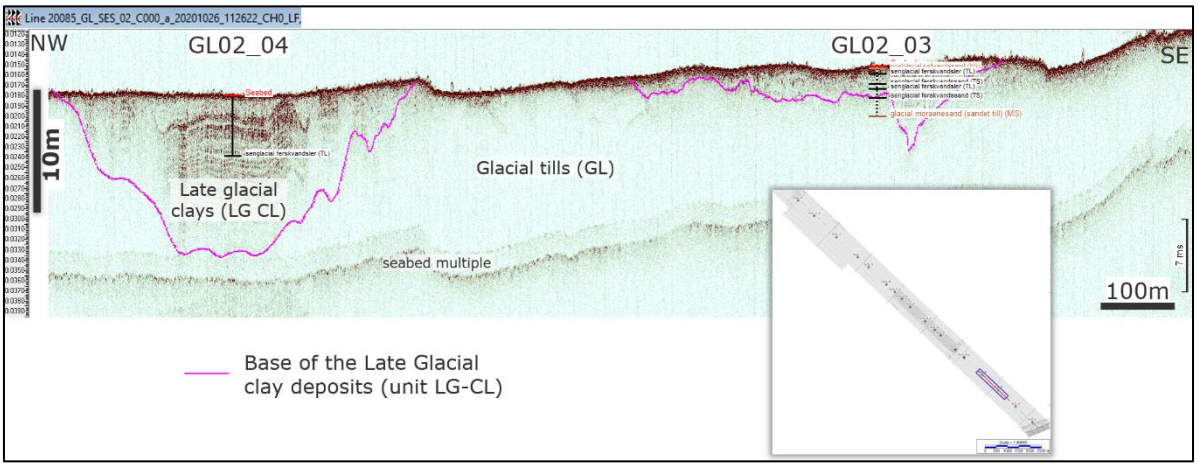

Figure 8-33 Late Glacial deposits forming channels within the glacial succession in the southern part of the cable corridor (south from the location GL03_08). Line 20085_MTK_GL_SES_02_C000_a_ _20201026_112622_CH0_LF.

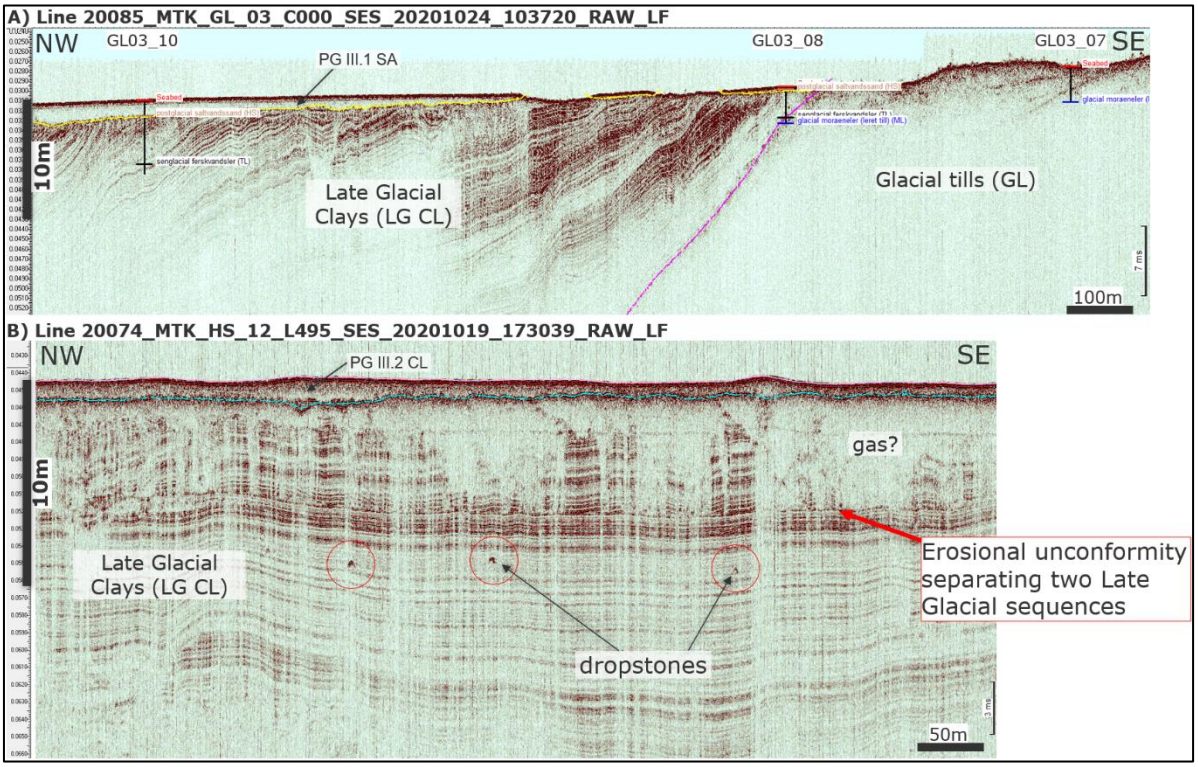

Figure 8-34 Late Glacial sediments deposited in the deeper parts of the Late Glacial basin depositional area. A) Line 20085_MTK_GL_03_C000_SES_20201024_103720_RAW_LF, B) Line 20074_MTK_HS_ _12_L495_SES_20201019_173039_RAW_LF. Note significant thickness of the Late Glacial succession with its base below the penetration depth of the SBP data.

Within the cable corridor this unit is generally composed of soft, silty, locally sandy (or with sand laminae) clays characterised by high plasticity- as described in the vibrocores GL11_04 and GL12_01 located close to the Hesselø OWF site. These soft clays are interpreted as glaciomarine infill of the Late Glacial basin. The acquired SBP data has not penetrated to the lower boundary of the Late Glacial glaciomarine deposits as they can reach significant thicknesses of up to 75 m /1/ (see Figures 8-34 and Figure 8-35). Therefore, the base of the Late Glacial clays could have been mapped in selected areas only.

The internal reflection pattern if the unit is characterised by presence of pronounced parallel and continuous reflections reflectors, as illustrated on the Figure 8-34.

The southern and the central parts of the cable corridor are located in the marginal part of the Late Glacial basin and the succession is represented here by coarser-grained deposits characteristic for more proximal environments.

Sand found at locations GL03_11, GL04_03, GL04_05, GL04_06, GL04_07 and GL04_08 forms the upper part of the Late Glacial sequence. Its precise thickness is unknown as the SBP-data did not penetrate the lower boundary of these deposits (see the Figure 8-35). Based on the available seismic data, it can be concluded that Late Glacial sands form a relatively thick upper part of the Late Glacial succession and extends along the block GL04 and GL05, between vibrocores GL04_03 and GL05_01.

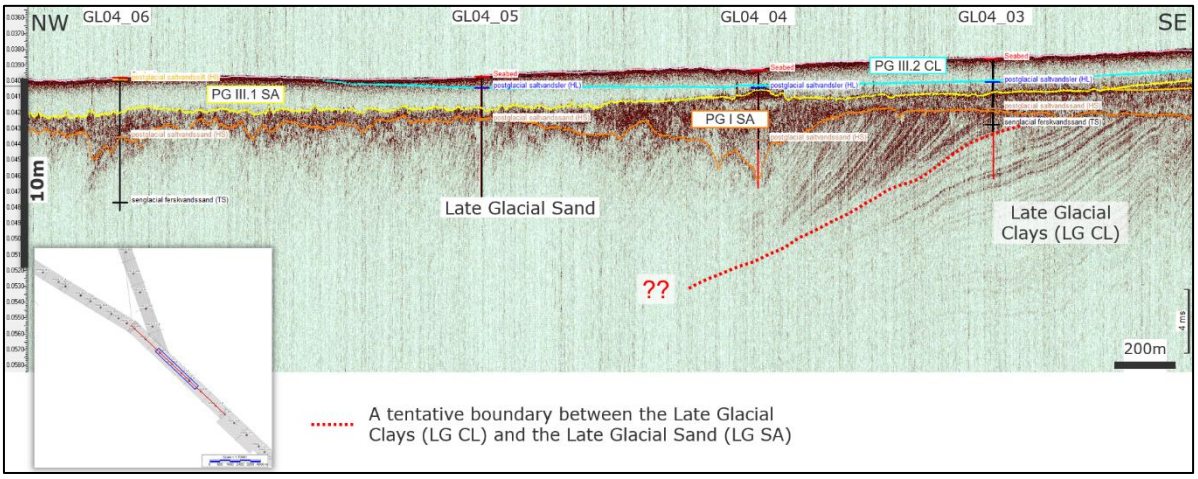

Figure 8-35 Seismic line 20085_MTK_GL_04_C000_SES_20201024_053005_RAW_LF showing a relatively thick succession of Late Glacial sands found in the central part of the cable corridor, block GL04.

Along the cable corridor block GL05 the Late Glacial sands have been described at locations GL05_01, GL05_05, GL05_07 as well as GL06_01, where they are underlying the Holocene units and are found next to glacial tills (see Figure 8-36). It should be mentioned that neither the base or the lateral boundary between the Late Glacial sands and glacial tills can be mapped on the available SBP-data due to the fact, that SBP signal penetration is limited in coarse or highly compacted sands as well glacial tills and no corresponding reflectors can be seen on the seismic section, as shown on the Figure 8-36.

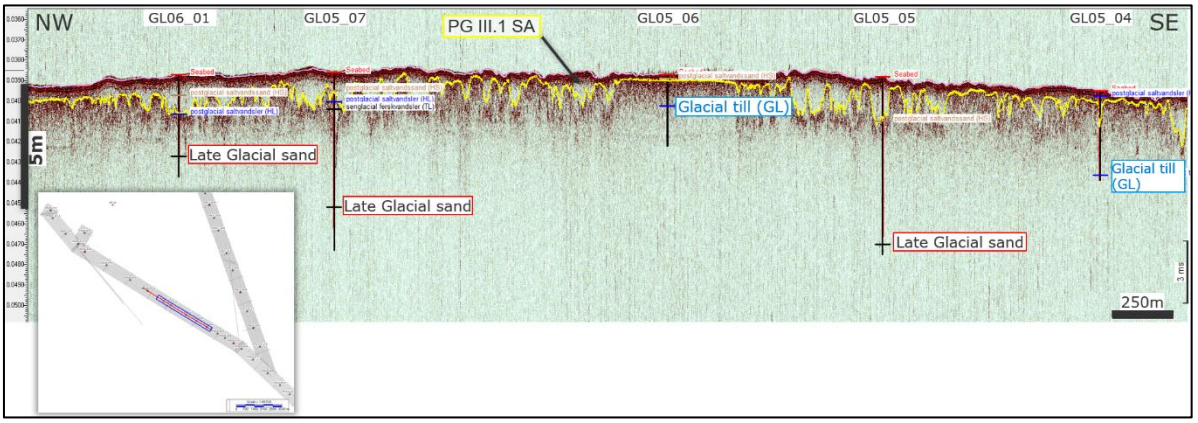

Figure 8-36 A composite seismic profile (lines 20085_MTK_GL_05_C000_SES_20201023_205938_ _RAW_LF and 20085_MTK_GL_05_C000_SES_20201023_163500_RAW_LF) showing the Late Glacial sand succession found in the central part of the cable route, block GL05. Note that the lateral boundary between the Late Glacial sands and glacial till deposits can't be mapped here as the SBP signal penetration is highly limited.

Late Glacial sands with gravel have also been penetrated by vibrocore GL02_01 located in the southernmost part of the cable route. The lateral boundary between the Late Glacial sands and adjacent glacial tills can't be mapped here due to limited signal penetration (Figure 8-37).

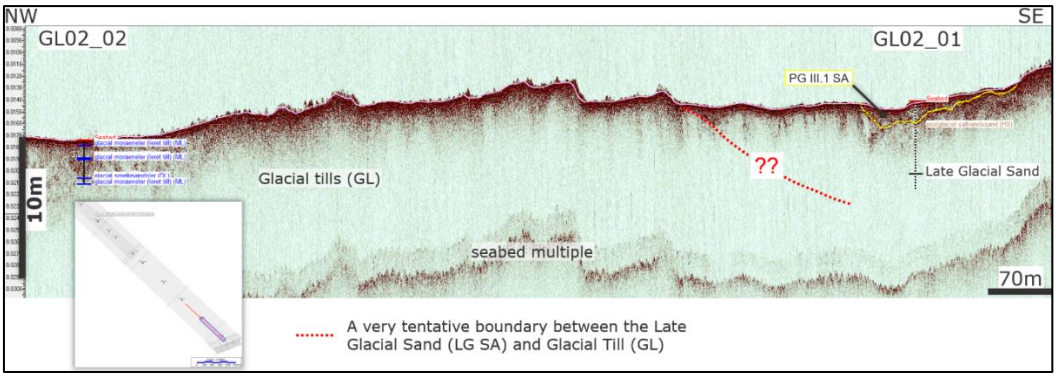

Figure 8-37 Seismic profile (line 20085_MTK_GL_SES_C000_0_20201025_152440_CHO_LF) showing Late Glacial sands found in the southernmost part of cable corridor, location GL02_01. Note that the lateral boundary between the Late Glacial sands and glacial till deposits can't be mapped here as the SBP signal penetration is highly limited.

An overview map presenting depth in meters below seabed to the top the Late Glacial deposits is shown on the Figure 8-38.

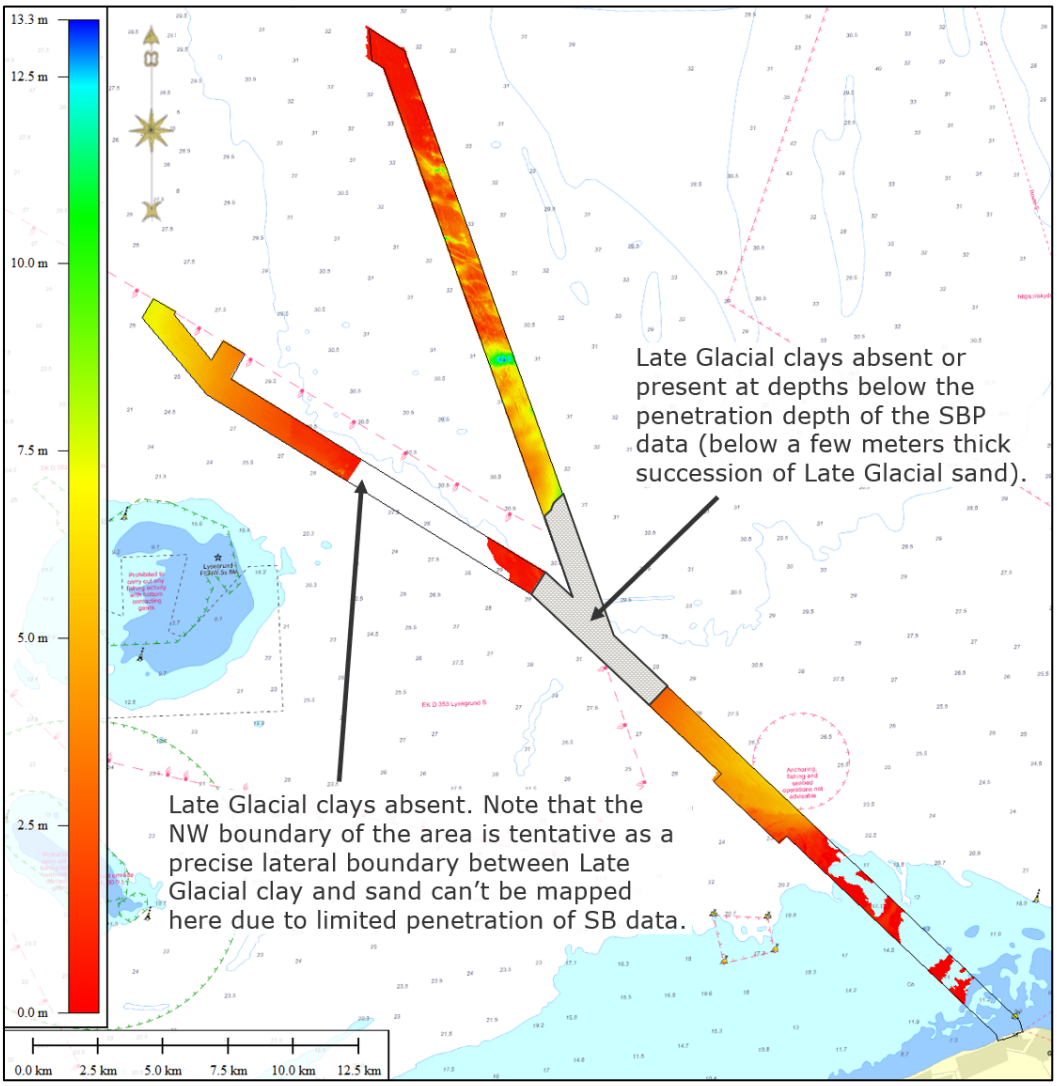

Figure 8-38 Depth in meters below seabed to the top of the Late Glacial succession (LG CL).

8.7.3.3 Post Glacial deposits (PG)

The Post Glacial deposits form the youngest sedimentary succession within the southern Kattegat region. Within the cable corridor they reach a total thickness of up to around 12 meters and can be found throughout entire survey area.

The lower boundary of the Post Glacial deposits is a pronounced erosional unconformity down to approx. 35 m below sea level (below which – a conformity prevails) /1/ (see Figure 8-39).

Based on the sedimentological composition and the internal reflection pattern the succession has been divided into a lower low stand systems tract (unit PG I) and an upper transgressive systems tract (units PG II and PG III). Additionally, a fourth unit PG IV composed of very coarse sediments has been mapped in the southernmost part of the cable corridor in order to align subsurface geology with the seabed geology observed on the side scan sonar data.

The PG I unit consist primarily of fine- to coarse grained sand deposited during the Early Holocene transgression and interpreted as lowstand post glacial sediments. It has been penetrated in, i.a., vibrocores GL04_02, GL04_04 and GL04_05 where it is described as clayey, silty or gravelly sand that might contain plant remains or high plasticity clay layers- as identified in the vibrocore GL04_01.

It has a characteristic seismic expression as the unit is semi-transparent with generally no internal layering. The lower boundary is uneven and truncates the underlying LG sediments (see Figure 8-39).

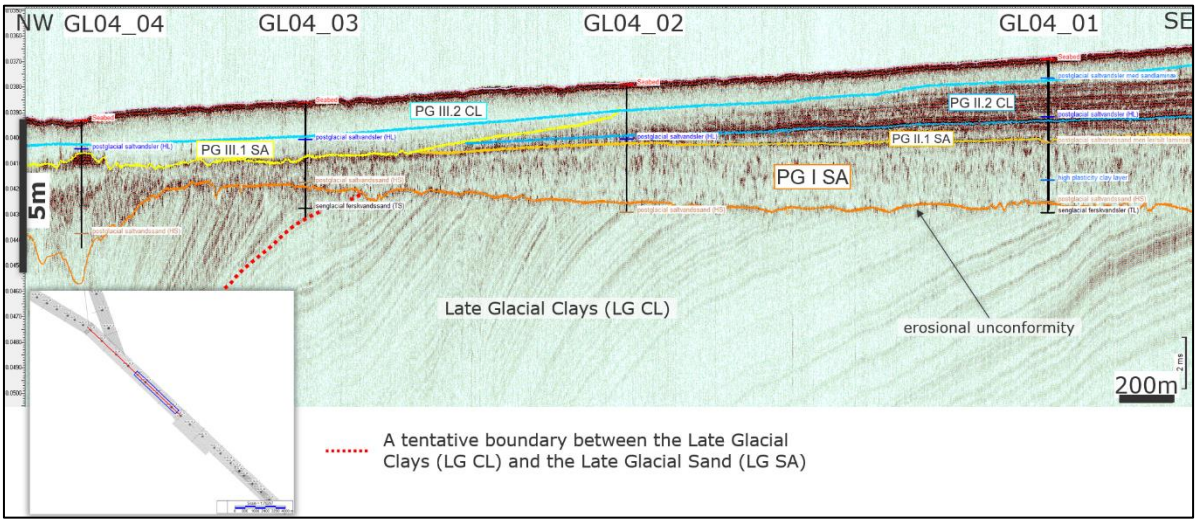

Figure 8-39 SBP profile 20085_MTK_GL_04_C000_SES_20201024_053005_RAW_LF illustrating the seismic character of the PG I unit interpreted here as marine coastal deposits.

In the cable corridor the PG I unit is limited to the central and north-western part of the corridor where it is laterally continuous and interpreted as coastal sediments deposited during Early Holocene coastal marine conditions.

At the area adjacent to the vibrocore GL06_02 PG I has been found to fill channel-like depressions in the glacial and late glacial deposits, as illustrated on the Figure 8-40. It should be noted that these channel-like features are characterised by small dimensions (up to 2-3 m deep) and lateral discontinuity. The origin of the features can't be indicated with confidence. However, their origin might be associated with presence of Late Glacial blocks of dead ice, minor fresh-water channels or iceberg scars subsequently filled with younger deposits.

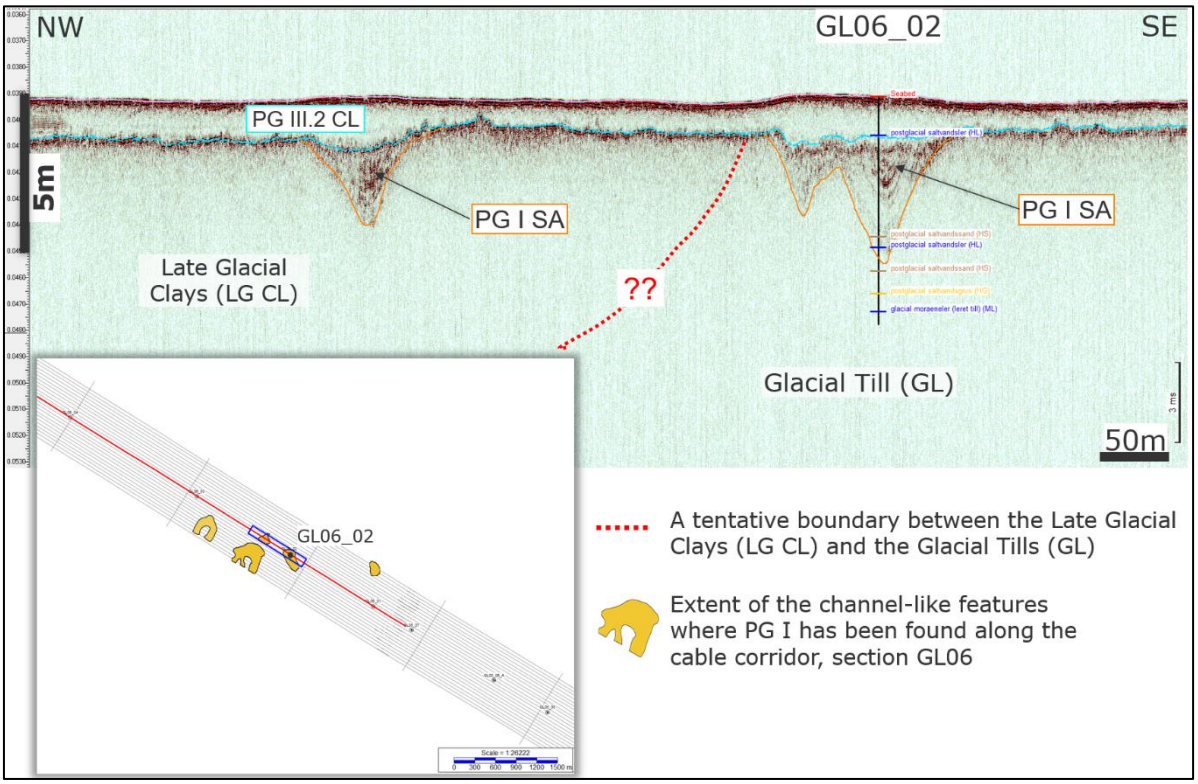

Figure 8-40 SBP profile 20085_MTK_GL_06_C000_SES_20201023_163500_RAW_LF illustrating the seismic character of the PG I unit at locations where it is found to form infill of channel-like depressions in the glacial and late glacial deposits along the cable corridor block GL06.

The thickness of PG I varies between 0 and 8 m, with typical values of around 1-2 m within most of the cable corridor. The thickest package is found in the central part of the cable corridor, adjacent to locations GL10_01 and GL04_04 (east from Lysegrund) where up to 8 m of the Early Holocene sands have been identified. The extent and thickness map of PG I are shown on the Figure 8-41.

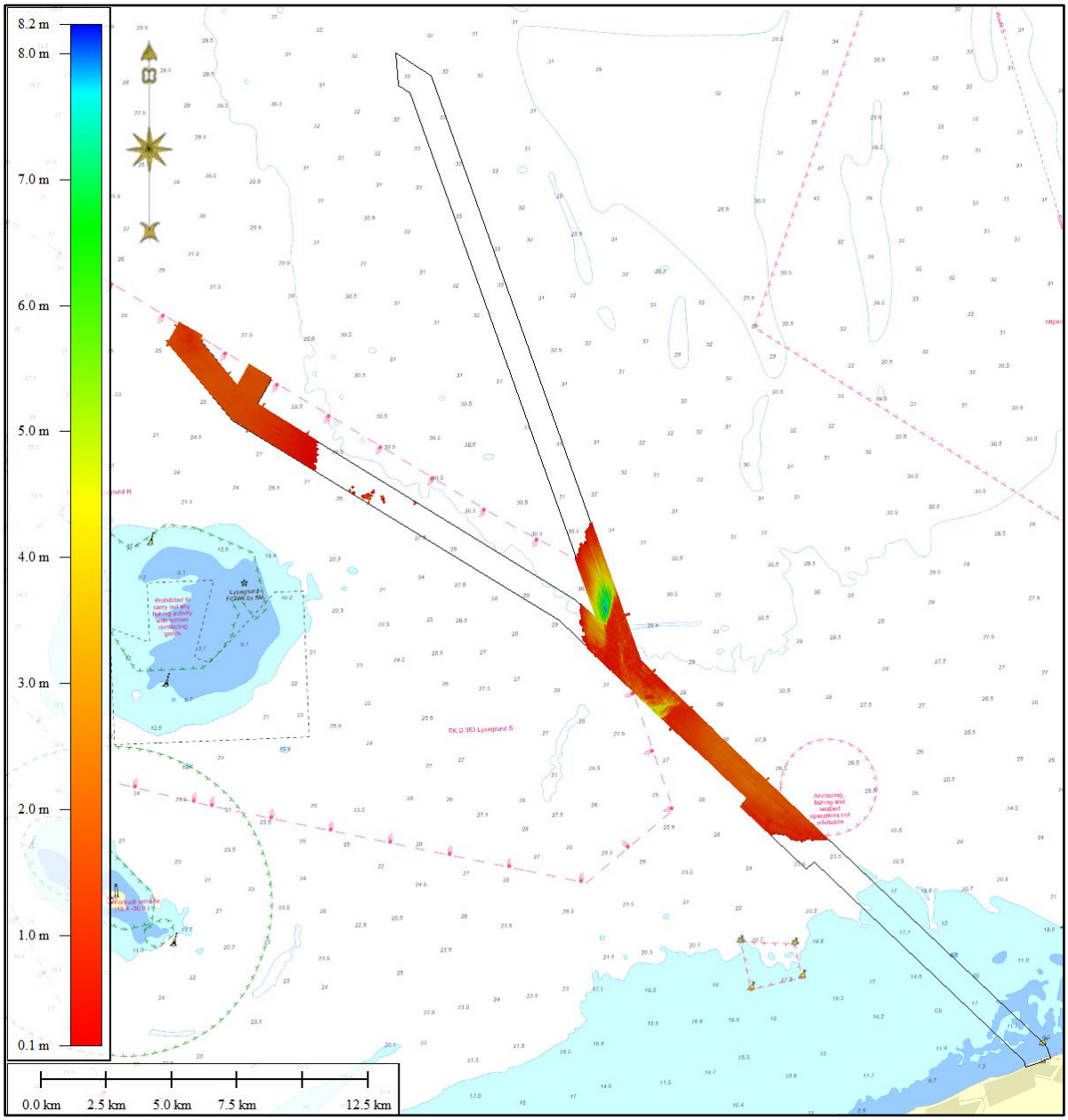

Figure 8-41 Thickness map of the Early Holocene sand unit PG I.

The unit PG II overlies PG I and has been divided into two separate units based on their sedimentological composition. The first one, PG II.1 is composed of sand and directly overlies PG I, while the upper part PG II.2 is composed of very fine-grained clays (see Figure 8-42).

PG II.1 has been found in the central part of the cable corridor (at locations GL03_11, GL03_12, GL03_13, GL03_12, GL04_01, GL04_02) as well as in the northernmost part of its western arm (at locations GL06_04, GL06_05, GL09_01, GL09_02, GL07_01, GL07_02 and GL08_01). Based on the vibrocore descriptions, it is generally composed of fine- to medium silty, clayey sand with thin clay layers and it might contain plant remains.

The unit PG II.1 has similar lithological composition to PG I, however, it shows a very different seismic reflection pattern as it is characterised by pronounced parallel reflections, as illustrated on the Figure 8-42 and Figure 8-43.

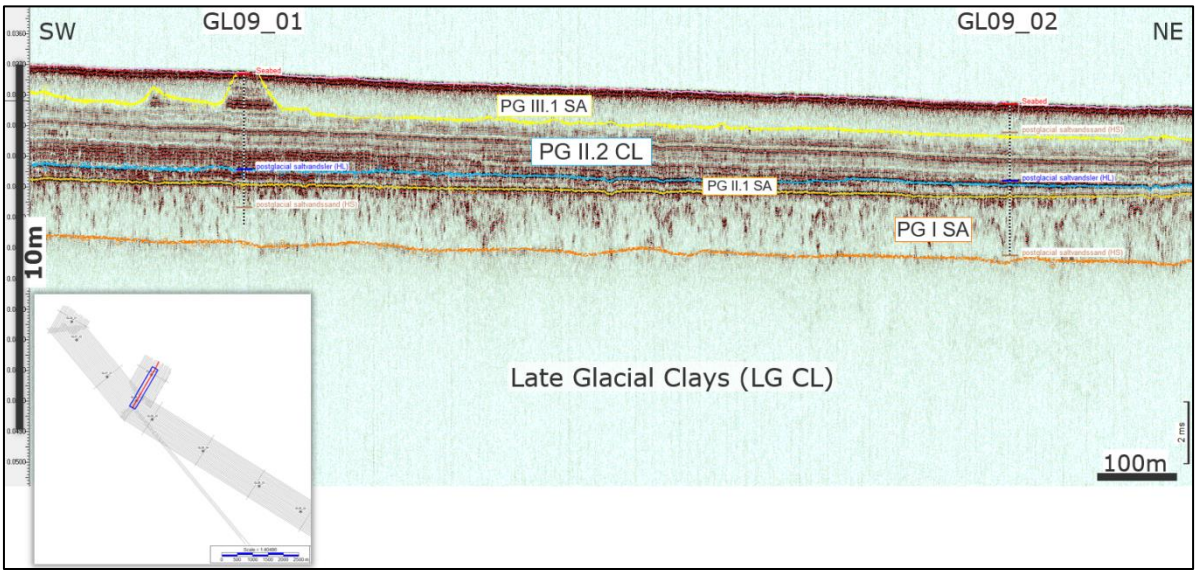

Figure 8-42 SBP profile 20074_MTK_HS_14_C000_SES_20201007_035343_RAW_LF illustrating the seismic character of the PG II units (PG II.1 composed of sand and PG II.2 represented by clays).

PG II.1 has a typical thickness of around 0.3-0.5 m. However, along the block GL12 located close the Hesselø OWF site it reaches its maximum thickness of up to 1.5m. The isopach map showing thickness of the PG II.1 unit is presented on the Figure 8-43.

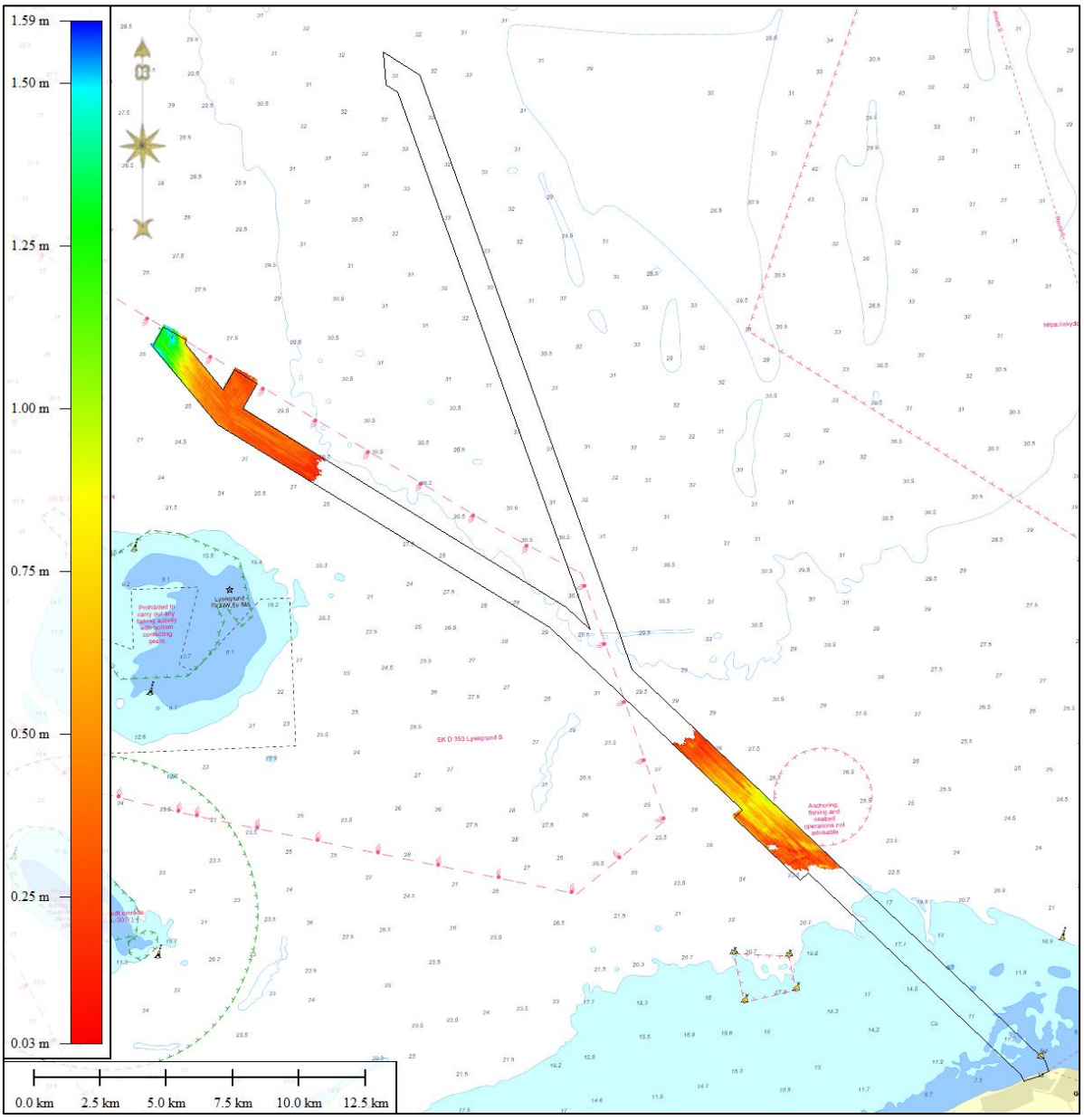

Figure 8-43 Thickness map of the Holocene sand unit PG II.1 SA.

PG II.2 comprises the upper, fine-grained part of the PG II sequence. It is composed of very sandy to slightly sandy clays with its lower part containing thin layers of sand or sand with gravel, as described for example in the vibrocore GL11_02. Like PG II.1, it has been found in the central part of the cable corridor as well as in the northernmost part of its western branch, where it conformably overlies PG II.1 (see Figure 8-42 and Figure 8-44). However, PG II.2 has been also penetrated along the eastern branch of the cable corridor, where it reaches significant thickness of up to 12 m within channels, as illustrated on the Figure 8-44, while in the western and central part of the cable corridor the unit PG II.2 has a typical thickness of 1-2m. The thickness map of the PG II.2 unit is shown on the Figure 8-45.

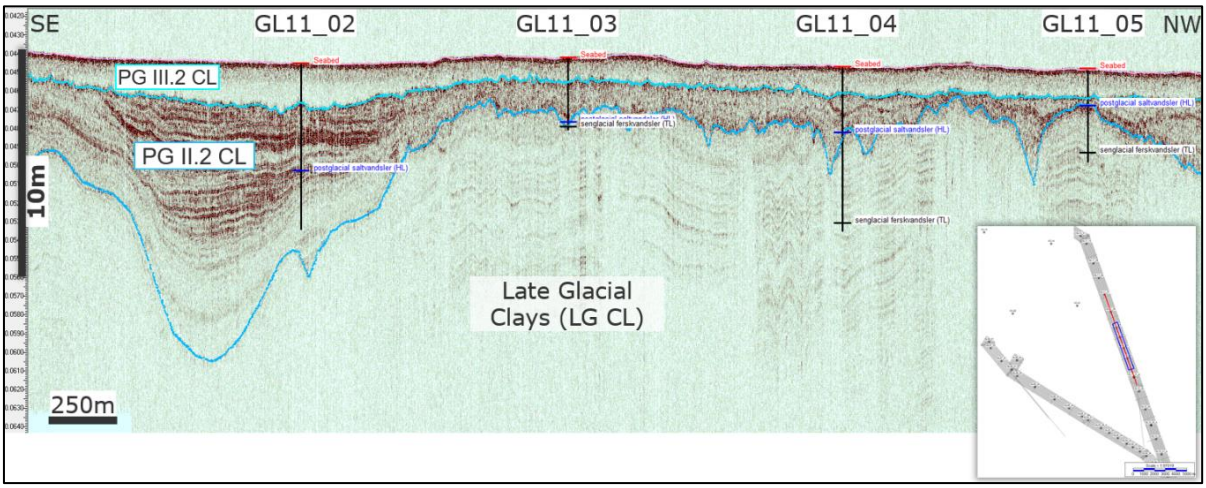

Figure 8-44 SBP profile 20074_MTK_HS_11_C000_SES_20201006_150620_RAW_LF illustrating the seismic character of the PG II.2 interpreted as channel infill along the eastern branch of the cable route (block GL10, GL11 and GL12).

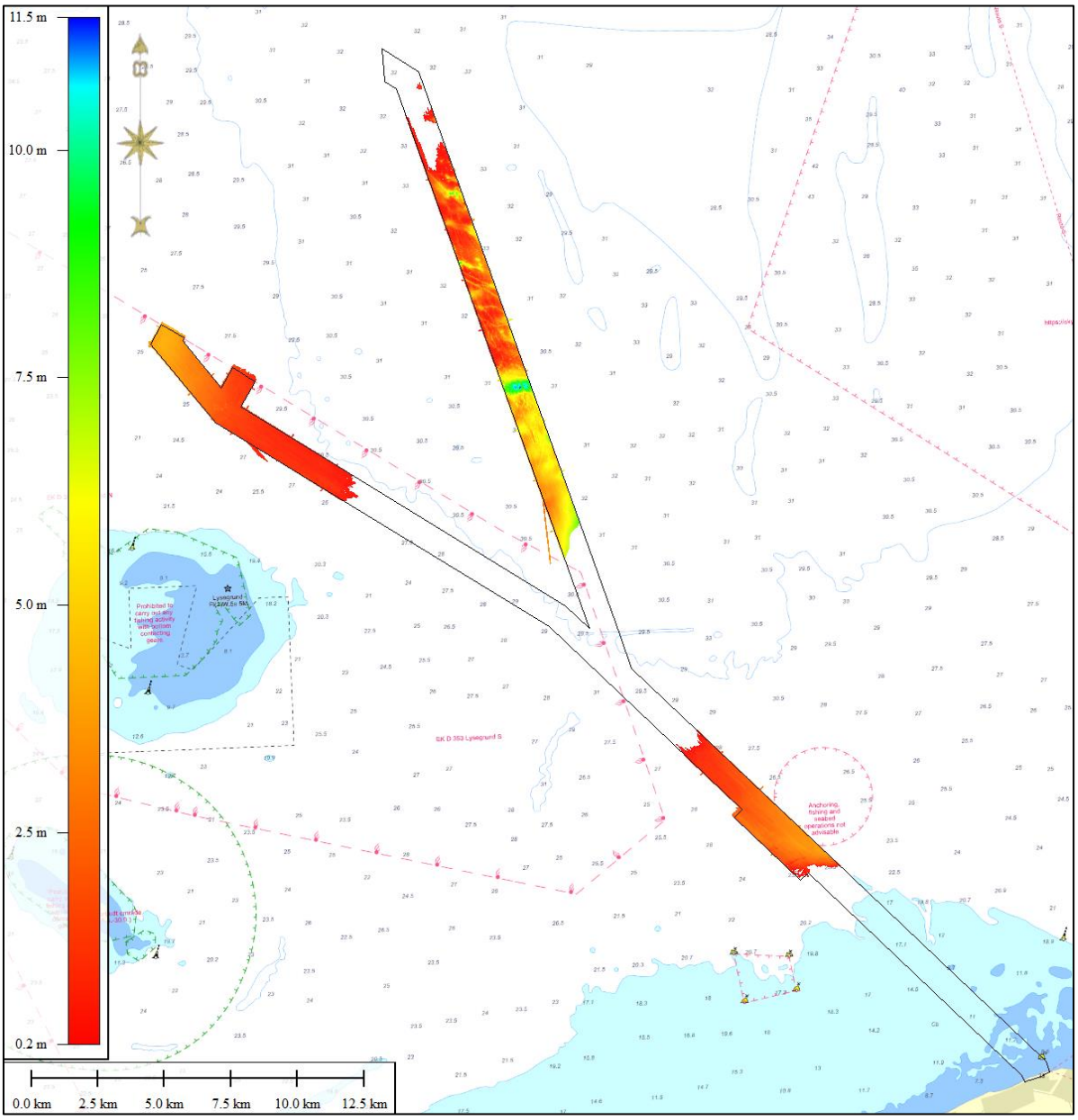

Figure 8-45 Thickness map of the Holocene clay unit PG II.2 CL.

In summary, the sediments of PG II are characterised by upwards thinning reflecting deepening of the basin and are is interpreted as transgressive systems tract deposited during the Early Holocene sea level rise. The lower unit PG II.1 forms initial sandy coastal deposits, while the younger unit PG II.2 is composed of primarily clays. PG II.2 forms both coastal deposits as well as channel infill, reaching significant thicknesses of up to 12 m along the eastern branch of the cable corridor, where its upper boundary of shows reflection truncation and is therefore interpreted as an erosional unconformity (see Figure 8-44).

The unit PG III represents the youngest highstand systems tracts sediments deposited after the latest marine transgression and it has been identified throughout entire cable corridor. It is composed of fine-grained sediments, typically silty clay grading into sand or clayey sand in more shallow parts of the survey area.

Based on sedimentological composition, PG III has been subdivided into two units, PG III.1 and PG III.2. The first unit PG III.1 is described as clayey, silty sand, while PG III.2 is composed of silty, sandy clays. Both units are of the same age and the lateral boundary between them is gradual. In addition, on the acquired SBP data both units show similar, very characteristic, transparent, or semi-transparent seismic expression with no clear reflectors (see Figure 8-42, Figure 8-44 and Figure 8-46). Therefore, mapping the extent and lateral boundaries between these two units have been governed primarily by the available geotechnical information, as illustrated on the Figure 8-46.

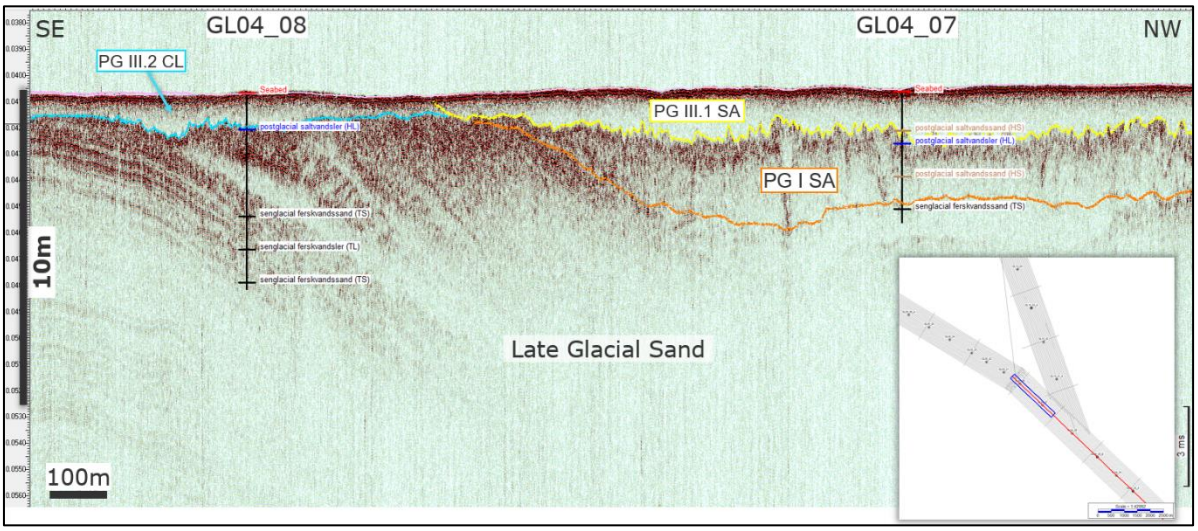

Figure 8-46 SBP profile 20085_MTK_GL_04_C000_SES_20201024_053005_RAW_LF illustrating the seismic character of the unit PG III.1 (sand) and PG III.2 (clay).

The total thickness of deposits belonging to unit PG III varies between 0 and 5 meters, lying typically between 0.5-3.0m throughout most of the cable corridor. Packages thicker than 3 m are interpreted at very few locations (see Figure 8-49). A map showing thickness of the unit PG III.1 is presented on the Figure 8-47 and an isopach map for PG III.2 is shown on the Figure 8-48.

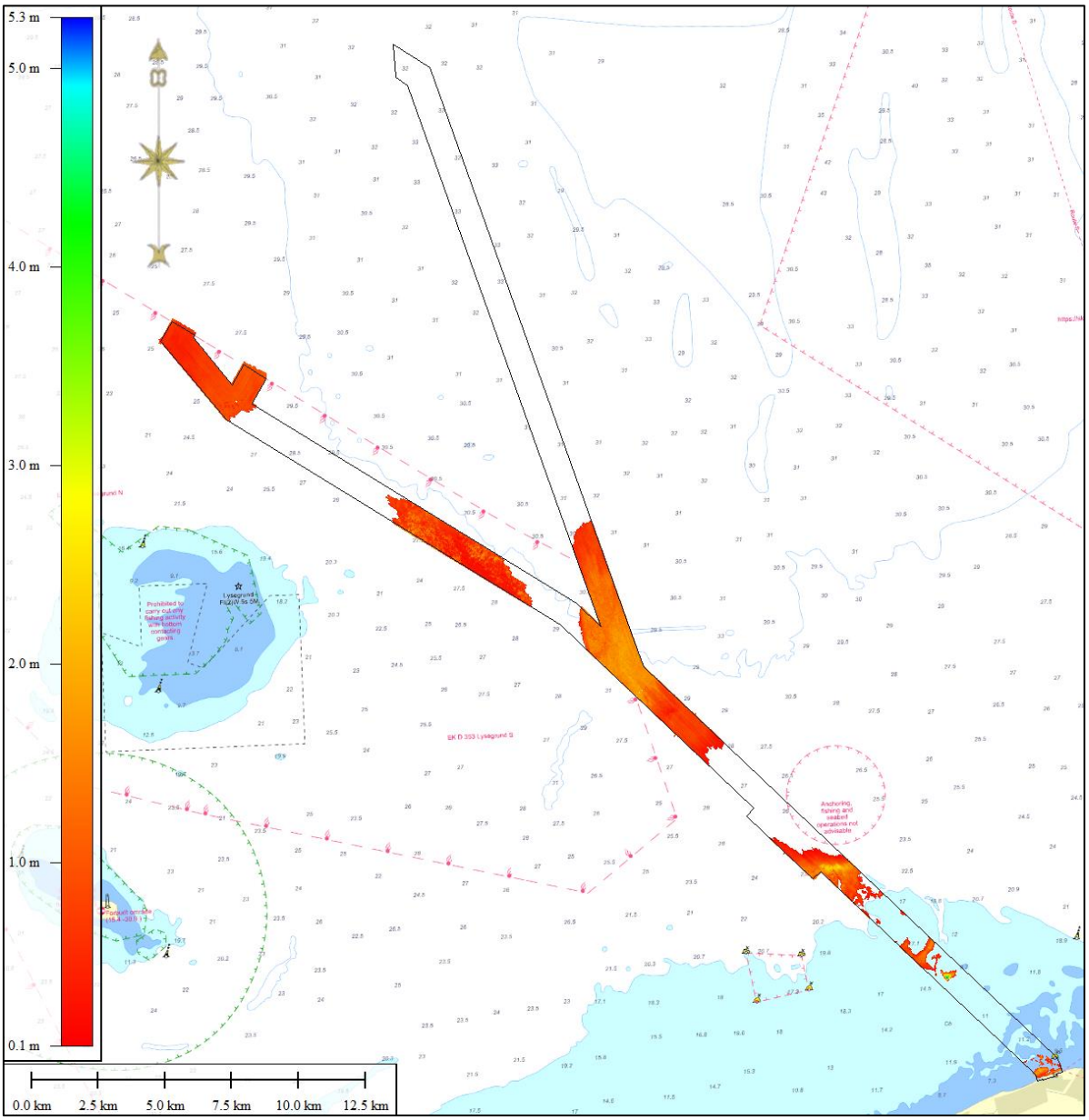

Figure 8-47 Thickness map of the Holocene sand unit PG III.1 SA, typical thickness of the unit: 0.5-2.5m.

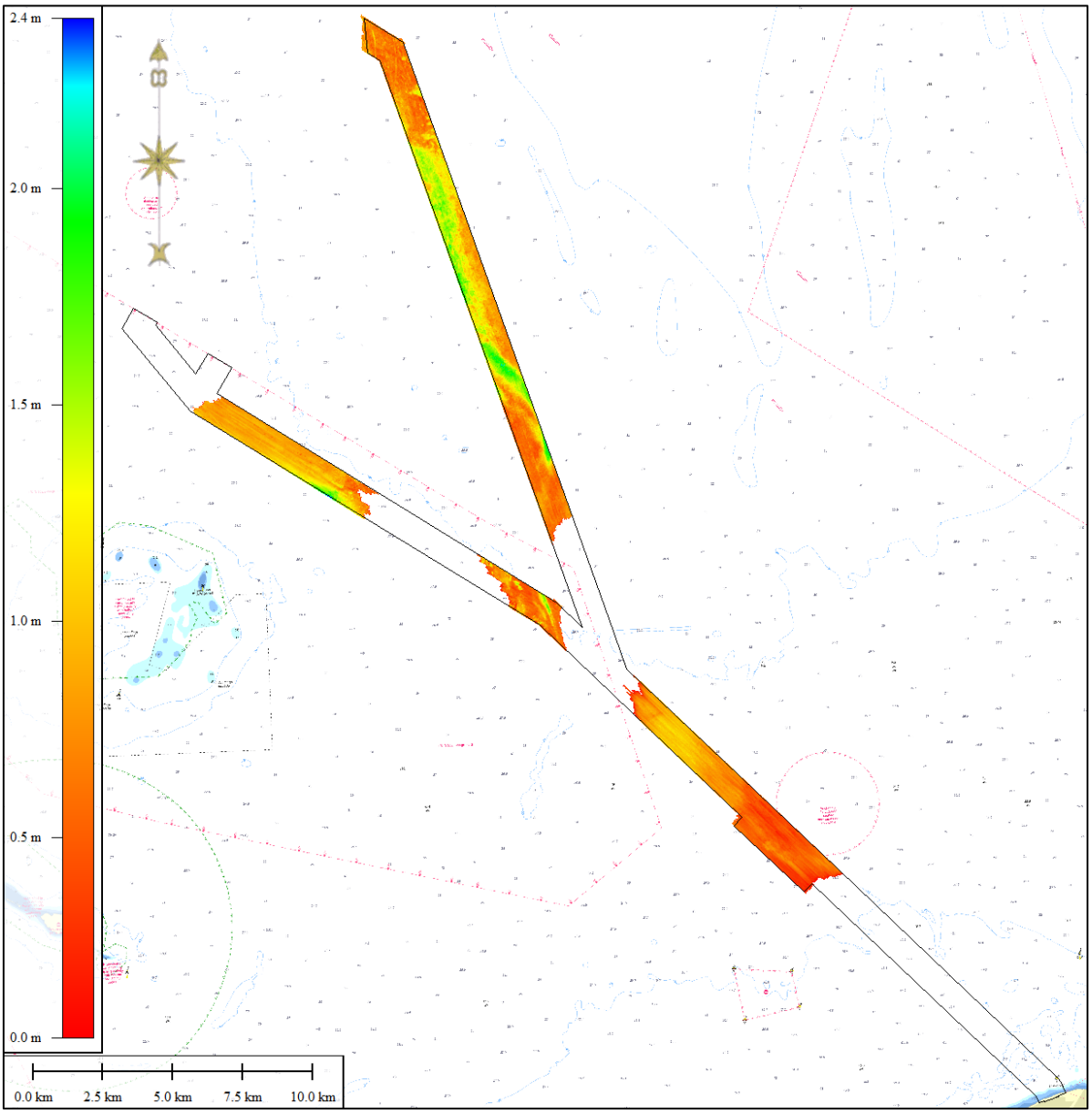

Figure 8-48 Thickness map of the Holocene clay unit PG III.2 CL, typical thickness of the unit: 0.5-2.0m.

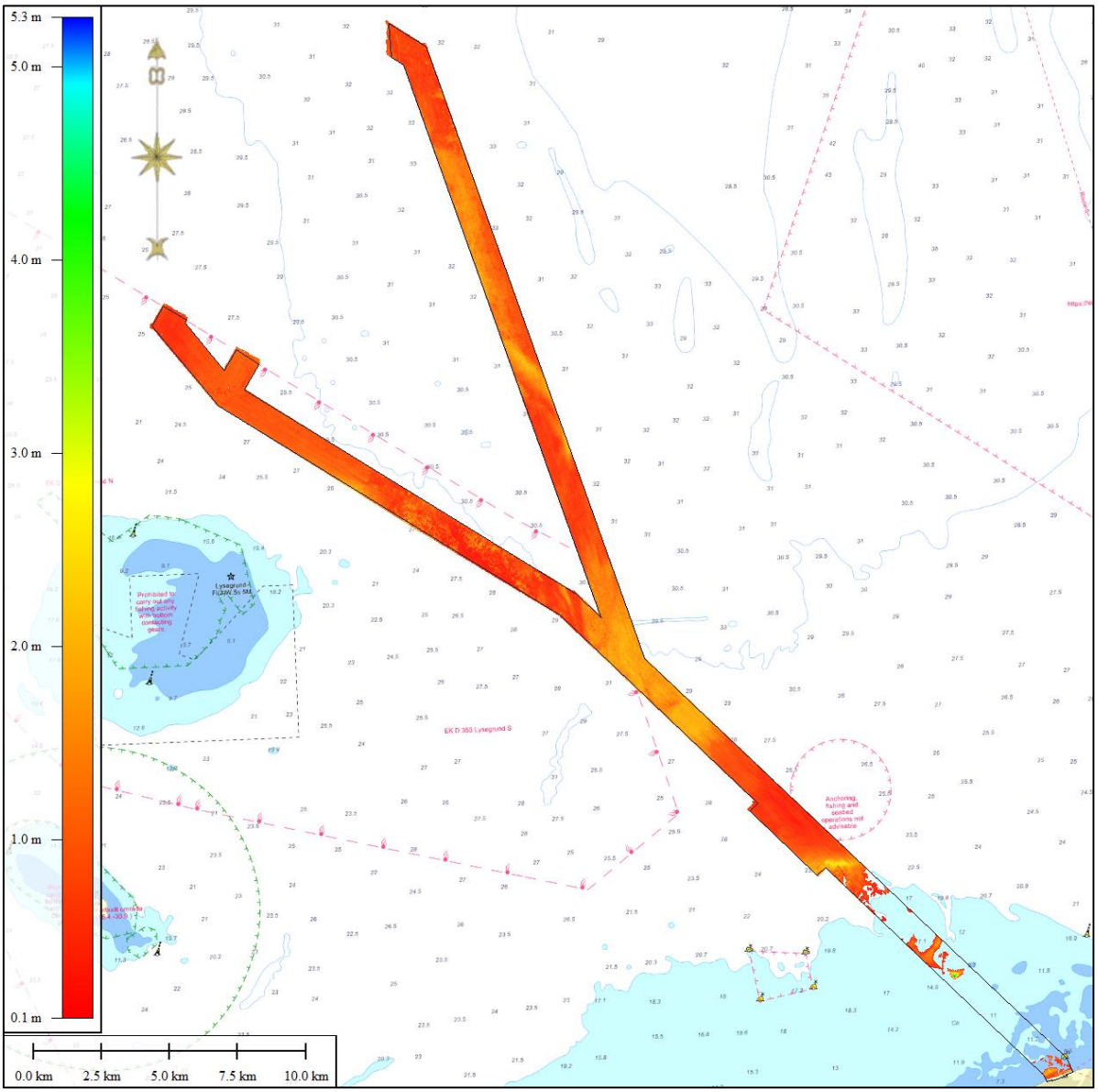

Figure 8-49 Total thickness map of the youngest Holocene deposits- unit PG III.1 SA and PG III.2 CL.

The last unit- PG IV, is composed of very coarse sediments found in the southernmost part of the cable corridor. It is interpreted as Holocene coarse sand and gravel as well coastal sediments eroded and redeposited on the margins of the till core and comprises a very thin cover layer at locations where glacial tills are present close to the seabed (see Figure 8-30). As the thickness of this unit does not exceed 1m (as shown on the Figure 8-50), mapping of this sediment package is based dominantly on the side scan sonar data.

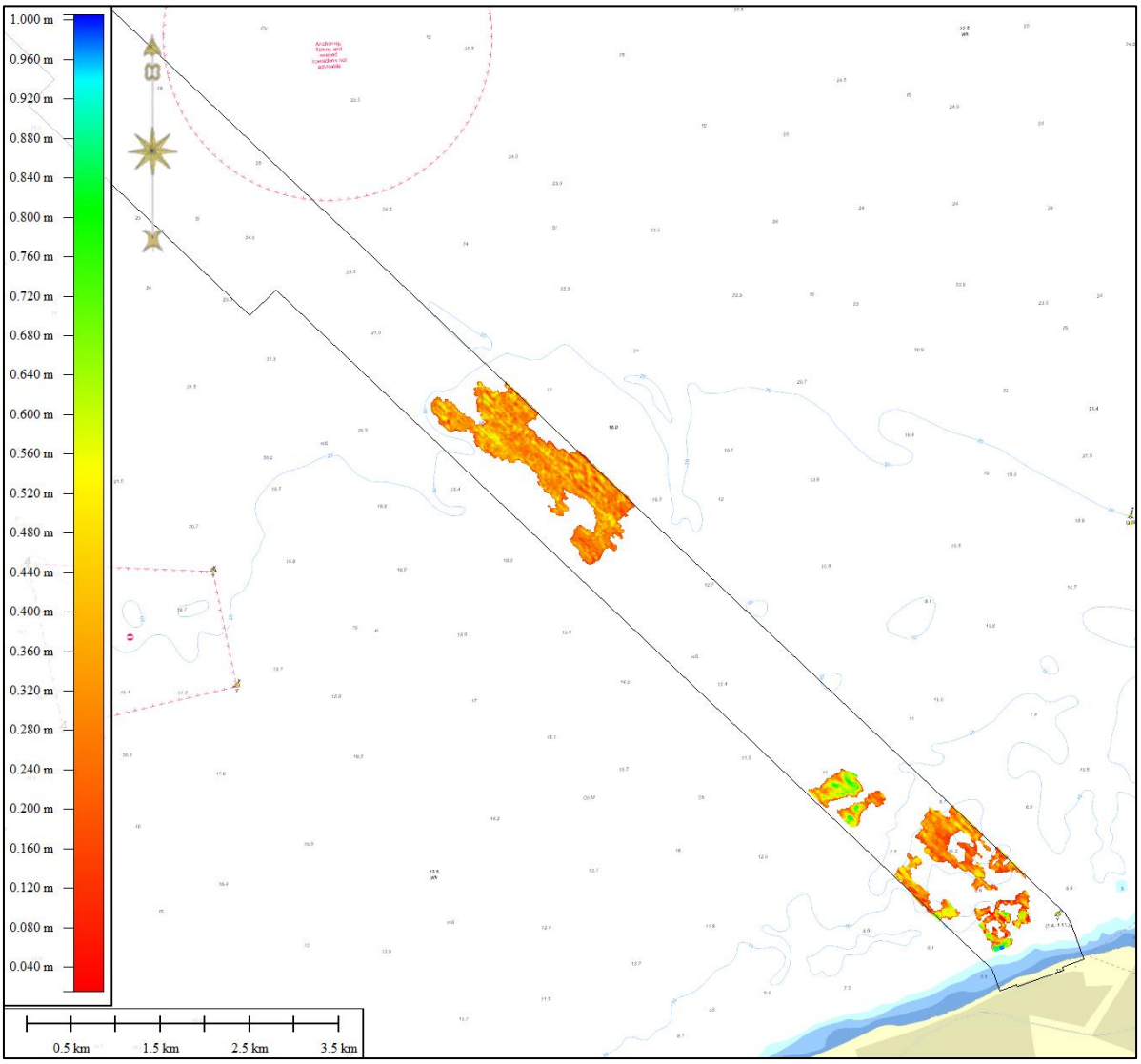

Figure 8-50 Thickness map of the Holocene unit PG IV composed of coarse-grained sediments, sand and gravel. Typical thickness of the unit: 0.2-0.5m.

8.7.4 Results summary

This study adopts GEUS' division of the Quaternary sediment succession into geological units that are described below. A summary of the interpreted horizons is shown in the following Table 8-3.

Table 8-3 Summary of the mapped geological units and interpreted horizons

Geological unit			
Glacial (GL)	GL (Sand till/Clay till)		*(Base of GL and LG SA has not been penetrated by the SBP recordings and therefore could not be interpreted)*
Late Glacial (LG)	LG SA (sand)		
	LG CL (clay)		Base LG CL
Post Glacial (PG)	PG I SA (sand)		Base PG I SA
	PG II	PG II.2 CL (clay)	Base PG II.2 CL
		PG II.1 SA (sand)	Base PG II.1 SA
	PG III	PG III.2 CL (clay)	Base PG III.2 CL
		PG III.1 SA (sand)	Base PG III.1 SA
	PG IV SA (Coarse sand and gravel)		Base PG IV

A more detailed division of the cable corridor in segments with similar subsurface geology can be found in Appendix 3. In general, based on results of the completed investigations, the following can be concluded:

KP = (0.0-9.2)

- Along the initial part of the corridor the subsurface consists generally of glacial tills formed out of the ground moraine material as well as late glacial sands found in the southernmost part of the corridor. The glacial deposits are cut by SW-NE running channels filled with late glacial-fresh water clays and overlain by a thin layer of Holocene deposits.
- Surface sediments consist of mainly till/diamicton with areas of coarse sand and gravels and mainly sand towards landfall. Late glacial clays are present at the seabed at locations where fresh-water channels eroded into the glacial deposits.

KP = (9.2-18.0)

- At this location, a transition from the area where glacial tills are found just below the seabed towards the Late Glacial basin occurs. A thick succession of Late glacial glaciomarine deposits (LG CL) is found north from KP=9.0, below a generally 0.5-2.5m thick layer of Holocene transgressive sediments.
- Surface sediments are interpreted as muddy sands and they occur at areas where most recent Holocene deposits belonging to units PG III.1 and PG III.2 outcrop the seabed. As mentioned in the paragraph 8.7.3.3 of this report, both of the PG III units are composed of fine-grained sediments, typically silty clay grading into sand or clayey sand in more shallow parts of the survey area. On the acquired SBP data they show similar, transparent to semi-transparent seismic character with no clear reflectors associated with the boundary between these two units. Correspondingly, given their similar sedimentological composition, PG III.1 and PG III.2 can't be differentiated on the side scan sonar data and based on the grab sampling description they have been classified as muddy sands.

KP = (18.0-27.0) western arm & KP = (21.75-27.0) eastern arm

- This segment of the cable corridor is located east (north-east) from Lysegrund and characterised by presence of a relatively thick succession of Late Glacial and Post Glacial sands underlying Holocene fine-grained sediments.

- Seabed sediments area dominated by muddy sand and sand.

KP = (27.0-35.0) western arm

- This segment is characterised by presence of 0.2-1.7m thick succession Holocene sands (PG III.1 SA) deposited on a very unevenly eroded surface representing the top of Glacial tills or Late glacial sands. The lateral transition from late glacial sands to glacial deposits can't be precisely indicated based on the available SBP data due to limited signal penetration.
- Surface sediments are sand which changes to coarse sand with gravel at locations where glacial tills are found at shallow depths below the seabed.

KP = (35.0-43.5) northern part of the western arm

- A typically 1m to 6m thick succession of post glacial deposits overlies late glacial clays.
- This section is dominated by muddy sand which changes to sand in the northernmost part, near the Hesselø OWF site.

KP = (27.0-35.0) eastern arm

- This part of the cable corridor can be characterised be presence of a very thick succession of generally soft and weakly consolidated clays belonging to the unit PG CL, overlain by PG II.2 and PG III.1.
- Surface sediments consist of muddy sand.

In summary, glacial tills are outcropping the seabed or are present at shallow depths below the seabed in the southernmost part of the cable corridor (KP=0.0-9.2) as well as in the central part of the corridor, north-east from Lysegrund (KP=27.0-35.0, western arm).

The central segment, between KP=(18.0-27.0, western arm) and KP=(21.75-27.0, eastern arm) located east from Lysegrund can be characterised by presence of a relatively thick succession of Late Glacial to Post Glacial sands found below approx. 0.5-2.0 m thick cover of Holocene fine-grained sediments.

Along the remaining part of the route, the Post Glacial deposits are underlain by Late Glacial clays. The acquired SBP data did not penetrate to the lower boundary of the unit as it can reach significant thicknesses of up to 75 m /1//2/.

The Holocene succession is 0-13 m thick (typically between 0.5-6.0m) and present throughout entire cable corridor, except along its southern part where the Holocene deposits are local and found at selected location only. The total thickness of the Post Glacial succession is shown at the Figure 8-51.

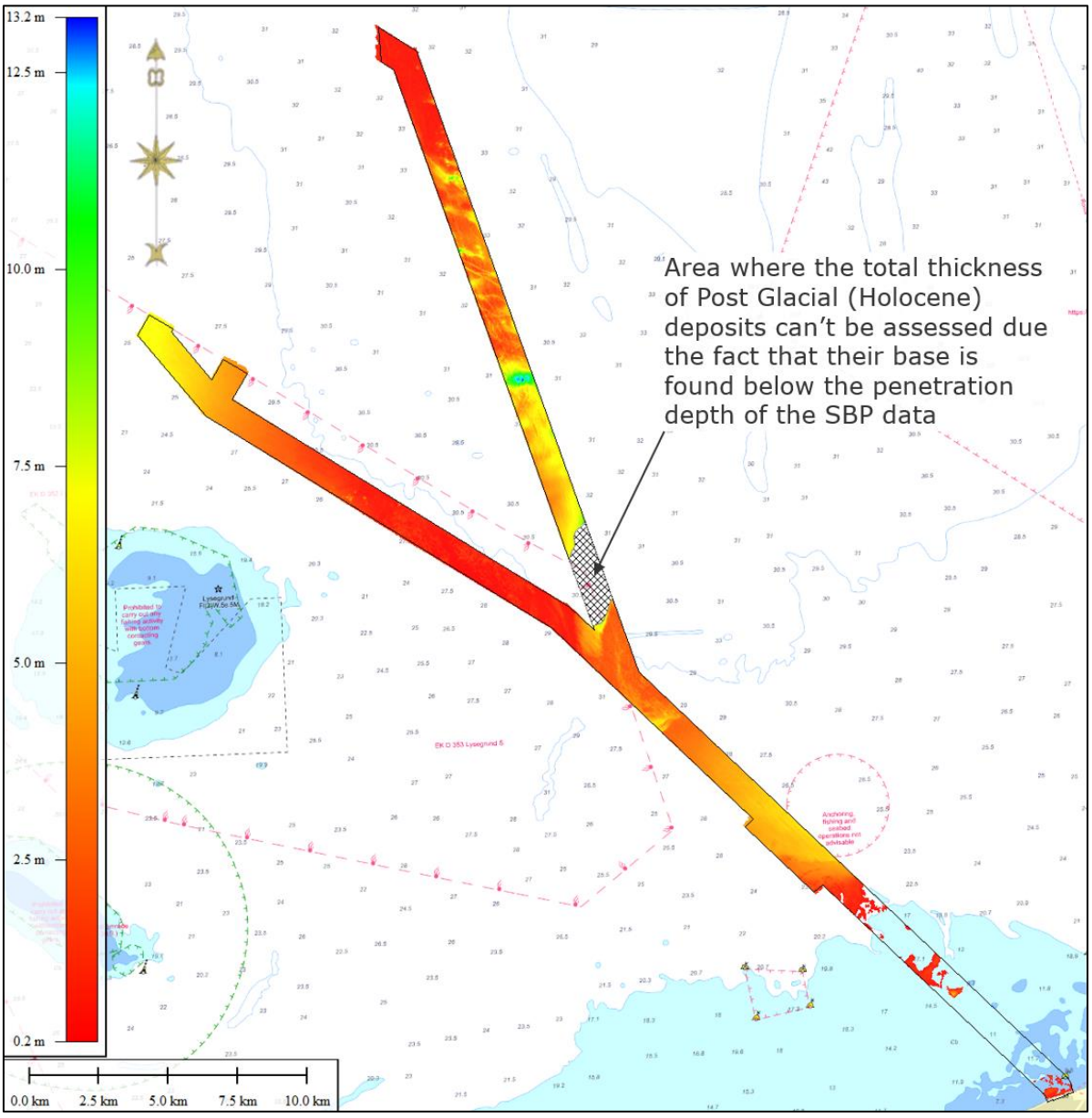

Figure 8-51 Total thickness of the Post Glacial sediments, typically: 0.5-6.0m.

8.7.5 Geohazards

As mentioned by GEUS in /1/, the geotechnical challenges for the Hesselø and cable corridor areas include neotectonics and earthquake activity within the Sorgenfrei-Tornquist zone, presence of gas in sediments and great thickness of weakly consolidated glaciomarine clay.

Based on the available SBP data, no recent faulting activity or sediment dislocation within the Holocene sequence has been observed along the cable corridor. However, given the fact that the Sorgenfrei-Tornquist zone is an active tectonic zone, risk for reactivation along the existing deeper fractures can't be fully excluded.

Late Glacial sediments composed of soft clays characterised by high plasticity are widespread in the southern Kattegat and have been identified at many locations throughout the cable corridor. In the southernmost part (along block GL02 and GL03) Late Glacial clays are found directly at the seabed and form laterally limited channel infill within the glacial succession (see Figure 8-33). Towards the north (north from the location GL03_08, approx. KP=9.0) both, thickness and lateral extent of this unit increase significantly. The total thickness of these deposits can't be defined as the acquired SBP data did not penetrate to their lower boundary. Based on the previous studies,

it can be concluded that Late Glacial clays within the Hesselø OWF site and cable corridor can reach significant thicknesses of up to 75 m, according to /1/ and /2/. It should be underlined that along the eastern arm of the cable corridor (block GL10, GL11 and GL12) the Late Glacial clays are overlain by a relatively thick (up to 12m) succession of Holocene clays belonging to the units PG II.2 CL and PG III.2 CL. These clays are also described as soft and weakly consolidated and together with the underlying Late Glacial clay deposits comprise a very thick (more than 20m) succession of weakly consolidated very fine-grained deposits present directly below seabed, as illustrated on the Figure 8-44.

Additionally, in the southern part of the cable corridor, a transition from relatively hard material comprised of glacial tills to soft sediments- Late Glacial clays, filling generally SW-NE running channels might be possibly also considered as one of the geotechnical challenges.

Presence of gas influences acoustic properties of sediments, typically leading to strong signal attenuation, masking of underlying reflectors and possibly the presence of phase-reversed reflection events. Accumulations of shallow gas within the cable corridor are manifested dominantly as acoustic blanking and occur primarily within the fine-grained units LG GL, PG II.1 SA and PG II.2 CL. One of the most pronounced shallow gas accumulations has been found in the southern part of the cable corridor, along the block GL03, and it is shown on the Figure 8-52.

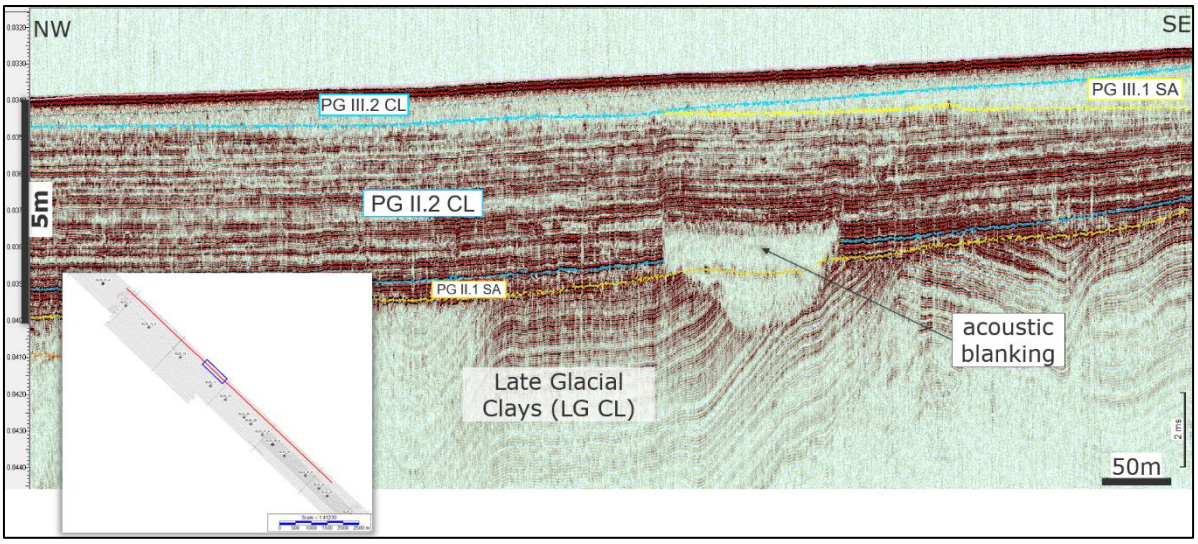

Figure 8-52 Example of a shallow gas accumulation identified, line 20085_MTK_GL_03_R405_SES_20201025_225420_RAW_LF

Pockmarks at the seabed have been only identified at one location, in the western arm of the cable corridor, along the seismic profile 20085_MTK_GL_07_L405_SES_20201107_200440_ _RAW_LF, as illustrated on the Figure 8-53. For more details regarding identification of pockmarks based on the MBES data see paragraph 8.6.

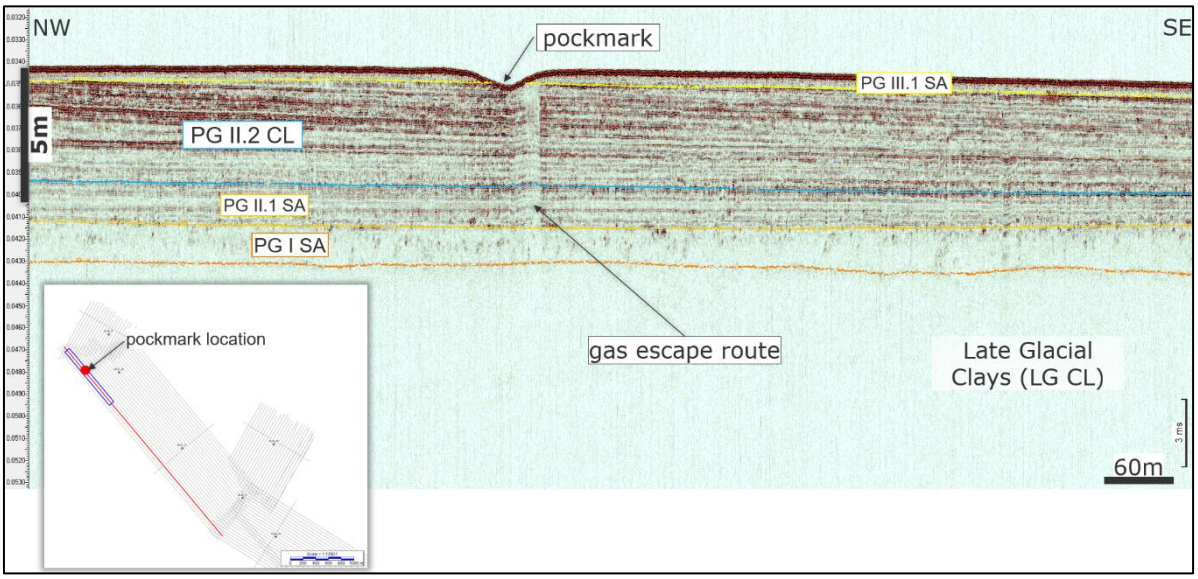

Figure 8-53 Location of the pockmark identified on the acquired SBP data, line 20085_MTK_GL_07_L405_SES_20201107_200440_RAW_LF

Results of geophysical mapping indicate that minor shallow gas accumulations occur within the fine-grained units LG GL, PG II.1 SA and PG II.2 CL throughout entire cable corridor and are manifested primarily as acoustic blanking observed on the SBP data. The occurrences can be characterised as minor and no evidence for large scale gas-filled structures have been found based on the available data. Selected, most evident manifestations of gas-filled sediments have been mapped on the SBP data and presented on the Figure 8-54.

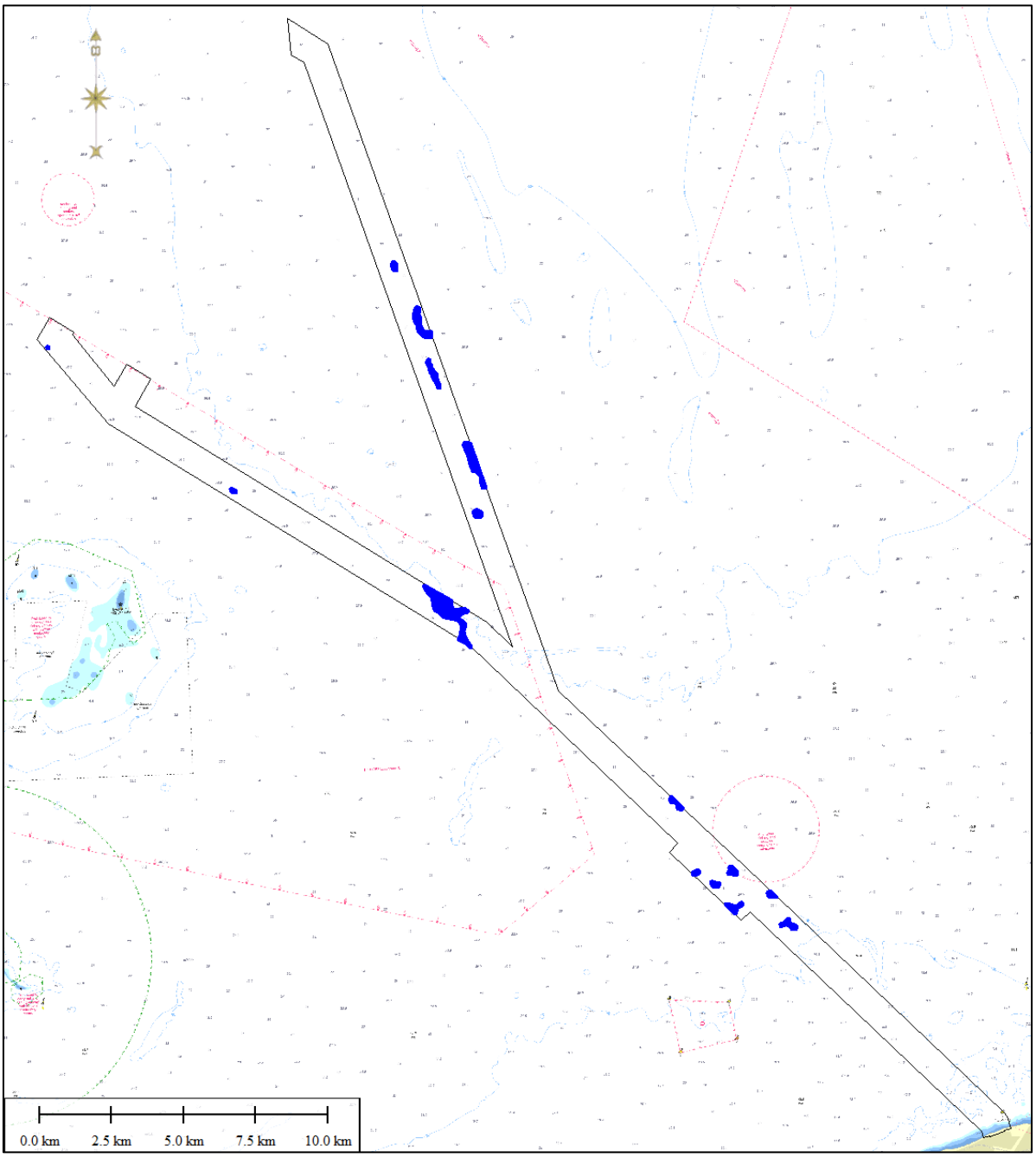

Figure 8-54 Overview over locations of the most pronounced presence of gas-filled sediments (marked with blue) within the Hesselø cable corridor.

8.8 Targets

Targets are picked on MBES, SSS and MAG data. These are correlated if there are two contacts from two different sensors within a radius of 5m. This radius is based on the uncertainty of the equipment and the detection range of the magnetometer. The positioning of the MBES targets is the most precise as the positioning on the SSS and MAG data relies on the USBL positioning.

8.8.1 MBES Targets

The MBES targets are detected down to 0.3m on the shortest axis including potential man-made objects. For the charts the MBES targets were sorted to include all MBES targets down to 1.5m on the shortest axis inside boulder fields and down to 0.3m outside the boulder fields.
Figure 8-55 shows the distribution of the MBES targets including all MBES targets down to 1.5m in boulder fields and down to 0.3m outside boulder fields, where the main part of all MBES targets is located around the boulder fields.

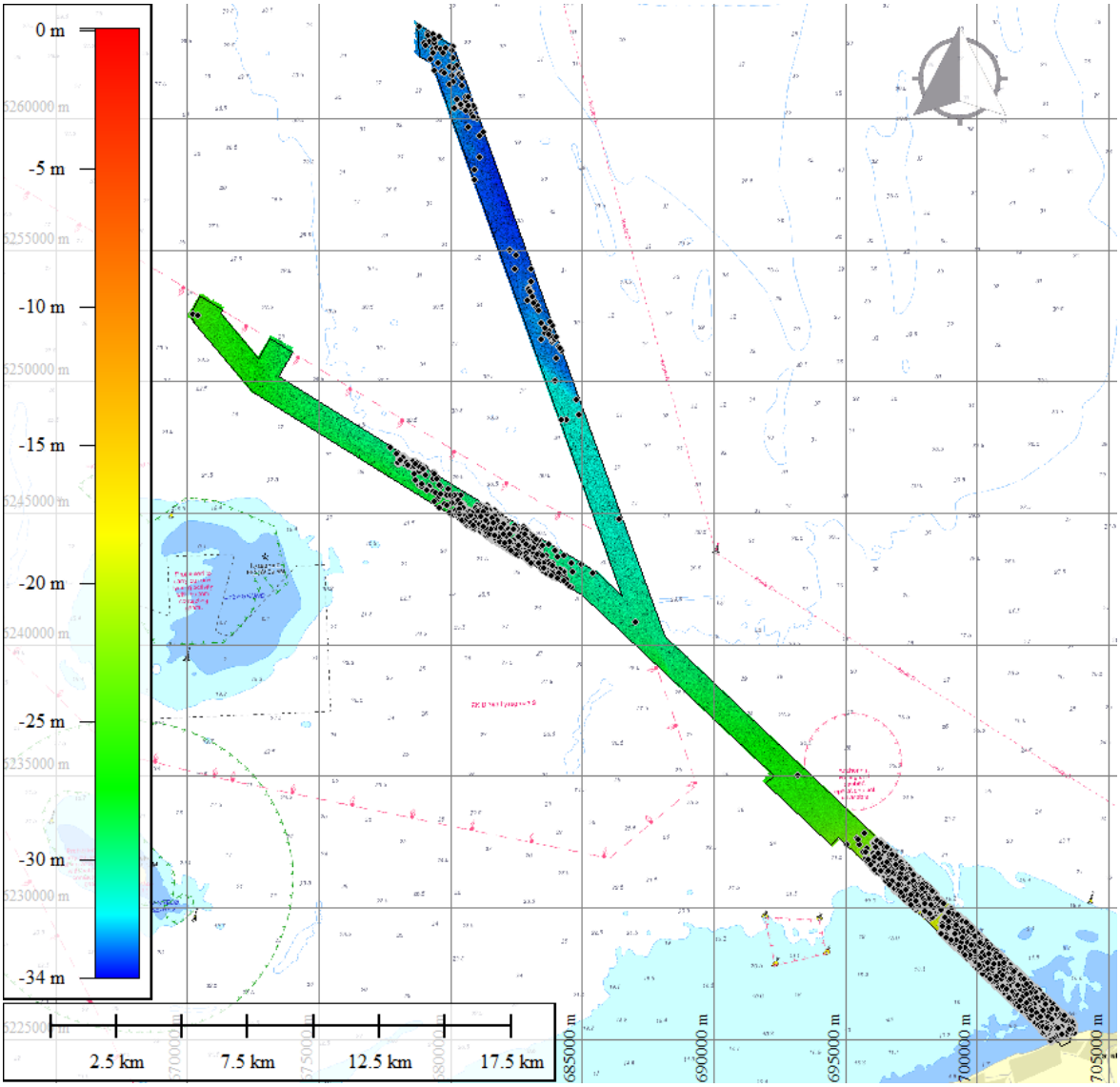

Figure 8-55 distribution of MBES contacts including targets with a dimension larger than 1.5m inside the boulder fields.

In total 89785 targets are detected on the MBES data, using the automated picking in Qimera. Qimera uses the plane between the 25cm grid cells to estimate height, length and width for each target. The MBES targets are detected down to 0.3m on the shortest axis and targets that was slighted outside the boulder fields was manually picked where the 25cm grid was screened for any irregular, linear and large features that might not be detected using the automated picking. In total 87651 of the detected MBES targets are inside boulder fields. When sorting all MBES targets to only include targets down to 1.5m on the shortest axis 26738 targets are detected along the cable corridor.
Approximately 2132 MBES targets are located outside the boulder fields, but the main part of these is also related to single boulder outcrops. 877 MBES targets are correlated with the magnetometer where 22 MBES targets correlates with the MAG targets outside boulder fields. Whereas 14 MBES targets are correlating with the side scan sonar targets.

The histograms in Figure 8-56 to Figure 8-58 shows the size distribution in height, length and width of the MBES targets outside boulder fields.

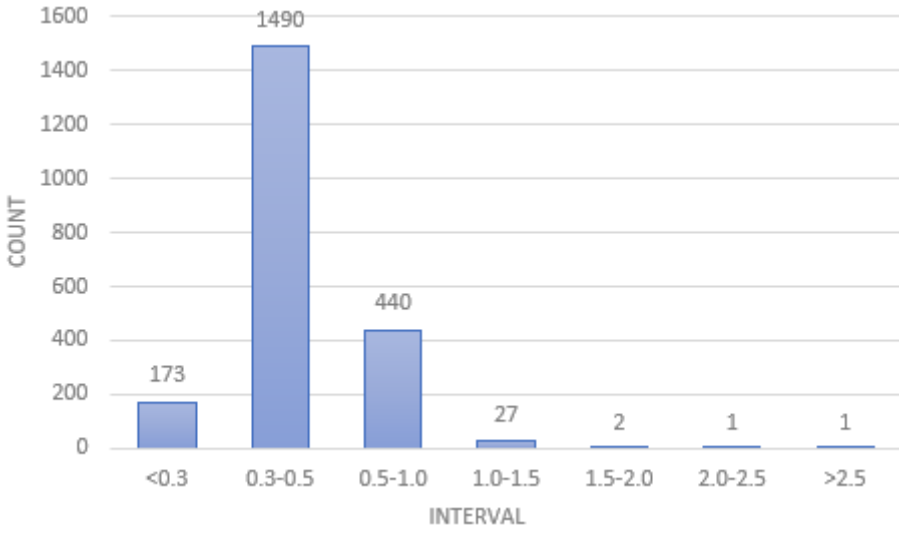

Figure 8-56 MBES targets outside boulder fields sorted by Height (Interval is in meters)

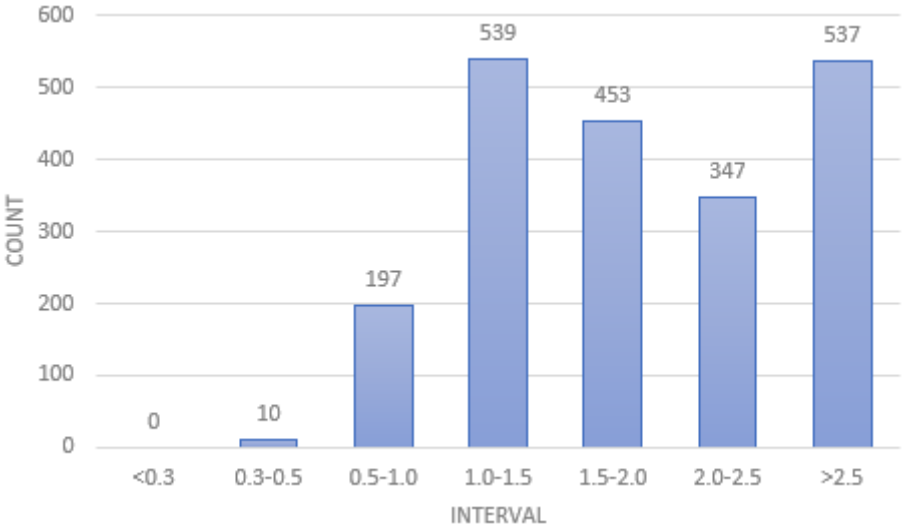

Figure 8-57 MBES targets outside boulder fields sorted by Length (Interval is in meters)

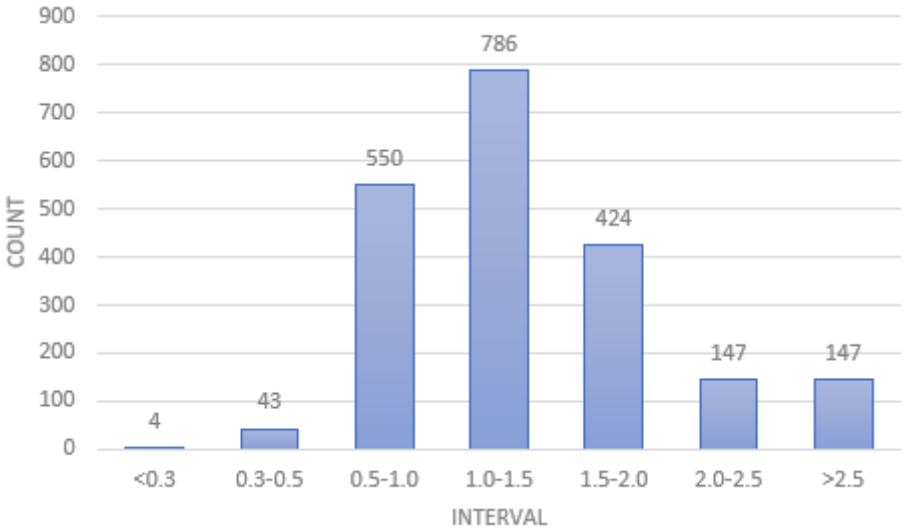

Figure 8-58 MBES targets outside boulder fields sorted by Width (Interval is in meters)

Some of the more significant MBES targets can be seen in Figure 8-59.

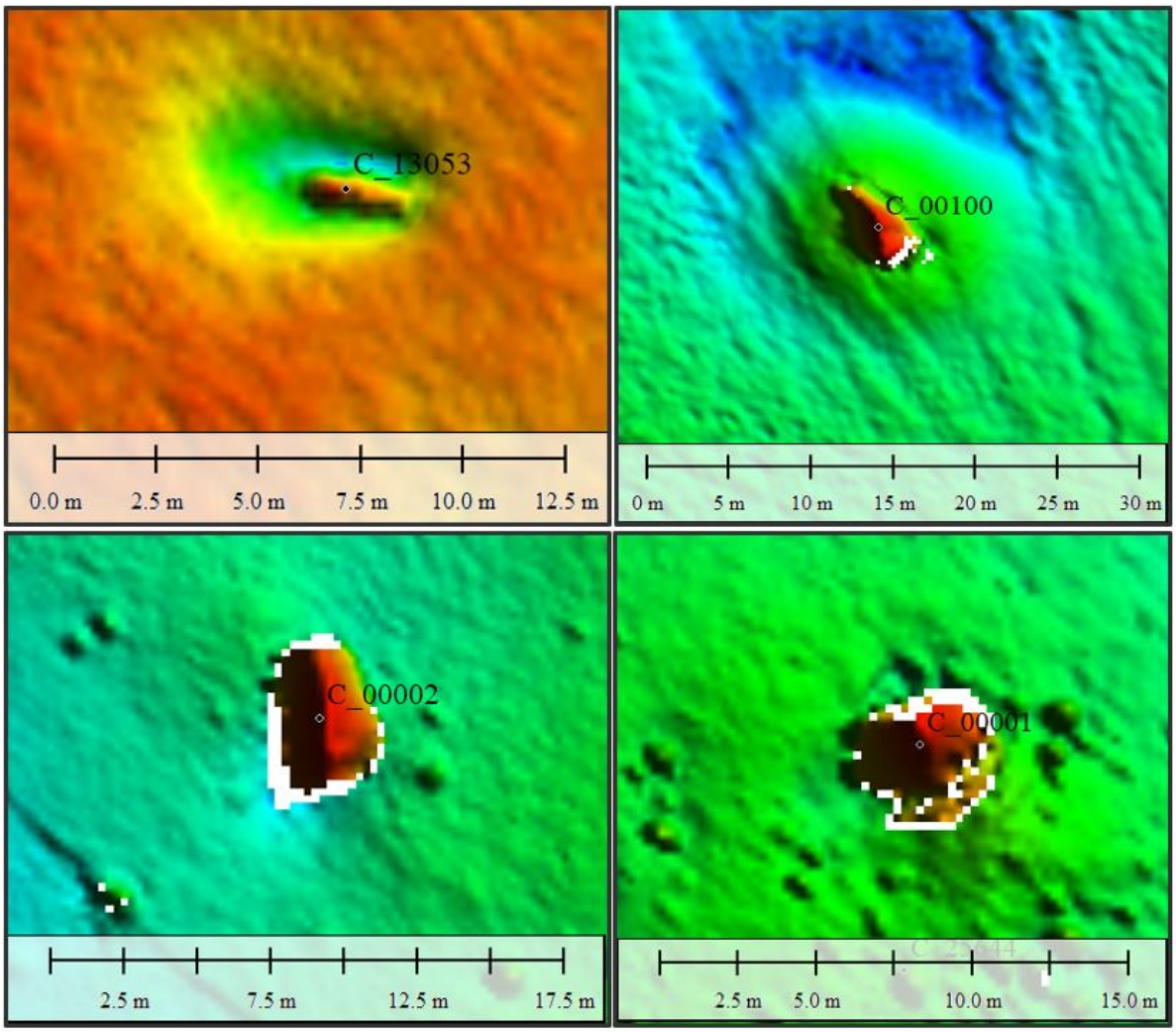

Figure 8-59 Different MBES targets. Upper left corner: the target is elongated and correlates well with the magnetometer and are located far away from boulder fields in block GL07. Upper right Corner: A large contact with an irregular shape with huge dimensions located in GL05. The lower two: are located inside boulder fields in block GL02 and GL03 and most likely large boulders.

8.8.2 SSS Targets

Once the side scan mosaics was processed, each finalized line was digitized in the waterfall view in SonarWiz. Length and width were manually measured for all targets outside boulder fields larger than 0.5 m on the shorts axis whereas inside boulder fields only man-made objects were to be detected especially detected using their shape deviating from boulders such as: linear, rectangular and irregular. If possible, any well-defined shadows were measured to calculate the height of the target. The final contact dataset was exported and correlated with MBES targets and MAG targets within a radius of 5m. Figure 8-60 shows some of the most conspicuous targets on the SSS images.

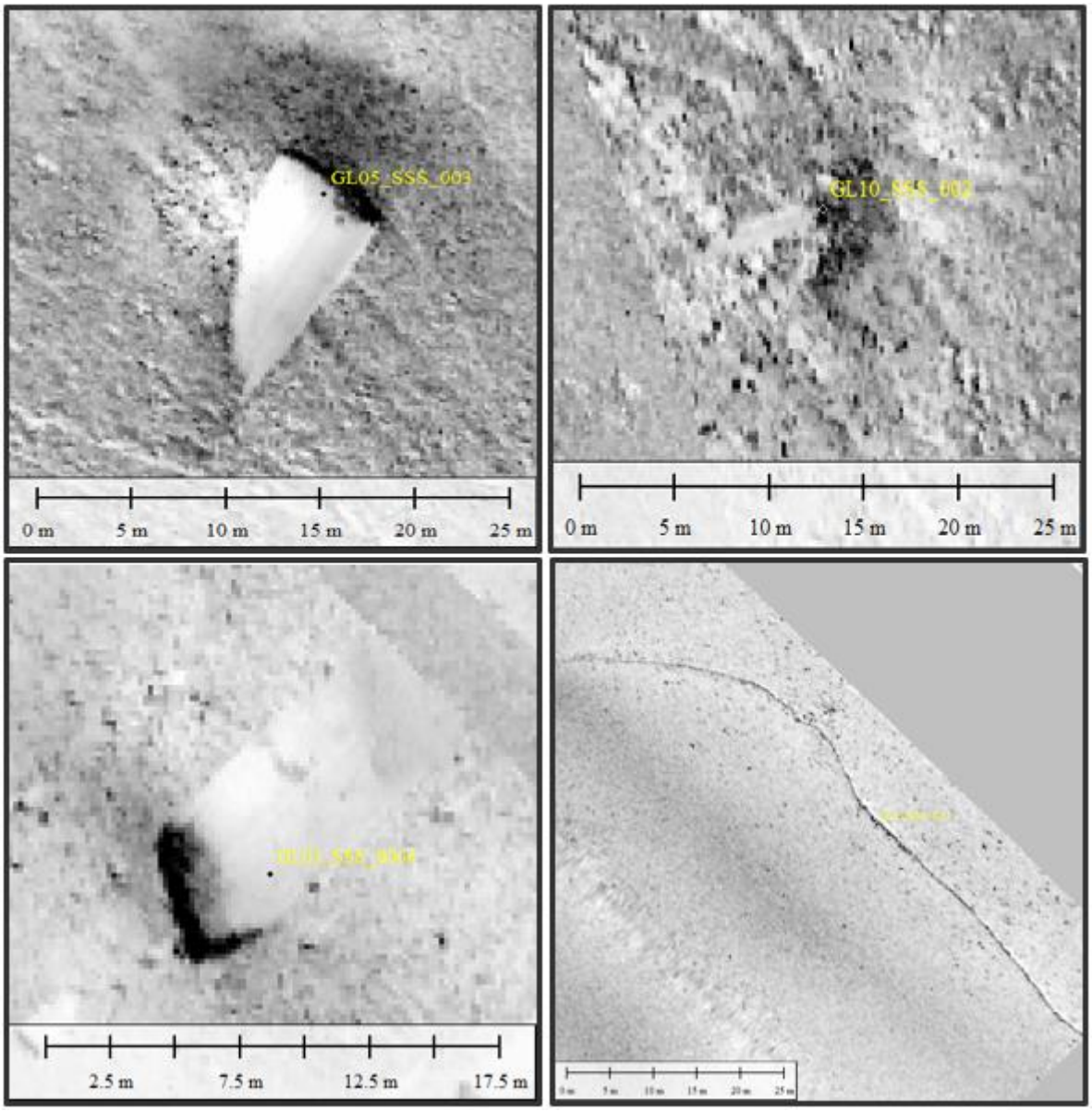

Figure 8-60: Upper left: Huge target which cast a large shadow located in GL05 (Target: GL05_SSS_003). Upper right: Seems to be some kind of debris consisting of several smaller parts (Target: GL10_SSS_002). Lower left: Huge boulder but have a rectangular shape (Target: GL03_SSS_004). Lower right: Rope in GL03 (Target: GL03_SSS_0011).

In total 28 targets are picked on the SSS based on the high frequency dataset where 14 of these are correlated with the MBES data and 1 with the MAG. Most of these or most likely related to geological features, outcrops and boulders. Man-made objects on the SSS data counts ropes, debris or unknown objects with an irregular or elongated shape.

8.8.3 MAG Targets

Magnetic anomalies down to 5 nT are detected in the residual field. A total of 1299 anomalies were identified along the corridor. The anomalies are picked using the pick-from-profile method in Oasis Montaj. The anomalies are picked at the highest peak if the shape is a monopole or a complex type and at the highest deflection point if it is a dipole, see Figure 8-61.

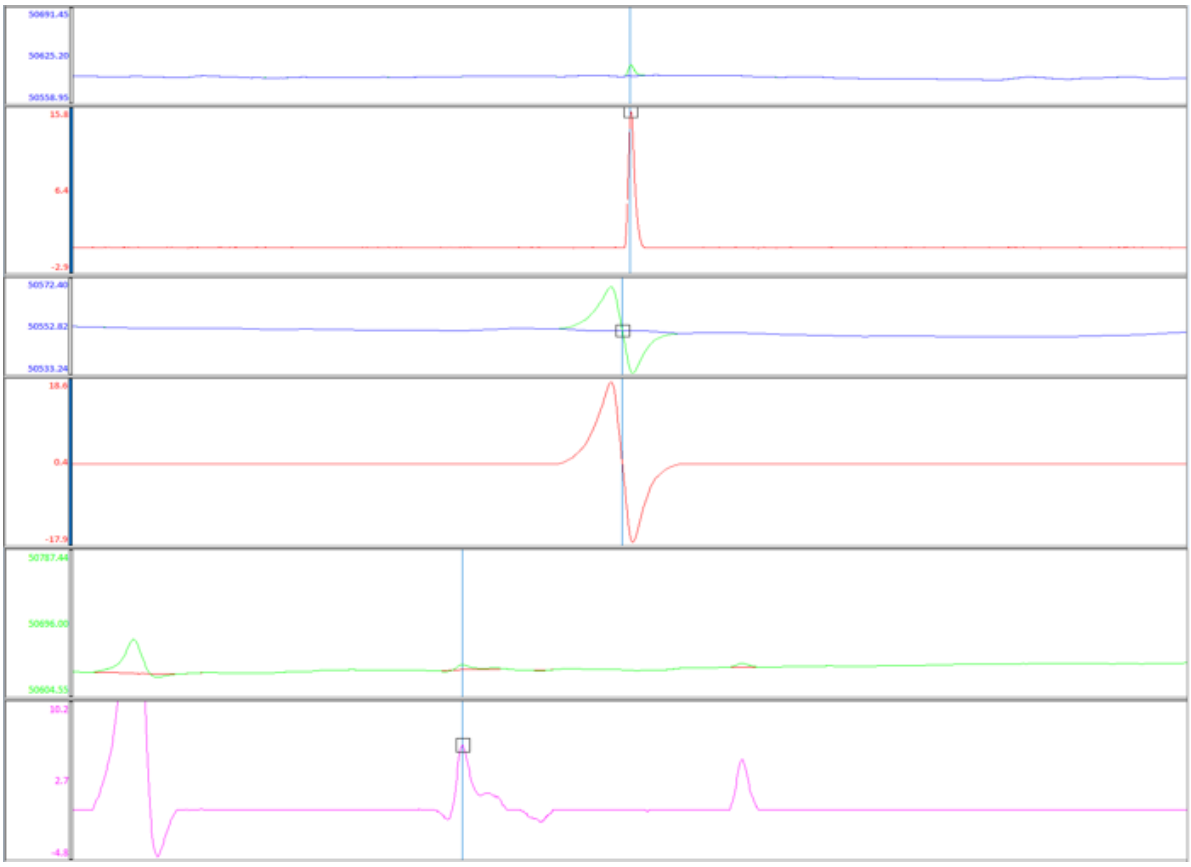

Figure 8-61: Illustration of picking anomalies (panel 1, 3 and 5 shows total field and background field, panel 2,4 and 6 shows the residual field): Upper panel: Positive Monopole, Middle panel: Dipole and Lower panel: Complex

In the dense boulder fields where the noise increases all anomalies are compared in both the residual field, total field and how the background field does fit the total field in order to identify potential noise. In general, the magnetic data are of good quality but in areas where dense boulder fields appear the noise level increases. For all lines the noise level were calculated as a tool to avoid noise detected as anomalies. A section across a boulder field can be seen in Figure 8-62 where the noise level increases as the magnetometer passes the boulder reef.

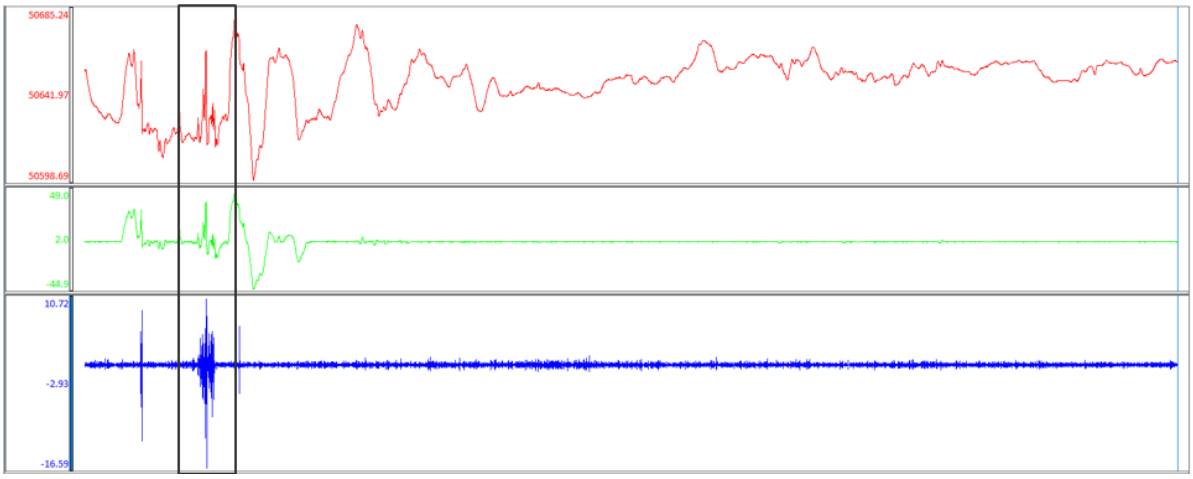

Figure 8-62 Illustrates how the noise is identified in boulder areas as a tool to avoid false anomalies. Upper panel: total field, middle panel: residual field and lower panel: noise channel

The magnetic amplitude of the anomalies along the corridor ranges from 5 nT to 720 nT with wavelengths ranging from 1.74 m to 55.26 m. The distribution of anomalies sorted by amplitudes can be seen in Table 8.4.

Table 8-4 shows the number of anomalies sorted by amplitudes

Amplitude range (nT)	Number of Anomalies
5-10	677
10-50	586
50-100	30
100-300	14
300-500	1
>500	1

From the magnetic anomaly map view in Figure 8-63 it can be seen that some concentrated zones of high magnetic intensity are found, these are located around the dense boulder zones and consists of both high and low amplitude anomalies. In these boulder fields it can be difficult to correlate the magnetic anomalies with targets from the SSS and MBES data, therefore, the correlation between the magnetic features and the SSS and MBES features in these areas must be evaluated with a significantly low confidence.

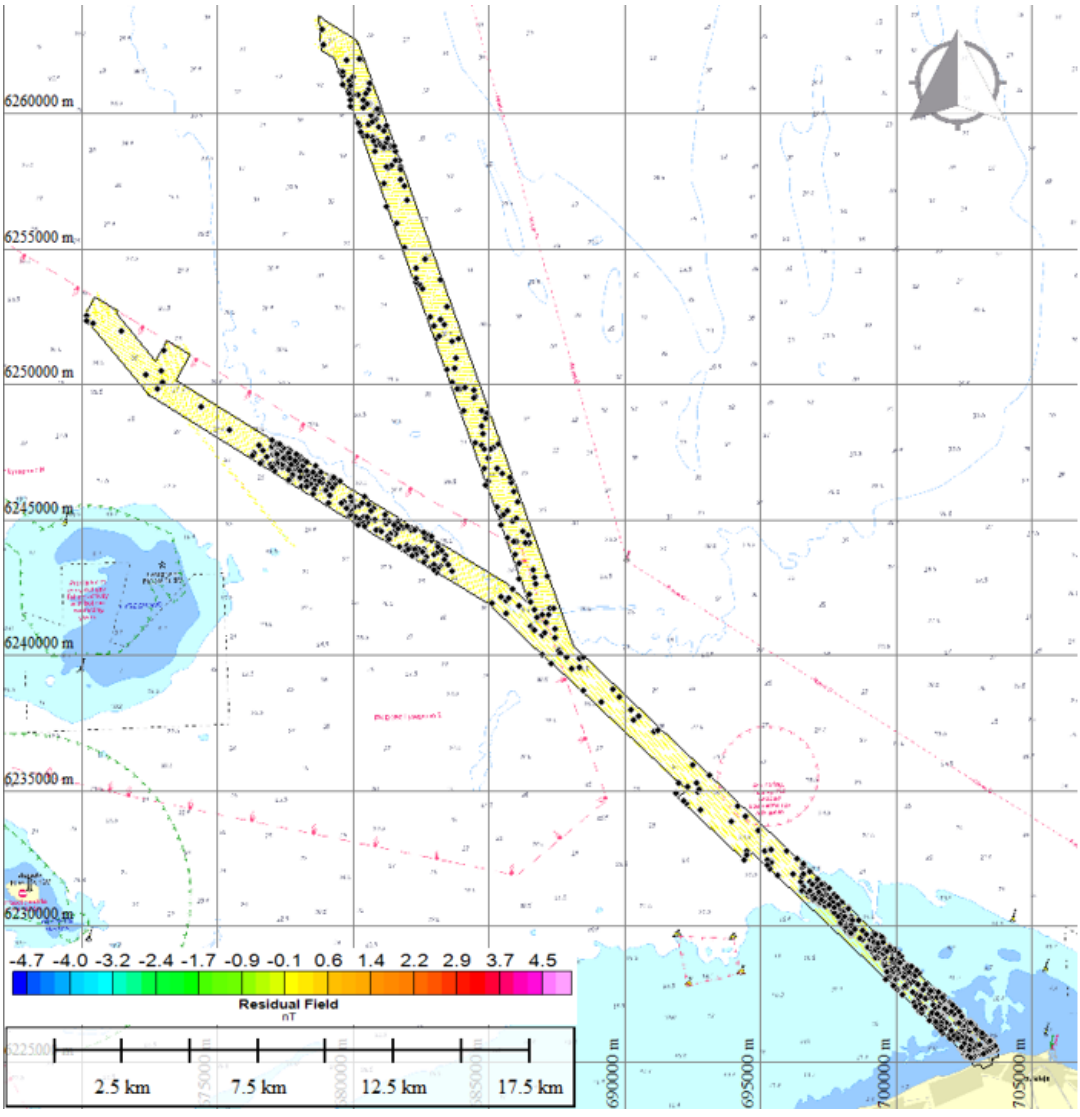

Figure 8-63 Map overview of the magnetic anomalies above 5nT with the residual field in the background

Outside the boulder fields many of the magnetic anomalies are not visible on the MBES and SSS data. These anomalies should however still be considered as objects that may be encountered during any activities on the seabed. These anomalies are most likely anthropogenic debris either

below the mudline or they are too small to detect on the MBES or SSS data. Figure 8-64 shows an example where the magnetic anomalies are present, but the main part of the anomalies cannot be correlated up against the MBES and SSS data.

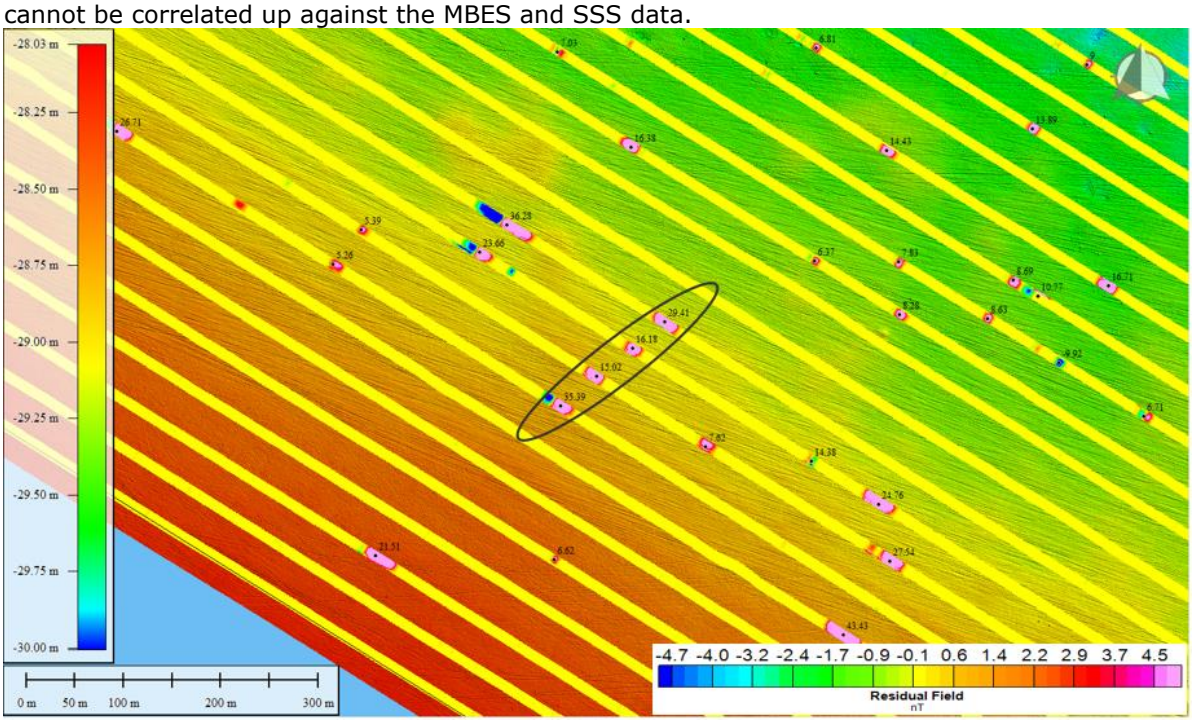

Figure 8-64 shows the residual field grid together with the MBES grid. A linear magnetic feature is marked but can't be seen on MBES nor SSS

In total 474 magnetic anomalies are correlated with the MBES data and where 19 magnetic anomalies correlate with the MBES targets outside boulder fields. 10 magnetic anomalies are correlated with potential man-made objects, the targets are correlated if each sensor identify a target within a radius of 5 m. If more targets were within a radius of 5m the targets were sorted and either the closest one or the most obvious ferrous object was correlated. The 5 m threshold is determined based on the detection range of the magnetometers and the uncertainty from the USBL compared to the MBES transducer.

8.8.4 SBP Targets

SBP anomalies have been mapped when diffraction hyperbolas have been observed on the seismic profile. Point diffractions represent objects in the subsurface- most probably boulders/ stones of different dimensions. The SPB anomalies observed within the Late Glacial glaciomarine succession can be interpreted as dropstones – as shown and indicated on the Figure 8-34B.

A total number of 249 of SBP anomalies have been interpreted. It should be underlined that:

- only point diffractions below the seafloor have been interpreted. Seabed anomalies are mapped based on the integrated interpretation of the MBES- and SSS-data;
- SBP anomalies related to presence of gas accumulations have been also interpreted- polygons representing the mapped gas occurrence within the sedimentary succession have been imported to the TSG (see 'Seabed_Features_POL' feature class).

The depth below the seabed (BSB) for each SBP target has been calculated using a constant assumed seismic velocity (ASV) of 1600 m/s and it varies between approx. 0.08 m and 11 m. Most of the SBP targets are found within the Late Glacial and Glacial succession.

SBP anomalies have been correlated with magnetic targets only as the other sensors (MBES and SSS) indicate objects located on the seabed. The targets are correlated if each sensor identify a target within a radius of 5 m. 4 SBP anomalies have been correlated with magnetic anomalies.

An overview over the interpreted SBP anomalies is shown on the Figure 8-65.

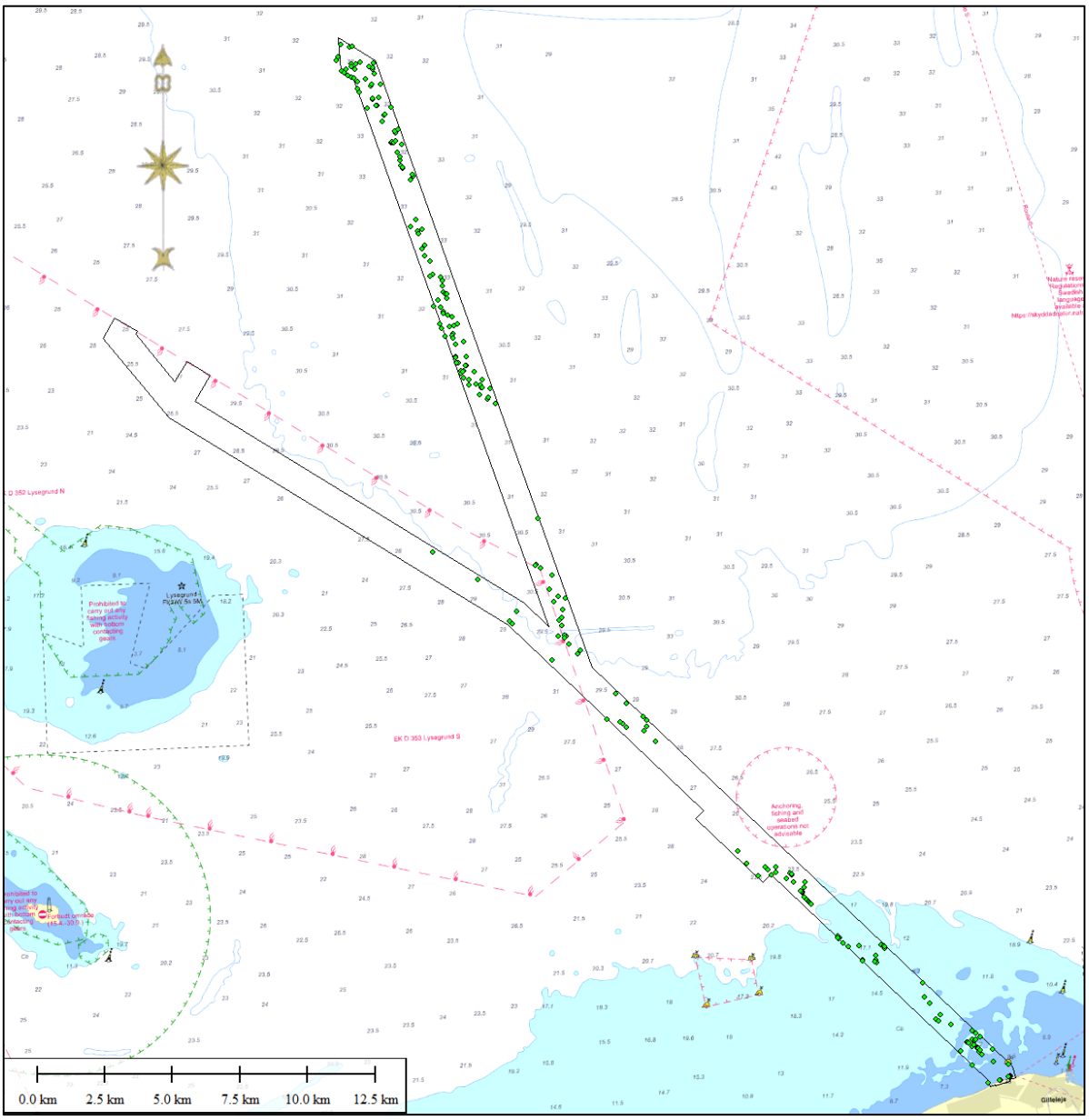

Figure 8-65 Overview over mapped SBP anomalies (green dots). A total number of 249 has been identified within the cable corridor. 4 SBP anomalies could have been correlated with magnetic anomalies.

8.8.5 Man-made objects

Man-made objects are identified along the cable corridor also inside high-density boulder fields even though it can be difficult to correlate between sensors and shapes. Man-made objects are interpreted using all sensors and correlated between the individual sensors if possible. MMO on the MBES and SSS data are interpreted by their size and shape and correlated with MAG. Targets from different sensors are correlated if they are within a radius of 5m between each other and if their shape on MBES and SSS matches reasonable. Inside the high-density boulder fields potential MMO's have attempt to be correlated with the MAG. However, in some cases more boulders correlate with one MAG anomaly, in such cases the boulders have been studied (by shape and size) to ensure no significant features has been neglected. In some cases, larger MAG anomalies doesn't correlate with other targets interpreted on MBES and SSS data, therefore attention must be paid to high amplitude anomalies inside and outside the boulder fields as these are not part of the MMO list, but can be an object just below the mudline or they are too small to

resolute on the other sensors besides the MAG. Table 8-5 highlights the different interpretations of MMO's.

Table 8-5 MMO classification and sensor ID

MMO ID	MMO Type	Comment	MBES ID	SSS ID	MAG ID	Lidar ID
MMO_0001	Other	Unknown	B_70084	GL03_SSS_0006		
MMO_0002	Other	Unknown	B_76966	GL03_SSS_0004		
MMO_0003	Other	Debris or boulder with magnetic response	B_05175		MAG_0047	
MMO_0005	Other	Debris or boulder with magnetic response	B_89820		MAG_0579	
MMO_0007	Other	Debris or boulder with magnetic response	B_05911		MAG_0125	
MMO_0009	Other	Unknown	B_88133	GL05_SSS_003		
MMO_0010	Other	Unknown	B_89352		MAG_0885	
MMO_0011	Other	Debris or boulder with magnetic response	B_89131		MAG_0903	
MMO_0012	Other	Debris or boulder with magnetic response	B_89186		MAG_0883	
MMO_0013	Other	Debris	B_89559		MAG_0919	
MMO_0014	Other	Debris	B_89512		MAG_1023	
MMO_0015	Metalic	Possible ferrous object	B_89835		MAG_1084	
MMO_0016	Other	Debris	B_00013			
MMO_0017	Other	Debris	B_89685			
MMO_0018	Non Metalic	Elongated object	B_33695	GL02_SSS_0006		
MMO_0019	Non Metalic	Elongated object		GL02_SSS_0007		
MMO_0021	Soft Rope	Possible rope		GL02_SSS_0005		
MMO_0022	Soft Rope	Rope		GL03_SSS_0010		
MMO_0023	Soft Rope	Rope		GL03_SSS_0005		
MMO_0024	Non Metalic	Elongated object		GL03_SSS_0009		

MMO_0025	Non Metalic	Elongated object		GL03_SSS_0012		
MMO_0026	Other	Debris		GL03_SSS_0013		
MMO_0027	Soft Rope	Rope		GL03_SSS_0011		
MMO_0028	Non Metalic	Elongated object		GL03_SSS_0008		
MMO_0029	Other	Debris or large trawl mark	B_88273	GL05_SSS_0001		
MMO_0031	Soft Rope	Rope	B_88711	GL05_SSS_004		
MMO_0032	Other	Debris or minor boulder outcrop		GL11_SSS_001		
MMO_0033	Soft Rope	Rope or anchor scar		GL11_SSS_002		
MMO_0034	Other	Unknown or larger boulder outcrop	B_86747			
MMO_0035	Other	Seems to be a depression with magnetic response		GL10_SSS_001	MAG_1204	
MMO_0036	Other	Monument				O_01
MMO_0037	Other	Monument				O_02

None of the MMO's are interpreted as archaeological origin based on the appearance on the MBES and SSS data and correlation with the MAG anomalies. Also, a huge part of the cable corridor is heavily affected by trawl marks meaning that potential archaeological findings on the seabed may have been ruined or dragged away from around KP 12.

8.9 Geotechnical investigations

The soil investigation campaign comprises:

- Vibrocore sampling and CPT at 60 positions (ECR)
- Grab sampling at 55 positions (54 were successful)

The vibrocores and CPT's aim at determining the soil conditions down to a target depth of 3 or 6 m depth. The grab samples aim at determining the soil conditions at the seabed level.

With respect to the vibrocores, it should be noted that for some positions, the penetration is considerably longer than the recovered core length. For other positions, more core length is recovered, compared to the penetration. This is related to two phenomenon's which are very common when retrieving vibrocores from very soft clays or very dense sands. The differences can be explained by:

- Core loss/compaction due to very soft soil, typically soft clay. The penetration is longer than the actual core length and air gaps may be seen in the cores. The locations where this occurs coincides with very low strength seen on the corresponding CPT

- Core gain due to bulking of relatively dense sand layers. When the vibrocore is retrieved, the sand gets looser, leading to additional core length observed, compared to the penetration.

This has been taken into account in combination with e.g. the seismic data during interpretation of the soil model. The vibrocore profiles and the Geogis database reflects the data as recorded in the laboratory.

After completed field work the core sections were shipped to Geo's laboratory where the cores underwent geological description. The grab samples were described at Rambøll's inhouse laboratory. The descriptions follow the specifications given in Bulletin No. 1 "A guide to engineering geological soil description" from Dansk Geoteknisk Forening (DGF) /2/. During the process of geological description, sub-samples for laboratory testing, in selected sections of the vibrocores, were extracted. The samples were sent to WBM Eurofins for classification testing. Thermal conductivity testing was carried out at Geo. Further, vane shear tests and pocket penetrometer tests were carried out during the description of the vibrocore samples.

8.10 Laboratory test results

The individual laboratory test results are described below and shown in Geotechnical data report, Appendix 2 to this report.

Natural Moisture Content
Natural moisture content determination was performed on several samples. The results of the natural moisture content determinations are given in the borehole and vibrocore logs (Geotechnical data report, sub Appendix 1 and 2) and in the Laboratory Summary Table (Appendix 2).

Particle density
Particle density was determined on selected samples. The results are found in Geotechnical data report, sub Appendix 2

Organic Content (loss on ignition)
Determination of the organic content of the encountered soils was performed for selected sub-samples. The results are presented on the vibrocore logs.

Particle Size Analysis
Particle size analyses were undertaken on sub-samples by sieving only or a combination of sieving and sedimentation (i.e. sieve or sieve/hydrometer testing). The detailed results from the sieve and sedimentation tests are presented on the Particle Size Distribution plots in the Geotechnical data reports, Appendix 2.4.

Atterberg Limit Testing
Atterberg Limit testing were performed on the cohesive soils encountered and presented on the vibrocore logs

Thermal Conductivity Tests
Determination of the thermal conductivity of the encountered soils, using a transient heat method (Thermal Needle Probe Procedure), was performed on a number of selected vibrocore sections. The results of the thermal conductivity tests are presented separately in the Geotechnical data reports Appendix 2.7.

8.11 Onshore lidar mapping

For the onshore part an airborne LIDAR survey was performed to acquire lidar data and orthophoto. The lidar point clouds are delivered in two different ways; one with all processed and accepted points and another as a terrain model as can be seen in Figure 8-66.

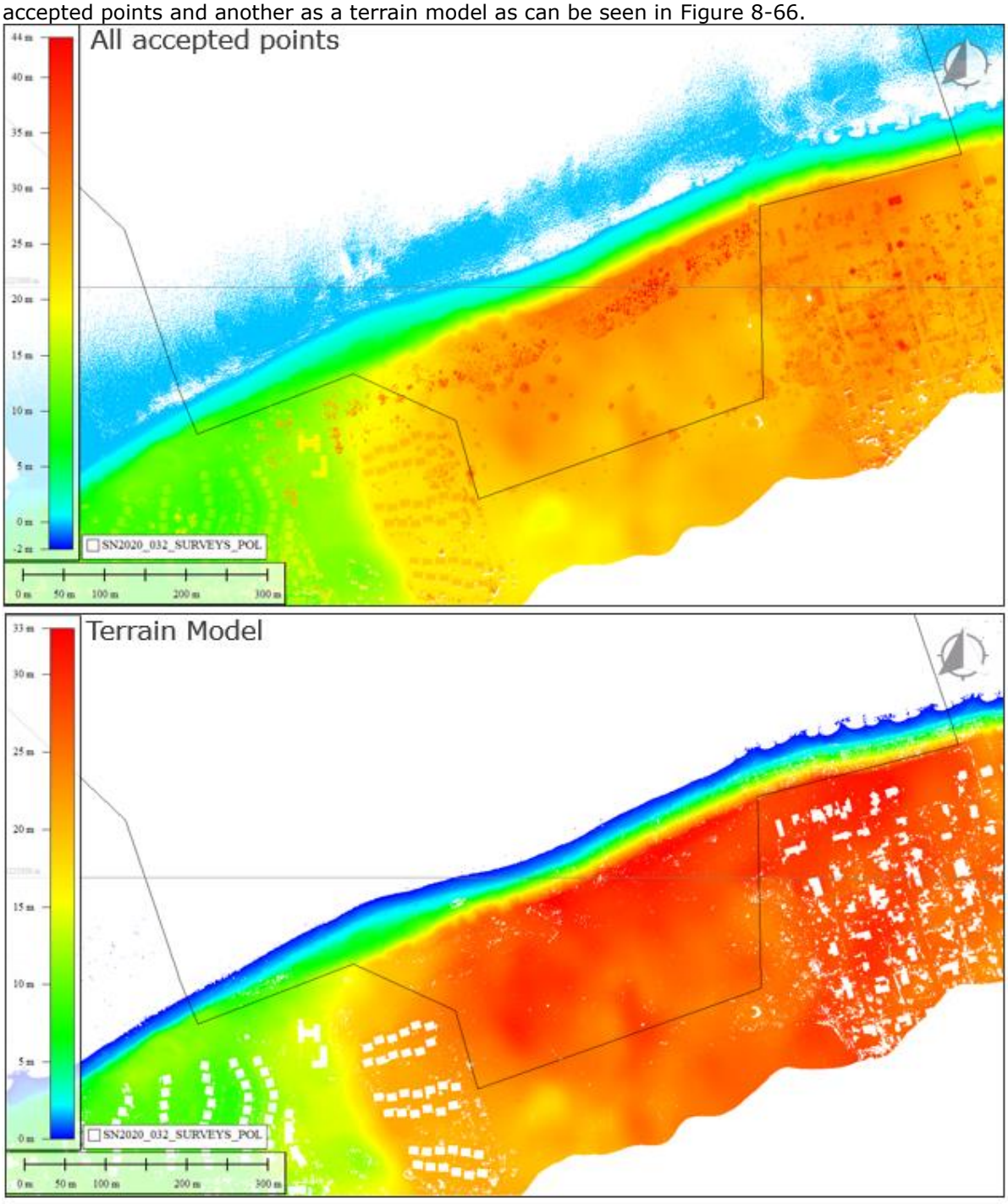

Figure 8-66: Onshore lidar data: Upper image shows the processed point cloud with all accepted points whereas the lower image shows the terrain model where all vegetation and man-made constructions are removed.

Based on the terrain model grids with cell sizes of 0.25m, 0.5m, 1.0m and 5.0m are created. Besides the point clouds an orthophoto with 2.8cm pixel resolution is provided which is useful to help identify any obstacles. For the onshore part no major obstacles are observed only two minor monuments which are most likely protected monuments. The orthophoto together with the two monuments can be seen in Figure 8-67.

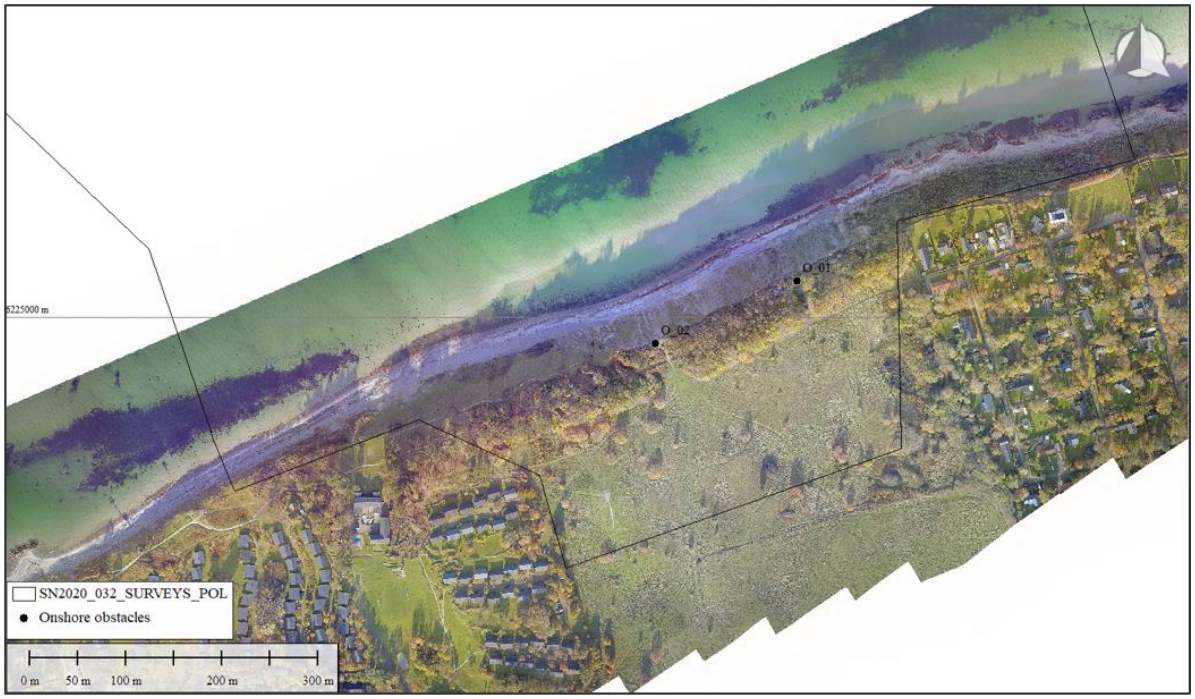

Figure 8-67 shows the orthophoto together with two identified monuments marked with two black dots.

When going from the offshore parts and towards the beach a steep cliff occurs along the beach of approx. 43.75 degrees in the survey area. On the top of the cliff a fence of trees and bushes appears and right after this a plain grass field covers the rest of the survey corridor. The transition from the offshore part towards land until the end of the survey corridor can be seen in Figure 8-68.

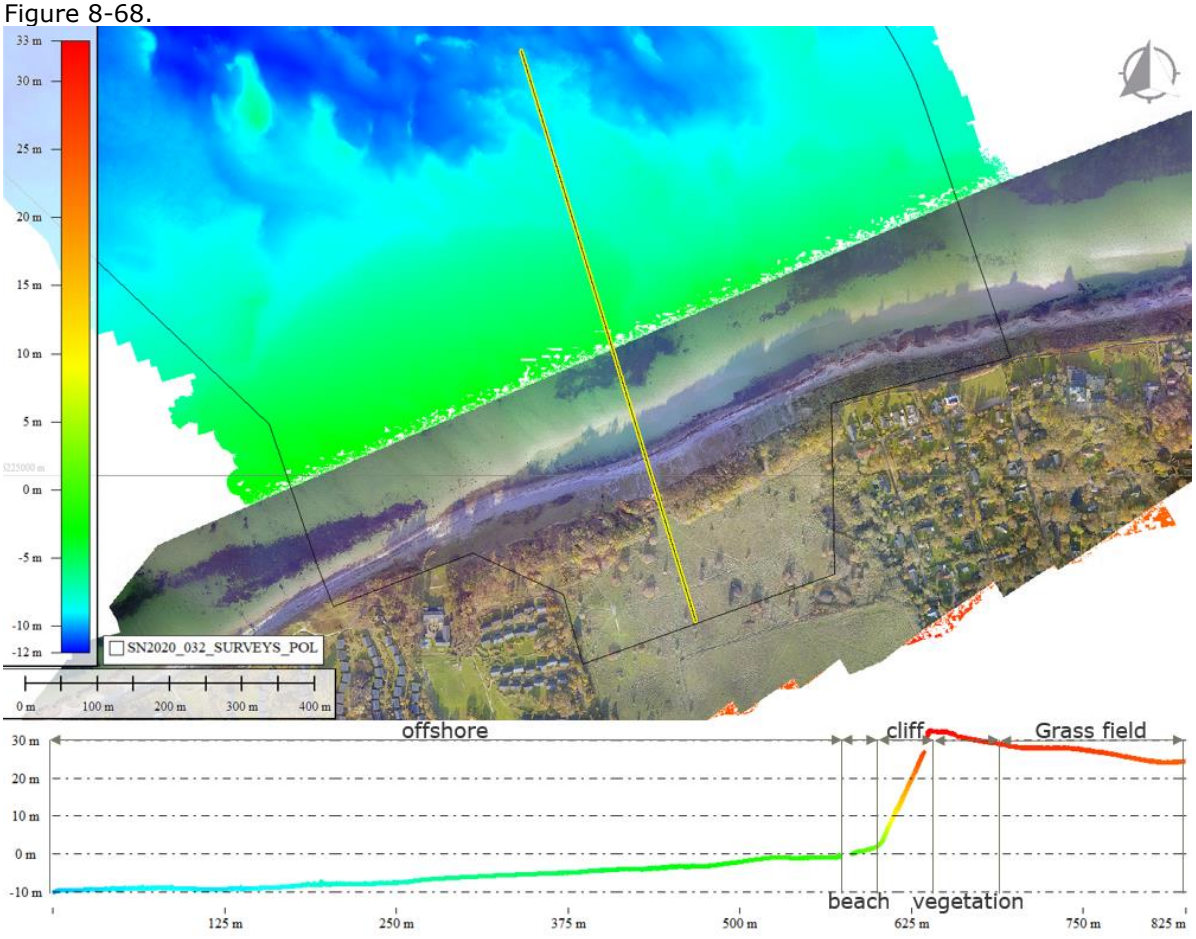

Figure 8-68 shows the transition from offshore to onshore and the terrain for the onshore parts

8.12 Detailed Route Analysis

A detailed route analysis can be found in Appendix 3 starting from KP 0.0 to KP 52.02. The route analysis includes bathymetry details, seabed sediments, seabed features, subsurface geology, targets and obstacles and geotechnical properties. The route is divided into 11 blocks – all divided in relation to the seabed sediment and subsurface geology.

9. SUMMARY

Ramboll Denmark A/S was commissioned by Energinet to perform a cable route survey between Hesselø landfall to the Hesselø OWF a corridor of approx. 70 km long and a width of 1000m with a local extension of 1400m. Based on the interpretation of geophysical, grab samples and geotechnical investigations, the following findings and conclusion are presented:

- Surveyed water depths ranged from 0.9 to 34 m.
- Typical seabed gradients are less than 1°. Seabed gradients of 10° or higher were identified around boulder fields where boulders are building up reefs.
- Towards landfall the seabed sediments are primarily dominated by till/diamicton with areas of coarse sand and gravels. Further offshore, the seabed sediment turns to be dominated by muddy sands.
- Dense boulder fields are observed nearshore (KP 0.5 to KP 10.00) and a minor one further offshore (KP 27.0 to KP 30.5). Also, the corridor has some areas with isolated boulders.
- In general, the seabed is mostly affected by the large nearshore boulder field and the remaining parts of the corridor are heavily affected by high density of trawl marks starting from KP 11.5 and slightly increases towards the OWF site.
- Targets were identified on MBES, SSS and MAG data, where most of the targets are related to the boulder fields. Also, multiple anomalies outside the boulder fields can't be identified on other sensors than magnetometer. These anomalies are most likely just below the mudline or too small to resolute but must be taken into consideration when preforming seabed activities.
- During the interpretation of the SBP data seven reflections were mapped.
- The subsurface geology can be summarised as; Glacial tills are outcropping the seabed or are present at shallow depths below the seabed in the southernmost part of the cable corridor (KP=0.0-9.2) as well as in the central part of the corridor, north-east from Lysegrund (KP=27.0-35.0, western arm). The central segment, between KP=(18.0-27.0, western arm) and KP=(21.75-27.0, eastern arm) located east from Lysegrund can be characterized by presence of a relatively thick succession of Late Glacial to Post Glacial sands found below approx. 0.5-2.0 m thick cover of Holocene fine-grained sediments. Along the remaining part of the route, the Post Glacial deposits are underlain by Late Glacial clays. The acquired SBP data did not penetrate to the lower boundary of the unit as it can reach significant thicknesses of up to 75m. The Holocene succession is 0-13 m thick (typically between 0.5-6.0m) and present throughout entire cable corridor, except along its southern part where the Holocene deposits are local and found at selected location only.
- From the onshore Lidar survey, no major obstacles were identified besides a steep cliff and two monuments. The terrain model shows a steep cliff with an incline of approx. 44° before reaching the coastline consisting of a plane grass field appears.

By investigating this area Ramboll has gathered significant amount of information and extensive knowledge of the seabed, sedimentary materials, sedimentation, seabed contacts and correlation of geophysical and geotechnical parameters in order to establish a solid geo-model.

10. REFERENCES

Ref. /1/ "General geology of southern Kattegat, the Hesselø wind farm area", Desk Study Report for Energinet Eltransmission A/S, Jørn Bo Jensen and Ole Bennike, GEUS, Rapport 2020/53

Ref. /2/ "Early Holocene estuary development of the Hesselø Bay area, southern Kattegat, Denmark and its implication for Ancylus Lake drainage", Bendixen C., et al., 2017

Ref. /3/ "The Holocene Great Belt connection to the southern Kattegat, Scandinavia: Ancylus Lake drainage and Early Littorina Sea transgression", Bendixen C., et al., 2015

11. LIST OF DELIVERABLES

Tracklines	MBES	.shp
	SSS	.shp
	MAG	.shp
	SBP	.shp
MBES	Tracklines	.shp
	Processed point clouds	.pts
	25cm gridded surface	.xyz
		.tiff
	1m gridded surface	.xyz
		.tiff
	5m gridded surface	.xyz
		.tiff
	Contours 50 cm intervals	.shp
	SVP	.txt
		.shp
Backscatter	24bit	.tif
	32bit	.tif
SSS	PROC files (LF, HF)	.xtf
	Mosaics (LF, HF)	.tif
	Navigation files	.csv
SBP	Processed files	.sgy
		.tif
MAG	Processed files	.csv
		.gdb
	Anomalies	.shp
		.csv
Seabed interpretation	Contacts (MBES, SSS, MAG)	.shp
		.csv
	Seabed Features	.shp
	Seabed Classification	.shp
	Seabed Substrate	.shp
	Boulder fields	.shp
		.csv

Subsurface interpretation	Horizons	.dat
	Elevation grids	.dat
		.tif
	Depth BSB grids	.dat
		.tif
	Isochore grids	.dat
		.tif
Geotech	Position	.shp
	Results	.pdf
		.xlsx
		.GeoXML
		.AGS4
Onshore	Processed files	.csv
		.laz
	Grids (0.25, 0.5, 1.0, 5.0m)	.xyz
		.tif
	Orthophoto	.ecw
	Contours	.shp
	Obstacles	.csv
GDB	Anomaly	MAG_PTS
		MBES_PTS
		SSS_PTS
		SBP_PTS
	Bathymetry	CONTOURS_LIN
	Geotechnic	GEOTECHNIC_PTS
	MMO	MMO_PTS
	SEABED	FEATURES_LIN
		FEATURES_POL
		FEATURES_PTS
		FEATURES_POL_BOULDERS_100x100m
		FEATURES_POL_BOULDERS_50x50m
		FEATURES_POL_BOULDERS_25x25m
		GEOLOGY_POL
		SUBSTRATE_POL
	SURVEY	CHARTS_POL

		KP_ROUTE_LIN_GL
		KP_ROUTE_LIN_HS
		SURVEYS_POL_GL_BLOCKS
		SURVEYS_POL_GL_CORRIDOR
		SURVEYS_POL_HS_BLOCKS
		SURVEYS_POL_HS_CORRIDOR
	TRACKS	TRACKS_LIN
RASTER GDB	BACKSCATTER	ALL_GL_Backscatter_25cm_32bit
		ALL_GL_Backscatter_25cm_8bit
	MBES	ALL_GL_MBES_AVG_1m
		ALL_GL_MBES_AVG_25cm
		ALL_GL_MBES_AVG_5m
		ALL_GL_THU_1m
		ALL_GL_TVU_1m
	SSS	ALL_GL_SSS_HF_20cm
		ALL_GL_SSS_LF_20cm
	Lidar	Gilleleje_ECR_Lidar_Ground_Model_1m
		Gilleleje_ECR_Lidar_Ground_Model_25cm
		Gilleleje_ECR_Lidar_Ground_Model_50cm
		Gilleleje_ECR_Lidar_Ground_Model_5m
	SBP	H01_Base_PG_III1_SA_mBSB
		H01_Base_PG_III1_SA_mMSL
		H02_Base_PG_III2_CL_mBSB
		H02_Base_PG_III2_CL_mMSL
		H03_Base_PG_IV_SA_GR_mBSB
		H03_Base_PG_IV_SA_GR_mMSL
		H04_Base_PG_II2_CL_mBSB
		H04_Base_PG_II2_CL_mMSL
		H05_Base_PG_II1_SA_mBSB
		H05_Base_PG_II1_SA_mMSL
		H06_Base_PG_I_SA_mBSB
		H06_Base_PG_I_SA_mMSL
		H07_Base_LG_CL_mBSB
		H07_Base_LG_CL_mMSL

		Isopach_LG_CL_m
		Isopach_PG_I_SA_m
		Isopach_PG_II1_SA_m
		Isopach_PG_II2_CL_m
		Isopach_PG_III1_SA_m
		Isopach_PG_III2_CL_m
		Isopach_PG_IV_SA_GR_m

APPENDIX 1
GEOTECHNICAL DATA REPORT

APPENDIX 2
CHARTS

APPENDIX 3
DETAILED ROUTE ANALYSIS

APPENDIX 4
BENCHMARK REPORTS

APPENDIX 5
OPERATIONAL REPORTS

APPENDIX 6
ACCEPTANCE TEST REPORTS

APPENDIX 7
ROUTE POSITION LIST (RPL)